

# Molecular Design of Solid-State Nanopores: Fundamental Concepts and Applications

Gonzalo Pérez-Mitta, María Eugenia Toimil-Molares, Christina Trautmann, Waldemar A. Marmisollé, and Omar Azzaroni\*

Solid-state nanopores are fascinating objects that enable the development of specific and efficient chemical and biological sensors, as well as the investigation of the physicochemical principles ruling the behavior of biological channels. The great variety of biological nanopores that nature provides regulates not only the most critical processes in the human body, including neuronal communication and sensory perception, but also the most important bioenergetic process on earth: photosynthesis. This makes them an exhaustless source of inspiration toward the development of more efficient, selective, and sophisticated nanopore-based nanofluidic devices. The key point responsible for the vibrant and exciting advance of solid nanopore research in the last decade has been the simultaneous combination of advanced fabrication nanotechnologies to tailor the size, geometry, and application of novel and creative approaches to confer the nanopore surface specific functionalities and responsiveness. Here, the state of the art is described in the following critical areas: i) theory, ii) nanofabrication techniques, iii) (bio)chemical functionalization, iv) construction of nanofluidic actuators, v) nanopore (bio)sensors, and vi) commercial aspects. The plethora of potential applications once envisioned for solid-state nanochannels is progressively and quickly materializing into new technologies that hold promise to revolutionize the everyday life.

## 1. Introduction

Solid-state nanopores have fascinated physicists, materials scientists, engineers, and chemists for nearly two decades, both in basic and applied research.<sup>[1,2]</sup> Consequently, the science related to this fascinating subject has expanded at a rapid pace and the field has become a cutting-edge area in nanoscience.<sup>[3,4]</sup> Much of the development of this field has been inspired by the unique functional properties of biological ion channels.<sup>[5,6]</sup> Ion channels are membrane proteins embedded within cell membranes where they represent key elements in living systems. Biological channels are in charge of regulating physiological parameters such as electric potential, ionic flow, and molecular transport inside and across the boundaries of the cells. These important operative functions control and regulate vital processes such as energy production and storage or signal propagation and processing, including, cardiac pulsing, memory, nerve signaling, etc.

Taking inspiration from these efficient biological machineries, many research groups worldwide embarked to develop nanofluidic architectures—such as nanopores, nanochannels and nanopipettes—to mimic their singular transport properties, and eventually use them for practical applications.<sup>[7–15]</sup>

At the same time, the rapidly developing fields of surface chemistry, materials science, and nanotechnology have provided the tools for the development of nanofluidic devices equipped with a wide range of functional molecular building blocks that ultimately confer them specific fluidic transport properties. This interdisciplinary approach in turn has successfully led to the construction of nanofluidic architectures which are able to mimic many ion transport functions of biological channels, such as ion selectivity, current rectification and flux inhibition by protons, among other examples.


In addition, nowadays, innovative research in solid-state nanopores is no longer circumscribed to the realm of fundamental science but has begun to enter the domain of nano-engineering. The field is particularly powered by the publication of several seminal works that proved the importance of nanofluidics for future technologies such as single molecule

Dr. G. Pérez-Mitta, Dr. W. A. Marmisollé, Prof. O. Azzaroni  
Instituto de Investigaciones Fisicoquímicas Teóricas y Aplicadas (INIFTA)  
Departamento de Química  
Facultad de Ciencias Exactas  
Universidad Nacional de La Plata (UNLP) – CONICET  
Diagonal 113 y 64, 1900 La Plata, Argentina  
E-mail: azzaroni@inifta.unlp.edu.ar

Dr. G. Pérez-Mitta  
Laboratory of Molecular Neurobiology and Biophysics  
Howard Hughes Medical Institute  
The Rockefeller University  
1230 York Avenue, New York, NY 10065, USA

Dr. M. E. Toimil-Molares, Prof. C. Trautmann  
GSI Helmholtzzentrum für Schwerionenforschung  
64291 Darmstadt, Germany

Prof. C. Trautmann  
Technische Universität Darmstadt  
64287 Darmstadt, Germany

 The ORCID identification number(s) for the author(s) of this article can be found under <https://doi.org/10.1002/adma.201901483>.

DOI: 10.1002/adma.201901483

analytics, lab-on-a-chip applications, micro total analysis systems ( $\mu$ TAS) and energy conversion.<sup>[16]</sup> Furthermore, in the past few years we have witnessed the uprising of the nanopore sequencing technology that is slowly becoming the future of genetic analysis.<sup>[16]</sup> This upward trend was further propelled and expanded with the development of new fabrication techniques which introduced alternative synthetic protocols to create nanopore platforms. During the beginning of the 21st century, the rise of experimental and theoretical information on solid-state nanopores stimulated an increased interest in how to harness their fascinating transport properties in suitable applications. Indeed, a careful look at the literature reveals that—since several years now—nanopore research has shifted from fundamental studies (“blue sky science”) toward much more concrete and tangible practical applications.

According to Eijkel and van den Berg, nanofluidics can be defined as the study of the motion of fluids within structures that have at least one dimension between 1 and 100 nm.<sup>[17]</sup> This definition includes nanochannels, nanopores and nanotubes as well as mesoporous materials. In many cases, for simplicity of expression, the term “nanopore” is used as a synonym of “nanochannel.” However, strictly speaking, a “nanopore” refers to a pore structure with a diameter in the 1–100 nm range, with the pore diameter larger than its depth; and a “nanochannel” refers to a pore structure in which the pore depth is much larger than the diameter. In other words, the use of the denomination “nanopore” should be restricted to structures with low aspect ratio (diameter to length) while the term “nanochannel” should be used for structures with high aspect ratio.

Finally, mesoporous materials are those containing a high density of nanopores or nanochannels, as traditional porous membranes do. In this work, we focus mostly on nanofluidic devices based on single nanochannels and nanopores with well-defined geometries. The application of nanotubes will not be discussed in this review.

Nanochannel model systems have enabled the investigation of their fundamental nanofluidic properties as a function of size and geometry. It is now clear that a wealth of interesting and new phenomena, including, e.g., ion current rectification and gating, arise when the channel surface is charged and the dimensions are comparable to the Debye length. It must be said that nanofluidics has provided the fundamental background to devise, design, and construct new addressable nanochannel-based devices relying on surface charge governed ionic transport. In the more recent years, this field is also known as “iontronics” and describes, whenever possible, ion-based processes and devices in close analogy to electronics.

Thanks to the efforts from many research groups, significant progress has been achieved regarding the various fabrication techniques in the last decade, generating nanochannels, nanopores, nanoelectrodes and nanopipettes with well controlled dimensions and a variety of materials.

It is generally accepted that the functionalization of the nanochannel walls with molecular assemblies may provide one of the most powerful (and yet versatile) means to command the transport properties of nanofluidic devices. The integration of adaptive/reconfigurable/responsive units into the nanochannels may result in different gating mechanisms controlled

by excluded volume effects, charge distributions, or specific recognition functions.

This is the main reason why the functionalization of nanochannels and nanopores with molecular systems capable of responding to specific target stimulus is of paramount relevance to attain addressable nanofluidic devices. Exciting opportunities in sensing, and signal transduction and amplification are revealed when we think that specific stimuli can finely modulate the physicochemical characteristics of the pore walls with a predictable effect on the ion transport properties.

Therefore, here, we take a closer look at what has been accomplished to date regarding functional ionic transport through nanopores, nanochannels, and nanopipettes. This review is divided into seven sections. Section 2 provides the fundamentals and theoretical concepts of nanofluidics. These fundamental notions are important to understand the functional properties of different nanofluidic elements. Section 3 discusses different strategies to fabricate nanopores, nanochannels, and nanopipettes. Section 4 describes the use of several general methods to functionalize the inner walls of nanofluidic devices. In Section 5 there is a detailed description of the integration of different molecular systems into solid-state nanopore-based nanofluidic devices aiming diverse applications. We focus on nanochannels, nanopores and nanopipettes, although some examples on other systems such as anodic aluminum oxide (AAO) membranes and  $\text{SiO}_2$  mesoporous thin films are also included with illustrative purposes. Section 6 highlights a range of prominent practical applications associated with the implementation of solid-state nanopores in different scenarios. In this regard, we should note that this review is not placing particular emphasis on functionalized nanopores for single molecule sensing provided that this topic has already been discussed in recent reviews.<sup>[18–20]</sup> Finally, our remarks on the evolution of the field and possible future directions are presented in Section 7.

Here, we attempt to give a comprehensive treatment and critical review of the subject, and to point to areas of future development. It is expected that the readers will find the concepts and ideas contained herein useful for their work. We hope that this article will be of help to researchers, postdocs, and graduate students with ambitions to explore new horizons in nanopore research and to discover new concepts, principles, and applications.

## 2. Theoretical Aspects

Different theoretical methods have been used to provide a better conceptual understanding of the physics underlining nanofluidic phenomena. Both classical continuous methods and molecular theories have been applied evidencing their complementarities. Typically, each method succeeds where the other fails. Continuous models fail for ranges of less than ten molecular dimensions ( $\approx 10$  nm) while, on the other hand, molecular methods cannot handle higher dimensions because computational times turn prohibitive. An interesting compromise can be found in hybrid models such as the molecular theory, where continuous equations that contain molecular information are used. In the following section we will proceed

to explain some general concepts that pervade the study of nanofluidics.

## 2.1. Fundamental Concepts

### 2.1.1. Electrical Double Layer (EDL)

The behavior of macroscopic systems breaks down when the characteristic lengths of the systems become comparable with, e.g., molecular distances or the characteristic distances for interactions. In particular, for nanofluidics, the characteristic length scale determining the electrostatic interactions of the ions in confined volumes is the dimension of the EDL. When an electrode is immersed in a solution and polarized, the EDL is formed consisting of a strongly adsorbed layer close to the electrode surface (Helmholtz layer) and a more loosely bound layer further apart (Stern layer). The thickness of the EDL is a function of the electrolyte concentration. For concentrations ranging from  $10 \times 10^{-3}$  to  $100 \times 10^{-3}$  M, the EDL thickness amounts 1 to 3 nm (Poisson–Boltzmann (PB) equation, Equation (8)). Therefore, while the EDL does not influence the ionic distribution in the interior of a micrometer-sized channel, its influence should be considered for pores 10–50 nm in size, and specially for pore sizes <5 nm. The latter is called extreme confinement, when overlapping of the EDL occurs. (Figure 1). In this case, the solution inside the pore is completely polarized, meaning that the concentration of counterions is enhanced and that the one of coions is depleted. This phenomenon is known as concentration polarization and is characterized experimentally as a plateau at low concentrations in a conductance versus concentration plot (Figure 1), meaning that in this region the concentration of current carriers is regulated by the surface of the channels and not by bulk concentration, outside this region the conductance increases linearly with the bulk concentration. The fact that in nanosized channels the control of the concentration of ions is regulated by the surfaces and particularly the surface charge distribution is of capital importance for every application in nanofluidics, due to the fact that changing this distribution allows regulating the concentration of carriers and ultimately the transport of such species within the channels.

A simplified model for explaining the conductance ( $G$ ) of a nanochannel was presented by Schoch and Renaud by considering both the bulk conductance and the excess counterion conductance that comes from the electroneutrality condition and the shielding of surface charges<sup>[21]</sup>

$$G = (\lambda_{\text{K}^+} + \lambda_{\text{Cl}^-}) c N_A e \frac{wh}{d} + 2\lambda_{\text{K}^+} \sigma_s \frac{w}{d} \quad (0)$$

where  $w$ ,  $h$ , and  $d$  are the width, the height, and the length of the rectangular nanoslit, respectively.  $\lambda$  is the ion mobility and  $\sigma_s$  is the surface charge density of the channel walls. Here, the first term is the bulk conductance while the second one is the excess counterion conductance (negative surface charges are considered). It can be readily seen that for high electrolyte concentrations, the first term prevails leading to the typical bulk linear behavior and approximate simplified dependence on the nanoslit dimensions is also presented.

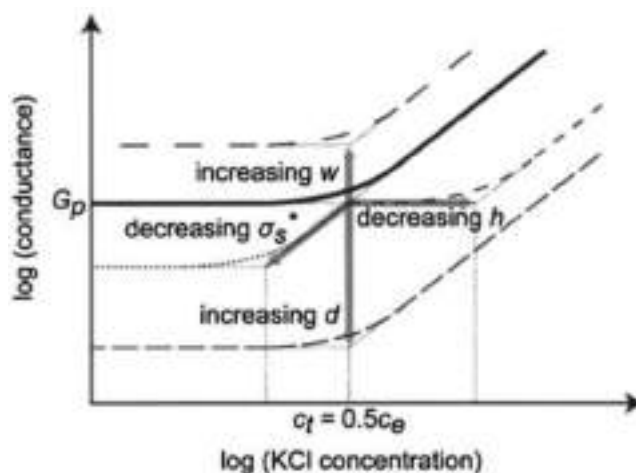


**Figure 1.** Schematic behavior of the conductance in rectangular nanoslits of width  $w$ , length  $d$ , and height  $h$  as a function of the electrolyte concentration. Reproduced with permission.<sup>[21]</sup> Copyright 2005, American Institute of Physics.

As it is known from fundamental courses of thermodynamics, a system at equilibrium in contact with thermal and pressure reservoirs minimizes the Gibbs free energy over the manifold states at the temperature and pressure of the reservoirs. Due to this, the Gibbs free energy is of great use for systems at constant  $T$  and  $p$ , which is the normal case for chemical reactions occurring in nature. The Gibbs fundamental equation can be written as

$$dG = -SdT + Vdp + \sum_i \mu_i dn_i \quad (1)$$

where the Gibbs free energy is defined as the product of an intensive quantity with the differential of an extensive quantity. For the case of  $n$  (number of molecules) the associated intensive quantity is called the chemical potential  $\mu$  of such species, which then is formally defined as

$$\mu_i = \left( \frac{\partial G}{\partial n_i} \right)_{n_j (j \neq i), p, T} \quad (2)$$

that gives a measure of the tendency of a species to change its position in space, to react with other substances, or to transform into another state of aggregation. For example, if the chemical potential of A is higher than that of B, a substance would be transported from A to B, or transform from A into B.<sup>[22]</sup> In equilibrium, the chemical potentials of all species are constant across the system; therefore there are no net flows of molecules or chemical reactions.

The chemical potential itself is separated into different contributions

$$\mu_i = \mu_{i0} + k_B T \ln \left( \frac{c_i(\mathbf{r})}{c^*} \right) + \mu_i^{\text{ex}}(\mathbf{r}) \quad (3)$$

where  $\mu_{i0}$  is the standard chemical potential of the species  $i$  at an ideal state (reference state),  $c_i$  its concentration,  $c^*$  the

standard concentration and  $k_B$  the Boltzmann constant. The last term is the excess chemical potential that is related to the presence of interactions with other particles or force fields such as, for example, an electrostatic field; it is therefore of great importance for nanofluidics as it will be seen in the next section.

## 2.2. Continuous Models

### 2.2.1. Poisson–Boltzmann Equation

The PB equation describes the electrical potential produced by the distribution of ions in space. Thus, different approximations of the PB equation have been applied to study and to model the EDL.

The first step toward the deduction of the PB equation is to obtain the contribution to the energy of the system related to the concentration of ions in solution which is, in turn, provided by the chemical potential of each ion. To consider the effects of electric fields stemming from the charged surfaces over the ions and from the ions themselves, we account for the effect of an external electrostatic field ( $\mu_i^{\text{ex}} = q_i\psi(\mathbf{r})$ ), and therefore Equation (2) can be rewritten as

$$\mu_i^{\text{eq}} = \mu_{i0} + k_B T \ln \left( \frac{c_i(\mathbf{r})}{c^*} \right) + q_i \psi(\mathbf{r}) \quad (4)$$

This expression is sometimes called electrochemical potential. As it was explained before, at equilibrium there is no gradient in the chemical potential ( $\nabla \mu_i^{\text{eq}}$ ), therefore the gradient of diffusional forces (stemming from the first two terms) must be equal to the gradient of the electrostatic forces (last term)

$$\nabla \mu_i = -q_i \nabla \psi(\mathbf{r}) \quad (5)$$

where  $\nabla = \text{grad}$ . If we solve this equation considering the bulk values ( $\psi = 0$ ,  $n_i = n_i^\infty = 1000 N_A c_i$ ), we can obtain the Boltzmann equation that provides the local spatial distribution of each type of ion in the diffusive layer as a function of the electrostatic potential

$$n_i = n_i^\infty \exp \left( - \frac{q_i \nabla \psi(\mathbf{r})}{k_B T} \right) \quad (6)$$

To determine how the distribution of different ions modifies the electric potential, the Poisson equation must be applied

$$\nabla^2 \psi = \frac{d^2 \psi}{dr^2} = - \frac{\rho}{\epsilon_0 \epsilon_r} \quad (7)$$

where  $\rho$  is the volume charge density of the total amount of ions close to the surface and  $\epsilon_0$ ,  $\epsilon_r$  the permittivity of vacuum and the solvent (water). Combining Equations (6) and (7) and considering the volume charge density  $\rho = \sum_i n_i q_i = e \sum_i n_i z_i$ , the Poisson–Boltzmann equation is obtained

$$\nabla^2 \psi = \frac{d^2 \psi}{dr^2} = - \frac{e}{\epsilon_0 \epsilon_r} \sum_i n_i^\infty z_i \exp \left[ \frac{-z_i e \psi(\mathbf{r})}{k_B T} \right] \quad (8)$$

The PB equation can be solved analytically by considering that within the EDL the electric potential is low, i.e., that  $z_i e \psi < 25.7$  mV. In this case the exponential can be expanded using the relation  $e^{-\alpha} = (1 - \alpha)$  and therefore Equation (8) can be approximated by

$$\nabla^2 \psi = \frac{d^2 \psi}{dr^2} = \kappa^2 \psi(\mathbf{r}) \quad (9)$$

where

$$\kappa = \left( \frac{e^2 \sum_i n_i^\infty z_i^2}{\epsilon_0 \epsilon_r k_B T} \right) \quad (10)$$

This equation is known as the Debye–Hückel (DH) approximation and the parameter  $\kappa$  is known as the Debye–Hückel parameter. Within the EDL, the electrical potential decays exponentially and the characteristic length of this decay is known as the Debye length ( $\lambda_d = \kappa^{-1}$ ). This value is normally regarded as a measure of size (or thickness) of the EDL and is widely used in different fields. The value of  $\lambda_d$  depends on the temperature and concentration of the ionic species in solution. **Table 1** shows values of  $\lambda_d$  for different concentrations of KCl.

The solution of the DH approximation is

$$\psi(x) = \psi_s \exp(-\kappa x) \quad (11)$$

where  $\psi_s$  is the electric potential at the surface. The PB equation for highly charged surfaces needs to be solved numerically with the exception of the case of symmetric electrolyte solutions, where the analytical result leads to the Gouy–Chapman equation.

### 2.2.2. Poisson–Nernst–Planck (PNP) Formalism

The Nernst–Planck equation can be seen as an extension of the Fick’s law for diffusion of particles for the case where their motion is also affected by electrostatic forces.

A flux of a certain species  $i$  will occur, either by diffusion or migration, in order to alleviate any difference of  $\mu_i$  as defined in Equation (4)

$$J_i(\mathbf{r}) \propto \nabla \mu_i \quad (12)$$

Taking the constant of proportionality to be  $-cD_i/RT$ , then

$$J_i(\mathbf{r}) = - \left( \frac{c_i D_i}{RT} \right) \nabla \mu_i \quad (13)$$

**Table 1.** Debye length  $\lambda_d$  for different KCl concentrations in water ( $\epsilon_r = 78$ ) at a temperature of 300 K.

C [mol L <sup>-1</sup> ]	$\lambda_d$ [nm]
0.001	9.62
0.01	3.04
0.1	0.96
1	0.30

where  $c_i$  is the concentration of the species and  $D_i$  its diffusion constant; here the minus sign indicates that the direction of the flow is opposite to the direction of the increasing chemical potential. Replacing Equation (4) in (13), we obtain the Nernst–Planck equation

$$J_i(\mathbf{r}) = -D_i \nabla c_i(\mathbf{r}) - \frac{z_i F}{RT} D_i c_i \nabla \psi(\mathbf{r}) \quad (14)$$

where  $z_i$  and  $F$  are the charge of species  $i$  and Faraday's constant, respectively. In this equation, the first term is related to the transport of species by diffusion while the second is for migration under an electric field.

When studying nanofluidic systems, the distribution of charges at the surface of the nanochannels or nanopores has a big influence on the spatial distribution of charged species in the electrolyte. In order to obtain the electric potential distribution of the nanochannel, the NP equations are solved along the Poisson equation (Equation (7)).

Solving of Nernst–Planck equations for the transport of ions along with the Poisson equation for the calculation of the spatial distribution of the electric potential allows obtaining a satisfactory model of the transport of ions across nanofluidic structures. Due to the fact that these equations allow flows as well as mechanical and electric forces to perform work on the system, they can be regarded as an extension of the PB model. Consequently, in absence of flows, the PNP–Navier–Stokes (NS) equations give the PB equation.

### 2.2.3. Navier–Stokes Equation

Finally, in order to consider the effect of mechanical forces acting in the system, the NS equations are used to calculate the velocity of fluids. NS equations can be regarded as a continuous analogous to Newton's second law  $F = ma$ . Due to the fact that fluids are continuous materials, continuous quantities such as densities and force densities must be used. In this regard, forces exerted on surfaces (stresses) and bulk forces (body forces) need to be considered. The Navier–Stokes equation can be written as

$$\rho \left( \frac{\partial \mathbf{u}}{\partial t} + \mathbf{u} \nabla \mathbf{u} \right) = \nabla \cdot \overset{\leftrightarrow}{\sigma} + \mathbf{f} \quad (15)$$

Here, the right side of the equation is the product of the inertial acceleration terms (accounting both a linear and a non-linear contribution) and the density of the fluid, while the left term accounts for the forces exerted to a volume element of the fluid, stresses  $\sigma$ , both tangential and normal and  $\mathbf{f}$  body forces exerted to the bulk of the element volume.

Taking pressure as the normal stress and viscous forces as tangential ones, considering an incompressible fluid with constant viscosity that does not depend on shear stress (Newtonian fluid) moving at a constant velocity, and considering that inertial forces are small compared with viscous forces (which is the case for nanofluidic devices), the NS equations adopt the general form

$$\rho \left( \frac{\partial \mathbf{u}}{\partial t} \right) = -\nabla \mathbf{p} + \eta \nabla^2 \mathbf{u} + \mathbf{f} \quad (16)$$

where  $\mathbf{p}$ ,  $\eta$ , and  $\mathbf{f}$  are the external pressure, the viscosity of the media and the body forces. Here, each term represents each different force acting on a volume element inside the nanofluidic system. The first term contains the forces generated by an internal pressure gradient, the second term stands for a force developed due to the concentration polarization within the nanochannel, while the third term represents the force produced by a streaming potential. The last term accounts for the viscous forces generated by the convective movement of the fluid and is balanced with the rest of the forces. In order to calculate the NS equations the no-slip boundary condition (zero relative fluid–solid velocity) is normally applied although it is known that many systems with low frictions do not satisfy such a condition.

### 2.2.4. Reynolds Number

To account for the influence of viscous and inertial components in the transport of mass through a system, the ratio between both components can be calculated and used as parameter to predict the behavior of fluxes.

$$\frac{\rho U_o L_o}{\eta} = Re \quad (17)$$

where  $\rho$  is the density,  $U_o$  is the velocity scale,  $L_o$  is a typical length scale, and  $\eta$  is the viscosity. This ratio is called the Reynolds number,  $Re$ , a dimensionless number widely used in many engineering applications to predict whether a flux is laminar or turbulent. If the Reynolds number is low (up to 100) the inertial component is less relevant than the viscous one and the flux is laminar. As it can be seen for Equation (17) the Reynolds number depends linearly on the characteristic length scale of the system. For nanofluidic systems, the  $Re$  values are very low and fluxes are always laminar. This is a well-known feature used in microfluidic applications such as separation and controlled mixing.<sup>[23]</sup>

## 2.3. Molecular Models

While for many nanofluidic applications continuous methods are normally sufficient, to understand phenomena below the range of 10 nm (about ten molecular units), where collisions between molecules and special characteristics of the surfaces have a large influence, molecular models are required. Computational limitations cause that only a certain range of geometries can be modelled. These limitations can be partly overcome without losing molecular information, by applying coarse grain simulations or statistical thermodynamic-based continuous models that account for microscopic information (molecular theory). In this section, we will describe some of the currently used molecular methods.

### 2.3.1. Molecular Dynamics (MD)

Molecular dynamics is an  $N$ -body computer simulation technique that is widely used for studying physical phenomena



at the atomic or molecular scale. Typically trajectories of each individual atom are calculated using interatomic potentials to model the forces between each atom in the system.

Molecular dynamics has been extensively used for modeling biological channels. It proves to be a useful tool for understanding experimental results and validating specific models. In recent years it has also been used for studying translocation of macromolecular species both in biological and synthetic channels within the size restrictions given to limit the computational times. Nanofluidic devices based on carbon nanotubes, graphene-like materials or SiN<sub>x</sub> have been studied.<sup>[24]</sup>

Up to date, interesting features of nanofluidics have been solved by MD, one example being the change on the direction of electroosmotic flow in 3.5 nm wide slit channels.<sup>[25]</sup>

In order to surpass the limits imposed by time consuming computations, coarse grained simulations have proven useful. In such simulations, instead of taking each individual atom into account, atoms are grouped following a functional criterion. Currently, new approaches such as the atomic resolution Brownian dynamics (ARBD) allow treating the solvent molecules implicitly while conserving the atomic information of the molecules of interest.<sup>[26]</sup> Other nondeterministic and stochastic approach is offered by Monte Carlo simulations which have been applied to provide information about the behavior of acid–base equilibrium of polyelectrolytes grafted in nanopores.

### 2.3.2. Molecular Theory

The molecular theory is a field-based theory that allows including features of molecular organization and physico-chemical states in the simulations. This theory is based on a description of molecular density distributions coupled with the interactions with different fields. It includes molecular parameters such as the size, shape, charge, chemical and conformational state of each molecular species in the system. A fundamental feature of this approach is that it allows handling both length and temporal scales of nanofluidic systems. It can be proved that this theory reduces into Poisson–Nernst–Planck equations when only electrostatic interactions are considered. Conceptually, this theory consists in writing the free energy of a system in terms of the spatial distribution of each species.<sup>[27]</sup> This theory has been successfully used to study the ionic transport of polyelectrolyte-grafted nanochannels and the influence of confinement over the behavior of the polymers. For such cases, the free energy functional describing the system is written as

$$\begin{aligned} \beta F = & \sum_{i=A,C,w,H^+,OH^-} \int \rho_i(\mathbf{r}) [\ln(\rho_i(\mathbf{r})v_w) - 1 + \mu_i^0] d\mathbf{r} \\ & + \sum_j \sum_\alpha P(j,\alpha) \ln(P(j,\alpha)) + \iint \frac{\beta \chi g(|\mathbf{r}-\mathbf{r}'|)}{2} \langle n_p(\mathbf{r}) \rangle \langle n_p(\mathbf{r}') \rangle d\mathbf{r} d\mathbf{r}' \\ & + \int \left( \langle \rho_Q(\mathbf{r}) \rangle \beta \psi(\mathbf{r}) - \frac{1}{2} \epsilon \beta (\nabla \psi(\mathbf{r}))^2 \right) d\mathbf{r} + \int \langle n_p(\mathbf{r}) \rangle [f(\mathbf{r}) \ln(f(\mathbf{r})) \\ & + (1-f(\mathbf{r})) \ln(1-f(\mathbf{r}))] d\mathbf{r} + \int \langle n_p(\mathbf{r}) \rangle [f(\mathbf{r}) \beta \mu_{A^-}^0 + (1-f(\mathbf{r})) \beta \mu_{HA}^0] d\mathbf{r} \end{aligned} \quad (18)$$

where  $\beta = 1/k_B T$  and  $\epsilon$  is the absolute permittivity. The first term is related to the contribution to the entropy of the translation

water, OH<sup>-</sup>, H<sup>+</sup> and both anions (A<sup>-</sup>) and cations (C<sup>+</sup>); here,  $\mu_i^0$  is the standard chemical potential of each species, while  $\rho_i$  is its position-dependent number density. The second term is the entropic contribution of the polyelectrolyte conformation, where  $P$  is the probability of finding polymer  $j$  in conformation  $\alpha$ . The third term accounts for the hydrophobicity of the chains and is the van der Waals attraction between polymer chains, here,  $\chi$  is the strength of the effective attractive interactions. The fourth term is the total electrostatic energy of the system, where  $\psi$  is the electrostatic potential,  $\epsilon$  the permittivity and  $\rho$  the average charge density at a particular position  $\mathbf{r}$ . The last two terms accounts for the acid–base equilibrium of the polymer.

As it can be observed, even though it is a mean-field approach, there are many molecular considerations in this theory what makes it a highly suitable approach for studying and modelling many nanofluidic applications.

## 3. Fabrication Techniques

Through the years, several techniques to fabricate nanopores in different materials were developed. In this review we focus mainly on strategies for fabricating solid-state single nanopores or nanochannels, we thus omit a comprehensive description of procedures that allow the production of multipore materials, such as sol–gel techniques or the production of anodized aluminum oxide. Synthetic methods for solid-state single pore fabrication have been reviewed extensively and many of them will not be described in detailed here.<sup>[28–32]</sup> Among the different techniques available for the fabrication of single nanopores, ion beam and electron beam techniques are by far the most commonly used ones.

### 3.1. Ion Beam Techniques

The velocity of ions represents a crucial factor that defines the interactions between them and the bombarded material during the ion bombardment process. Elastic collisions with the target atoms take place during bombardment at low kinetic energies (keV), whereas at higher energies ( $\approx$ MeV–GeV) the ions interact with the target electrons. The damage process produced by the ions in the material is very different in each of these cases. Under low kinetic energy conditions, atoms can be directly displaced from their lattice sites. Conversely, at GeV energies, the ions transfer their energy first to the electrons of the solid, thus triggering a cascade of secondary electrons. After a certain time, the energy is transferred into atomic motion, resulting in the modification of the solid structure. The damage produced along the straight ion trajectory is called ion track.<sup>[33]</sup> Both low- and high-energy ions have been used to produce solid-state nanochannels.

#### 3.1.1. Low-Energy Ions

Using focused ion beams (FIB) was one of the first techniques specially developed to fabricate nanopores. FIB ions are

accelerated typically to  $\approx$ keV energies, and applied to sequentially “drill” pores in different materials, such as thin layers of silicon, silicon nitride or silicon carbide. When the accelerated ions impact on the surface, some atoms are removed by a sputtering process that ultimately leads to the formation of a nanopore (Figure 2).<sup>[34]</sup>

An important drawback of this technique is that it is very difficult to obtain nanopores with diameters below 30 nm in a reproducible manner. Nevertheless, several technical improvements have been developed to overcome this limitation, allowing the production of pore diameters of  $\approx$ 5 nm in SiC and 5.5 nm in SiN.<sup>[37,38]</sup>

Further disadvantages are related to the substrates, which should be thin  $\approx$ 50 nm, exhibit certain conductivity, as well as low roughness. The thinner the supportive membrane, the smaller the resulting pore diameter.<sup>[39]</sup>

The FIB technique was significantly improved with the arrival of the scanning helium ion microscope (HIM) (Figure 2b), which allows obtaining a better resolution and precision compared with the typical gallium based FIB devices. Moreover, the HIM has proved to be useful for a large variety of materials including graphene and even gold. The resolution of this technique is better, mainly due to the smaller mass of the gas species (He) used, which allows producing a highly controlled drilling process.<sup>[35]</sup> Diameters down to 4 nm in a one step process have been reported with this technique.<sup>[40]</sup>

An approach complementary to FIB consists of using a low-energy ion beam and sample temperature modulation to partially close the pores instead of open them. This procedure is called ion beam sculpting. Golovschenko’s group proposed that there are two processes competing during the milling of a pore with an ion beam.<sup>[34]</sup> The first one is a sputtering process that removes atoms from the surface leading to the formation or opening of pores and the second is a lateral diffusion process where material moves induced by the ion beam finally leading to a pore area decrease or even closing the pores. By using this last phenomenon a feedback controlled device was designed using the transmitted ion counts as monitor, i.e., the higher the counts, the larger the pore (Figure 2a). With this approach, nanopores down to 1.8 nm have been fabricated. It has been shown that the prevalence of one or the other phenomenon is related to the temperature of the experiment. Thus, diffusional processes can be slowed down at low temperatures. Moreover, there is a minimum initial diameter of the pores up to which the opening process is the prevailing mechanism (Figure 2c,d). Some experiments have shown the feasibility of this procedure for making sensor devices for a number of biomolecules.<sup>[41]</sup>

Recently, this technique was further improved by cooling the sample with liquid nitrogen, therefore reducing the surface diffusion that leads to the typically observed “volcano shape” during the common ion sculpting technique. With this new approach, named cold ion beam sculpting, pores of 6 nm could be made in a reproducibly manner.<sup>[36]</sup>

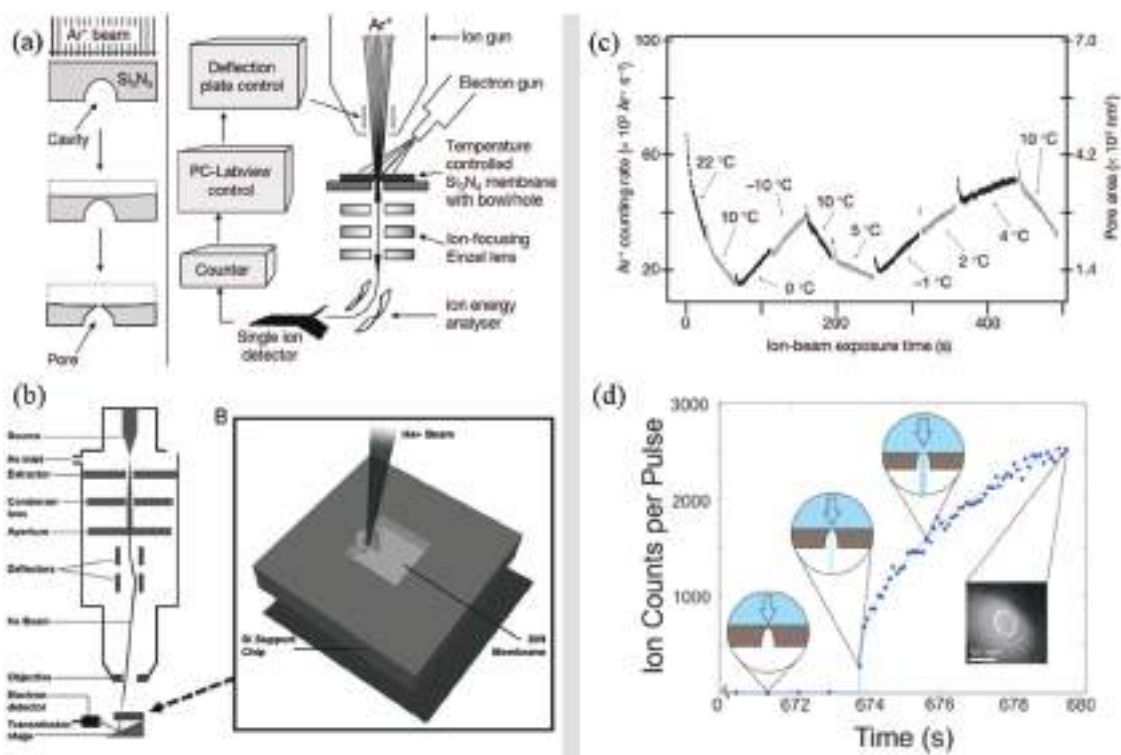


**Figure 2.** Low-energy ions. a) Scheme of the fabrication of nanopores using Ar beam technique. Reproduced with permission.<sup>[34]</sup> Copyright 2001, Springer Nature. b) Scheme of the scanning helium ion microscope. Reproduced with permission.<sup>[35]</sup> Copyright 2012, Wiley Periodicals Inc. c) Temperature dependence of pore area during ion-beam exposure; a low temperature leads to the opening of the pore while a high temperature leads to closing. Reproduced with permission.<sup>[34]</sup> Copyright 2001, Nature. d) Count rate trace of cold ion beam sculpting of a 50 nm diameter nanopore in a SiN membrane. Inset: TEM image of resulting nanopore. Reproduced with permission.<sup>[36]</sup> Copyright 2012, American Institute of Physics.

### 3.1.2. High-Energy Ions

At large accelerator facilities high-energy ion beams (energy  $\approx$  MeV–GeV) can be used to produce highly localized nanometer-sized ion tracks in dielectric materials.<sup>[42–44]</sup> Subsequently, the damage along the ion tracks can be selectively dissolved to form nanopores. The pore size and geometry is controlled by adjusting suitable etching parameters (concentration, temperature, time, etc.). This technique is known as “ion-track etching.” To successfully fabricate nanopores, it is important that the ion track is well defined. This requires that the energy loss ( $dE/dx$ ) of the ions in the material surpasses a material-dependent threshold energy loss, which is for polymers  $\approx 5$  keV nm<sup>-1</sup>.<sup>[33]</sup> Typically, irradiations are done using heavy ions such as <sup>197</sup>Au, <sup>206</sup>Pb, and <sup>238</sup>U, which produce more pronounced and continuous damage. At these high energies, the dominant process for forming the ion tracks is the electronic energy loss. The damage produced by the ion in the solid is straight and radially isotropic around its trajectory producing a cylindrical volume within the solid. In polymers the damage produced by swift heavy ions consist of radicals, unsaturated bonds, amorphization and outgassing of small organic fragments leading to a decrease of the material density along the track.<sup>[45–48]</sup>

The ion range, which is the distance the ions can travel before they stop, is determined by their initial kinetic energy  $E_0$  and the energy loss  $dE/dx$

$$R = \int_0^{E_0} \left( \frac{dE}{dx} \right)^{-1} dE \quad (19)$$

As an example, for Au ions with a specific kinetic energy of 11.4 MeV u<sup>-1</sup> the projected range in polycarbonate (PC) is  $\approx 150$   $\mu$ m. Given this large range, foil stacks (e.g., ten foils 12  $\mu$ m thick, or four foils 30  $\mu$ m thick) can be irradiated.

For sample irradiation, the ion beam is typically defocused in such a way, that an area of 5 cm  $\times$  5 cm is homogeneously illuminated. Since each ion creates one individual track, the number of tracks per square centimeter can easily be adjusted via the beam flux (ions s<sup>-1</sup>) and irradiation time. The ions in the beam are randomly distributed. At fluence above approximately 10<sup>10</sup> ions cm<sup>-2</sup>, track overlapping becomes an issue. To produce a regular track pattern requires a so-called heavy ion microprobe that shoots individual ions at a kHz rate to predefined position with an accuracy of around 1  $\mu$ m.<sup>[49]</sup>

The fabrication of membranes with one single track,<sup>[41]</sup> involves the use of a mask with a small circular aperture (diameter  $\approx 200$   $\mu$ m). During the fabrication process the mask is placed in front of a stack of foils (Figure 3c) and the ion beam characteristics are adjusted in order to promote the passage of single projectiles through the aperture with a frequency of about 1 Hz. After passing through the foil stack, the bombarded ion is detected by a particle detector placed behind the sample. Immediately after the detector has registered the single ion impact, the ion beam is deflected by an electrostatic chopper system.

In order to convert ion tracks into nanopores, the damage produced along the ion track needs to be selectively removed by a wet chemistry etching procedure. The etchant depends on the nature of the irradiated material (Figure 3). For polymers (poly(ethylene terephthalate) (PET), PC, polyimide (PI)), which are the most widely used materials for nanofluidic applications, the etching procedure is usually an alkaline hydrolysis.

Selective chemical track etching is described by two processes occurring at different rates: the hydrolysis of the undamaged polymer matrix, denoted as bulk etching is competing with the dissolution of the damaged material created along the ion track, known as track etching. Each process is characterized by a specific rate, namely bulk etching rate ( $v_b$ ) and track etching

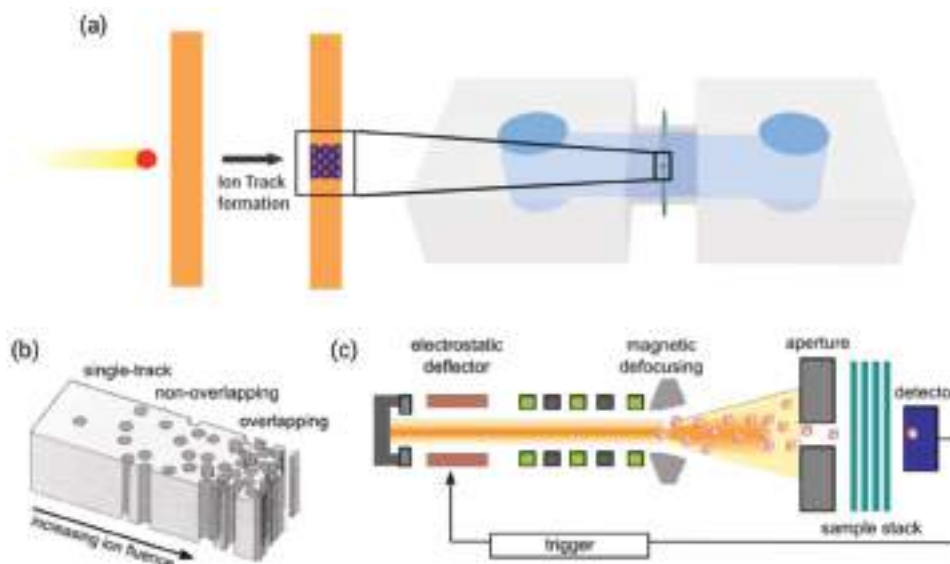


**Figure 3.** High-energy ions. a) Scheme showing the procedures of the ion-track-etching technique and b) different fluence regimes from single tracks to heavily overlapping tracks. c) The ion irradiation setup used for single ion irradiations at the GSI Helmholtz zentrum consisting of the linear ion accelerator with magnetic defocusing, the aperture in front of the sample stack and the detector behind. b, c) Reproduced under the terms of the CC-BY 2.0 Creative Commons Attribution License (<http://creativecommons.org/licenses/by/2.0>).<sup>[50]</sup> Copyright 2012, Beilstein-Institut.



rate ( $v_t$ ). The ratio of these factors ( $v_t/v_b$ ) determines the geometry of the pore. For high ratios, the resulting channel geometry is cylindrical while for low ratios the geometry is conical (or double conical). In addition, the geometry of the channel can be adjusted by applying symmetric or asymmetric conditions on each sides of the irradiated polymer foil, as well as by varying the composition, concentration, and temperature of the etching solution. The channel size increases proportionally to the etching time. Variation of the etching procedure allows the fabrication of nanopores with a large variety of shape and size. For different application the flexibility of this technique is extremely helpful.<sup>[51–53]</sup> Other approaches use coupled electrical fields (polarization-assisted etching) and/or surfactants to further influence the shape of the etched nanopores.

### 3.2. Electron Beam Techniques

Focused electron beams can be also used to produce nanopores. In this case, an intense electron beam produced by transmission electron microscope can be used to “drill” the pores directly (Figure 4a). By using this technology, pores with diameters of  $\approx 5$  nm can be obtained.<sup>[54–58]</sup> There is correlation between the velocity of the pore formation and the thickness of the foils which makes that the drilling of pores in thick membranes become prohibitive for time reasons. However this technique has been heavily used for applications requiring two dimensional materials, for example resistive pulse sensing using graphene nanopores or even for the fabrication of nanopore transistors in materials with a bandgap such as molybdenum disulfide.<sup>[59]</sup>

Another similarity with the focused ion beam technique is that the electron beam can be also used to reduce the pores from a larger one. In order to achieve this, the electron beam intensity needs to be lowered so that the main process occurring is the fluidization of the membrane instead of the sputtering of atoms from the surface (Figure 4c). Nanopores as small as 2 nm could be obtain with this sculpting technique. Moreover, it was shown that a size control of 0.5 nm can be reached.<sup>[57]</sup>

Regarding the electron sculpting technique, Storm et al. showed that there is an interesting change of the pore formation dynamics at a diameter of 80 nm for silicon oxide pores. Below this size, the pores shrinks when electron beams of intensities from  $10^5$  to  $10^7$  are applied, but they expand when the diameter is larger than 80 nm.<sup>[54]</sup>

### 3.3. Nanopipettes and Glass Nanopores

There are other approaches to fabricate nanofluidic devices that do not include drilling with ion or electron sources. Among these, two fundamental approaches are the fabrication of nanopipettes and glass nanopores. Due to the small sizes that nanopipettes can reach using current technology, nanopipettes have been used for resistive pulse sensing and also for ionic current rectification.

Pipette based electrodes have been used since decades in analytical chemistry, electrochemistry and life sciences to characterize the transport phenomena in biological cells due to its capacity to determine the local activity of different ions among other things.<sup>[61]</sup> Furthermore, there have been applications

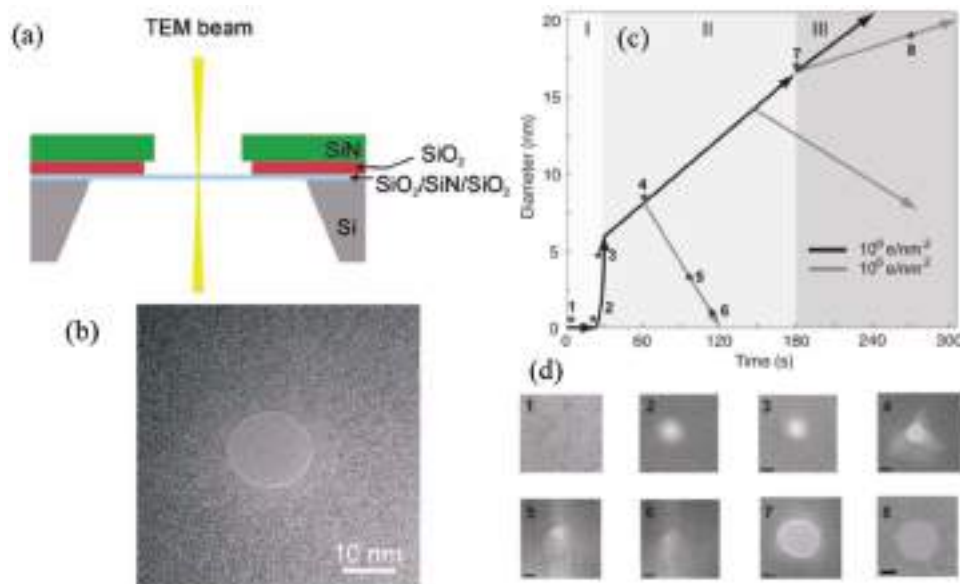


**Figure 4.** Electron beam techniques. a) Scheme showing the construction of a nanopore by using an electron beam. The different materials in the substrate are shown. b) Transmission electron micrograph of a nanopore fabricated by electron beam drilling. a,b) Reproduced with permission.<sup>[60]</sup> Copyright 2006, American Chemical Society. c) Diagram showing different steps of the fabrication of silicon nitride nanopore by electron beam technique. It shows average nanopore diameters versus irradiation time. Three regions are shown, I, initial pore formation followed by a rapid growth; II, expansion or contraction (e-beam intensity dependent); III, further expansion, at this point it is very difficult to contract the nanopore. d) TEM images of the nanopores created at different steps indicated in (c). Scale bars correspond to 5 nm. c,d) Reproduced with permission.<sup>[57]</sup> Copyright 2006, Wiley-VCH.

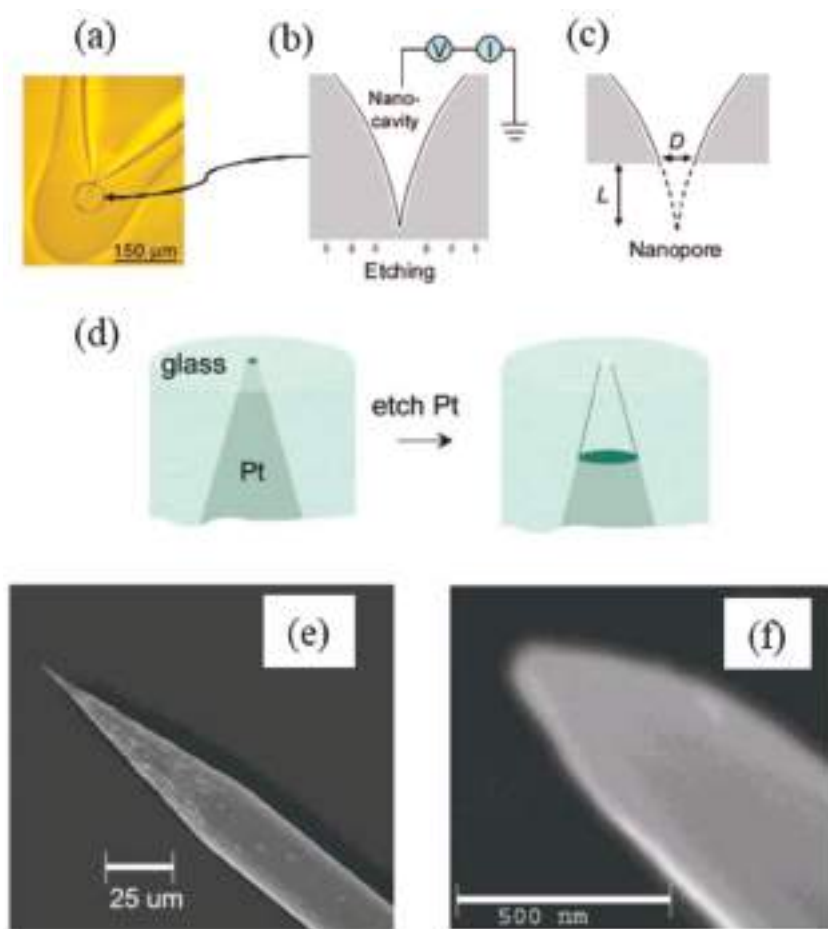


**Figure 5.** Nanopipettes and glass nanopores. a) Nanopipette fabrication from a sealed glass ball. b) External etching from bottom-up with external monitoring. c) Perforation on nanocavity terminal and nanopore formation. a–c) Reproduced with permission.<sup>[67]</sup> Copyright 2009, American Chemical Society. d) Scheme of the fabrication of nanopore electrodes. e, f) SEM images of a sharpened Pt electrode. d–f) Reproduced with permission.<sup>[68]</sup> Copyright 2004, American Chemical Society.

that use nanopipettes as probes for scanning probe microscopy. This is the case of scanning ion conductance microscopy (SICM).<sup>[62,63]</sup>

The fabrication procedure includes first using a pulling device that transform a commercial glass capillary into a micropipette by melting the tip with a microforge (laser) forming two micropipettes at a time with tip diameters that can reach sizes <10 nm.<sup>[64,65]</sup> Even though most conventional glasses can be used, quartz glass (fused silica) is often preferred due to the fact that quartz has advantageous properties such as high rigidity, low noise and does not contain any of the typical metals found in normal glasses. Furthermore, different capillary types and sizes can be used for different applications.<sup>[66]</sup>

Nowadays there have been advances in the design of nanopipettes aiming to reduce its size or to enhance certain features. One strategy aimed to achieve the first goal described by Gao et al. is the closing and etching of a micropipette. In this technique the tip is melted using a microforge and then selectively etched using a feedback controlled device that controls the current between the interior and exterior of the pipettes

(Figure 5). The advantages of this process is the enhanced control over the diameter of the pores, which can be predicted from the calculation of the conductance of the pipettes which were recorded to be <1 nS.<sup>[67]</sup>

A long time pursue in electrochemical sciences was the development of ultra-microelectrodes (UME), defined as electrodes whose critical dimension is smaller as the diffusion characteristic length. The underlying idea is that by reducing the radial dimension to a value under the diffusion of the system, significant steady state currents can be obtained even for very fast scan rates allowing then to study fast electrochemical conversions as well as reactions occurring in nonaqueous conditions (organic solvents). Bringing the dimension of these electrodes to even lower values (sub-micrometers) saw a rapid increase during the 1980s. More recently, in the 2000s, White and co-workers pioneered a relatively straight forward way to fabricate glass capillary supported sub-micrometer Pt electrodes called glass nanopores ever since.<sup>[68]</sup> Another feature of such electrodes is that the Pt electrode is embedded in a conically shaped femto-liter chamber with a nanometer aperture (Figure 5d). It has been shown that for ratios between the depth of the pore ( $d$ ) and the length of the opening ( $a$ ),  $d/a > 50$  the current falls into a limiting state where the current is independent of the depth of the pore and the steady state current depends on the aperture size and concentration of species in the bulk, making it therefore a very appealing system for analytic electrochemical studies of fast kinetic species. On top of that the glass surrounding the electrodes can be modified to control or

modify the access of different species to the electrodes. The procedure of fabrication of glass nanopores is as follows: 1) a metallic wire (Pt) is electrochemically etched to produce a sharp tapered tip. 2) The metallic tip is sealed into a glass capillary. 3) The glass is polished to until the wire is exposed (nanodisk). 4, optional) The glass tip is chemically modified. 5) The metal is etched to a specific value to obtain the glass nanopore.<sup>[69–71]</sup> With this method, nanopores with openings of less than 100 nm were produced. These nanopores present the advantage of having the sensing part (the Pt wire) inside the nanopore and this allows to finely studying the transport of molecules in nanoconfined structures.<sup>[68]</sup> Even though this approach offers many possible advantages for analytical purposes, the low currents recorded by the system (pA) make them more difficult to use as other commercially available UMEs due to the low signal to noise ratio (SNR) and most labs tend to choose other fabrication approaches to develop analytic nanofluidic devices.

In summary, each fabrication technique has its advantages and disadvantages including simplicity in the operation, affordability, type of material, which should be considered before a

**Table 2.** Comparison of the advantages and disadvantages of each fabrication method.

Fabrication technique	Minimum radius <sup>a)</sup> [nm]	Advantages	Disadvantages	Refs.
Focused ion beam	2–6 (HIM)	Small openings with good reproducibility	Nonscalable Limited geometries Time consuming Only thin samples Expensive	[34,37,38,72]
Ion track etching	3–10	Scalable Different geometries can be achieved Samples up to 100 $\mu\text{m}$ can be used Compatible with any dielectric material Easy to modify (postfunctionalization)	Noncommercially available equipment Difficult to control small apertures	[42–48,51–53]
Electron beam	2–5 (TEM)	Easy control of the aperture dimensions at small values	Nonscalable Limited geometries Limited range of fabrication materials Only samples of <200 nm thickness Expensive	[54–58]
Nanopipettes	10	Easy to fabricate Reproducible apertures Easy to modify (postfunctionalization) Cheap	Nonscalable Limited range of fabrication materials Limited geometries	[61,64–67,73]
Glass nanopores	10	Scalable Easy to modify (postfunctionalization) Easy to fabricate Cheap	Low signal to noise Limited geometries Limited range of fabrication materials	[68–71]

<sup>a)</sup>Except otherwise noted these values were calculated from conductivity measurements. TEM: transmission electron microscopy. HIM: helium ion microscopy.

decision is made. For example, silicon nitride and silicon oxide are typical materials used in FIB fabrication where polymers are the chosen materials for ion track fabrication. In general terms, the available minimum pore size, as well as the scalability of the fabrication process, depends on the chosen technique, as summarized in **Table 2**.

## 4. Functionalization of Solid-State Nanopores

The enormous potential of nanochannel research to mimic the nanofluidic transport in biological systems as well as to develop efficient biological and chemical sensors is based on the enormous variety of surface functionalization strategies that can be applied to modify the nanochannel walls. This variety allows scientist to develop their creativity and to integrate adaptive/reconfigurable/responsive units into the nanochannels, resulting in different gating mechanisms controlled by excluded volume effects, charge distributions or specific recognition functions. The different functionalization approaches can be applied individually or in combination, enlarging even more the possible nanochannel designs, and their nanofluidic operational functions. Here we describe the solid-state nanochannel functionalization techniques that have been reported up to now in literature.

### 4.1. Physical Vapor Deposition

Ion sputtering is a method of depositing thin films that involves the bombardment of a solid target with energetic ions ( $\text{Ar}^+$ ).

The momentum transfer from the bombarded energetic ions to the atoms on the solid target causes the ejection of surface atoms that are then deposited onto a given substrate to form a thin film. This deposition technique is compatible with different materials and has proved very useful in facilitating the modification of nanopores with homogeneous layers exhibiting good adhesion properties.<sup>[74]</sup> The versatility of this technique has been demonstrated by Jiang and co-workers through the fabrication of single asymmetric nanochannels with controllable ionic rectification by asymmetric modification with ion sputtering.<sup>[75]</sup> In this example, each side of the nanochannel was independently sputtered to control the pore size.

Nanopores have also been modified by electron beam evaporation. In this physical deposition technique the target material is bombarded with an electron beam generated from a charged tungsten filament. This process leads to the evaporation of the target material that is then deposited onto the working substrate to form a homogeneous thin film. Electron beam evaporation enables the direct transfer of energy from the electron beam to the target material, thus rendering this technique very effective to deposit metals with high melting points. In addition, by focusing the energy on the target rather than on the entire vacuum chamber, this technique also helps minimize or prevent any possible damage to the substrate due to thermal effects. The main advantages of this method are fast deposition, good adhesion properties, and broad compatibility with substrate materials. Based on this deposition method, Kalmán et al. successfully prepared a nanofluidic transistor through subsequent e-beam deposition of gold and silicon dioxide layers on the small opening of asymmetric nanopores.<sup>[76]</sup>

#### 4.2. Chemical Vapor Deposition (CVD), Asymmetrical Functionalization

CVD is a versatile deposition method based on the deposition of gaseous reactants onto a substrate. In this regard, Asatekin and Gleason reported an interesting CVD strategy to modify nanoporous membranes.<sup>[77]</sup> The proposed method directly translates free radical polymerization into a CVD process. The strategy relies on placing the substrate on a chilled stage in the CVD reactor. Then, monomers and a thermally labile initiator are fed into the reactor where heated filaments trigger the decomposition of the initiator leading to the formation of free radicals in the vapor phase. Concomitantly, monomers and free radicals adsorb on the substrate, and the polymerization is initiated on the surface. This method has demonstrated great versatility to modify polymer nanopore membranes with nominal pore sizes, as low as 5 nm in which pore size and surface chemistry of these membranes have been tuned at will. As an example, these authors showed that two consecutive layers can be deposited on the nanopore. First a highly crosslinked layer of poly(divinylbenzene) (pDVB) was deposited for narrowing the pores and then a layer of poly(1H,1H,2H,2H perfluorodecyl acrylate) (pPFDA) was deposited to confer hydrophobic characteristics to the nanoporous membranes. The proposed CVD process is reasonably straightforward, although some specialist equipment is necessary.

#### 4.3. Electroless Plating

Electroless plating represents a simple, low cost technique enabling the preparation of high quality metallic films at room temperature (RT). This technique is especially suitable for polymeric substrates provided that it is generally implemented under mild conditions and does not require the high-temperature conditions demanded by traditional vapor deposition strategies. The electroless deposition process can be described as an autocatalytic redox reaction in which metal cations in solution are reduced onto a substrate to form a metal layer. In most of cases, this process is accomplished in the presence of surface-immobilized Pd nanoparticles that act as catalysts responsible for initiating the reaction.

Different metals, such as Au, Ni, Ag, or Pt can be used for electroless metallization of polymeric nanochannels. In a typical metallization procedure, the first step is the pretreatment of the nanochannels with the catalyst. Then, the pretreated sample is immersed in the plating solution in which the metal ions react with a reducing agent at the nanochannel surface. This process results in the formation of dense metal layers that ultimately leads to a decrease in the nanochannel diameter. The flexibility of this method to tailor the surface chemistry of polymer nanochannels through metallization processes has been demonstrated by several authors, who have shown that electroless deposition not only provides a good platform for the further nanopore functionalization via thiols self-assembly but also as a strategy to image the shape of the nanopores.<sup>[78–85]</sup>

#### 4.4. Atomic Layer Deposition (ALD)

ALD is a vapor phase technique capable of producing thin films of a variety of materials on different substrates. The technique is based on successive, separated, and self-terminating gas–solid surface reactions of two gaseous reactants. The self-limiting nature of ALD offers precise process control in terms of film thickness and composition. One of the attractive features of ALD is that even confined surfaces with high aspect ratio such as the inner walls of nanochannels can be completely coated with a uniform film. Another attractive feature of ALD is its capability to decrease the diameter of the nanochannels in a very controlled manner without distorting the nanochannel geometry. In the recent past, it has been demonstrated that it is possible to deposit different metal oxides on nanoporous structures by ALD. TiO<sub>2</sub>, SiO<sub>2</sub>, and Al<sub>2</sub>O<sub>3</sub> films were successfully deposited on AAO membranes.<sup>[86,87]</sup> By way of example, Romero et al. coated AAO with SiO<sub>2</sub> up to an aspect ratio of 3000 and performed ionic transport measurements AAO membranes.<sup>[88]</sup> The same materials were also deposited in etched ion-track PC nanomembranes.<sup>[89–95]</sup> In a similar vein, ALD has been employed to modify silicon nitride nanopores with TiO<sub>2</sub>,<sup>[96]</sup> Al<sub>2</sub>O<sub>3</sub>,<sup>[97]</sup> and Al<sub>2</sub>O<sub>3</sub> bilayers.<sup>[98]</sup>

#### 4.5. Plasma-Induced Graft Polymerization

Plasma polymerization offers an interesting approach to functionalize surfaces. Thin polymer coatings can be obtained easily in a one-step process. Plasma polymerized thin films are conformal and can be deposited onto a variety of substrates with good adhesion properties. Despite the fact the density of functional groups in the polymer layer is not very well controlled, one of the attractive features of this technique is its robustness. Jiang and co-workers have shown that this technique can be employed as a valuable tool to create pH-gated single nanopores through asymmetric chemical modification of a symmetric hourglass-shaped channel with a plasma-polymerized poly acrylic acid (PAA) layer.<sup>[99]</sup> The same group explored a similar strategy to create dual-responsive nanochannels through plasma-induced asymmetric modifications inside the single nanochannels.<sup>[100]</sup> To this end, PET symmetric hourglass-shaped nanochannels were modified with a plasma-polymerized PAA layer on one side of the nanomembrane and with a temperature-responsive polymer, poly(*N*-isopropylacrylamide) (PNIPAM), on the other side. This strategy based on asymmetric modification led to the construction of a nanofluidic element displaying pH- and thermoresponsive transport properties.

#### 4.6. Covalent Grafting of Organic Molecules and Biomolecules

Covalent grafting of organic molecules on the nanopore walls is one of the simplest ways in which a specific function can be conferred to the nanochannel. In the case of PET nanopores, the chemical etching procedure generates residual carboxylate groups that are readily available for chemical grafting via

*N*-(3-dimethylaminopropyl)-*N'*-ethylcarbodiimide (EDC) chemistry in the presence of molecular building blocks bearing primary amines.<sup>[101]</sup> This is one of the most traditional techniques for linking ligands covalently to a solid surface through amine coupling via reactive esters. EDC participates in the activation of carboxyl groups to react with primary amines. In many cases the use of EDC is combined with *N*-hydroxysulfosuccinimide (NHS) or sulfo-NHS to increase the reaction efficiency. This straightforward chemical strategy to functionalize nanopores and nanochannels has been successfully implemented by different research groups. By using EDC chemistry, these authors developed some protocols to modify different regions of asymmetric PET nanopores. Primary amines were grafted on the PET surface by reacting ethylene diamine in the presence of EDC. Then, depending on the desired function surface amino groups can be transformed back to carboxyl groups by reaction with succinic anhydride. This strategy enables the symmetrical or asymmetrical functionalization of the nanopore depending on the use of EDC + ethylene diamine or succinic anhydride solutions in both sides of the nanomembrane or only at the tip side, respectively. By this method, they were able to create nanofluidic diodes with enhanced rectification properties<sup>[102]</sup> as well as bipolar ionic transistors.<sup>[103]</sup>

This approach has proved successful in the construction of nanopore-based biosensors through the covalent integration of aminated biotin for further recognition of avidin or streptavidin.<sup>[104]</sup> The modification of the tip of a conical pore with biotin caused the formation of a diode junction under acidic conditions when the nanopore was exposed to streptavidin. The bioconjugation of streptavidin, bearing positive charges, on the pore walls led to the generation of a well-defined ionic signal. The same protocol based on EDC chemistry was employed by Jiang and co-workers to attach DNA motors onto the inner walls of PET nanopores resulting in systems exhibiting pH responsive properties.<sup>[105]</sup>

#### 4.7. Formation of Self-Assembled Monolayers (SAMs) via Thiol or Silane Chemistries

SAMs refer to ordered molecular assemblies that are formed spontaneously by the adsorption of an amphiphilic molecule with a specific affinity of its headgroup to a particular substrate. For example, SAMs consisting of thiol- or disulfide-containing molecules are readily formed on gold surfaces by simple exposure to a dilute solution of the sulfur-containing amphiphiles. Depending on the nature of the terminal group, the one-step self-assembly process can lead to the formation of a monolayer of predefined functional groups on the surface. This method has been commonly used for the functionalization of gold surfaces due to its ease of preparation and the relative stability of the gold–thiolate bond under ambient conditions. By using a thiol assembly strategy, Martin and co-workers anchored DNA strands on polycarbonate nanopores that were previously metallized with a gold layer via electroless deposition.<sup>[106]</sup>

Siwy and co-workers created a “hydrophobic gate” on gold-coated PET nanopores by assembling thiols with different chains lengths at the pore entrance.<sup>[107]</sup> This technique was

also employed to decorate pore walls with nitrilotriacetic (NTA) groups<sup>[108]</sup> or polyethyleneglycol (PEG) chains<sup>[109,110]</sup> in order to create protein-detecting nanopores or prevent the unspecific adsorption of proteins into the nanopores, respectively.

For many years, in the realm of organic thin films, self-assembled monolayers of sulfur-containing molecules have played a prominent role on the production of substrates with tailorable surface properties. However, alkylsilane monolayers on oxide surfaces also possess attractive features for those willing to use molecular films for modifying surfaces. In the case of alkylsilane monolayers, the assembly process involves the formation of covalent bonds between the silane molecules and the substrate that, in turn, results in molecular films with superior stability. Nanopore functionalization via silanization is a straightforward protocol that can be achieved by vapor phase or solution routes.<sup>[111]</sup> Organosilane assembly takes place via hydrolysis of the silane group that proceeds through a condensation reaction with the hydroxyl groups exposed on the substrate surface. In the case of the SiN nanopores, the pretreatment of the substrate with piranha solution favors the formation of surface hydroxyl groups. By using organosilane assembly, Wanunu and Meller were able to functionalize nanopores with amine, epoxy, PEG and carboxyl groups.<sup>[112]</sup> The formation of organosilane SAMs has been also employed to functionalized polymeric nanopores that were previously modified with a ZnO layer deposited by atomic layer deposition.<sup>[95]</sup>

#### 4.8. Layer-By-Layer (LBL) Assembly

In recent years, the modification of solid-state nanopores via polyelectrolyte assembly/adsorption has gained increasing interest.<sup>[113–119]</sup> The LbL assembly of polyelectrolytes represents a very simple and versatile chemical method to create functional thin films with nanoscale precision.<sup>[120–130]</sup> This functionalization method is based on the alternate deposition of polyanions and polycations on solid surfaces leading to the formation of polyelectrolyte multilayers.<sup>[131]</sup> This technique provides access to the straightforward construction of nanoscopic functional multilayer systems and distinguishes itself in its simplicity from other surface modification methods requiring special/sophisticated equipment. Different groups explored the modification of asymmetric solid-state nanopores via LbL assembly observing that the rectifying properties are strongly affected by the assembly conditions and the nature of the polyelectrolytes as well as the nature of the capping layer.<sup>[132,133]</sup> Furthermore, the physicochemical properties of confined assemblies differ from those produced on flat surfaces.<sup>[116]</sup> However, these apparent drawbacks are not determining factors in whether or not one can succeed in the pore functionalization. In fact, the efficiency of surface modifications achieved by the LbL technique is probably higher than those obtained by covalent routes. This surface modification approach has been employed by Jiang and co-workers to create a highly sensitive acetylcholine (ACh)-sensing nanopore based on the LbL assembly of polyethylenimine and sulfonatecalixarene on the pore walls.<sup>[134]</sup>



#### 4.9. Polymer Brushes

Polymer brushes are assemblies of macromolecules that are tethered by one end to a surface. These macromolecular architectures bearing different functional groups<sup>[135–137]</sup> along their backbones can be grafted on different surfaces,<sup>[138–143]</sup> and even in constrained environments.<sup>[144–150]</sup> There are two main strategies for generating polymer brushes on solid surfaces: “grafting to” and “grafting from.” In the “grafting-to” technique, presynthesized polymers are anchored to a surface from solution. In contrast, the “grafting-from” approach involves sequential growth of polymer chains from the surface.<sup>[151]</sup> Different research groups have demonstrated that polymer brushes offer a versatile chemical approach to molecularly design solid-state nanopores by using homo- or copolymer brushes equipped with predefined functionalities in their monomer units. If we consider that the degree of rectification strongly relies on surface charge density; then, one of the most appealing aspects of modifying nanopores with polymer brushes is the possibility to sensitively increase the number of fixed charges on the nanopore walls by simply increasing the degree of polymerization of the grafted chains. This notion was initially put into practice by Yameen et al. to create highly rectifying nanopores decorated with phosphate-bearing polymer brushes,<sup>[152]</sup> thermoactuated nanopores through the modification with thermoresponsive poly(*N*-isopropylacrylamide) brushes<sup>[153]</sup> and zwitterionic nanofluidic devices displaying pH-reversible rectifying characteristics.<sup>[154]</sup> Since then, different groups explored the use of polymer brushes as a chemical strategy to functionalize solid-state nanopores for different purposes, including the construction of multiresponsive nanofluidic architectures.<sup>[110,155–162]</sup>

### 5. Rational Integration of (Bio)Molecular Architectures into Nanopores and Nanochannels—Gating, Switching, and Sensing through Integrated Molecular Systems

#### 5.1. DNA Oligonucleotides as Versatile Mechanical Transducers

Recent advances in DNA bio-nanotechnology provide new insights to incorporate integrated molecular systems within nanofluidic solid-state channels looking for specific responsiveness, high efficiency and selectivity. In this context, the rational design of oligonucleotide-based molecular architectures has paved the way to the generation of nanostructures exhibiting adaptable conformational as well as exceptional molecular recognition properties.

Early in 2004, Harrell et al. demonstrated the use of DNA oligomers decorating solid-state nanochannels as electromechanical gates.<sup>[163]</sup> Since then, several investigations have employed DNA oligomers to induce or modulate gating behaviors based on a variety of mechanisms.<sup>[164,165]</sup>

Harrell and co-workers proposed that rectification in DNA-grafted nanochannels entails electrophoretic insertion of the DNA chains into (OFF state) and out of (ON state) the pore depending on the polarization of the transmembrane potential, yielding a marked diode-like behavior.

A close related example was presented some years later by incorporating the pH responsiveness of DNA oligomers to create a pH- and voltage-gated nanochannel.<sup>[166]</sup> In that case, DNA oligomers containing protonable A and C bases were densely attached at the tip side of conical nanochannels (diameter <14 nm). Under neutral pH conditions voltage switching promotes the (in/out) nanomechanical movement of the DNA strands (“ON” state). Then, under acidic pH conditions (<5.5), positively charged DNA strands bind to other strands bearing negative charges in their backbones, thus leading to the formation of an electrostatic mesh that, in turn, produces the closure of the pore (OFF state).

##### 5.1.1. DNA Complex Structures as Mechanical Transducers

In 2008, Xia et al. presented a pH-responsive solid-state nanochannel employing the mechanochemical transformations of DNA oligomers caused by protonation–deprotonation equilibria.<sup>[105]</sup> This concept was based on the integration of *i*-motifs, constituted of four-stranded DNA structures formed from sequences containing stretches of cytosine (C), into the nanochannels.<sup>[167]</sup> At mild acidic pH, a protonated cytosine forms a base pair with an unprotonated C, and these base pairs interdigitate to form a quadruple helix. At high pH values, the cytosine deprotonates and an extended duplex structure is formed. Thus, switching of folded and extended conformations can be achieved by altering the solution pH.

Bound to the surface of a conical etched PET nanochannel by EDC/NHSS crosslinking, the ssDNA oligomers allowed transforming the pH-induced conformation changes into changes in the transmembrane ionic current behavior. At low pH, the DNA motor transforms into the quadruplex *i*-motif structure decreasing the effective diameter of the nanopore, whereas at high pH, the DNA structure relaxes to a loosely packed single-stranded and more negatively charged structure enhancing the ionic conductivity.

Other specific DNA secondary structures are G-quadruplexes (G4), which refer to highly ordered DNA structures derived from G-rich sequences formed by tetrads of hydrogen-bonded guanine bases. Particularly, the G-rich human telomere strand d[AGGG(TTAGGG)3] has been employed for the construction of K<sup>+</sup>-gated nanofluidic channels (**Figure 6**),<sup>[168]</sup> owing to the formation of G-quadruplexes dependent on the alkali metal ion concentration, as revealed by circular dichroism. The enhanced stability of the G4 structures by increasing the potassium concentration gradually diminishes the effective pore size in the range  $0 \times 10^{-6}$  to  $750 \times 10^{-6}$  m.

Also based on a DNA quadruplex, Liu et al. presented a pH and K<sup>+</sup> double gated cigar-like nanochannel. In this setting, two separate gates can be actuated—alternately or simultaneously—in the presence of a specific stimuli combination.<sup>[169]</sup> For this nanodevice, C4 and G4 DNA molecules were covalently immobilized (EDC/NHS) onto the top and bottom tip side of cigar-like single pore track-etched PET membranes. C4 DNAs undergo well-defined pH-induced structural changes switching from a four-stranded *i*-motif structure, at pH 4.5, to a random single-stranded structure at pH 7.5. On the other hand, G4 DNAs undergo potassium-induced structural

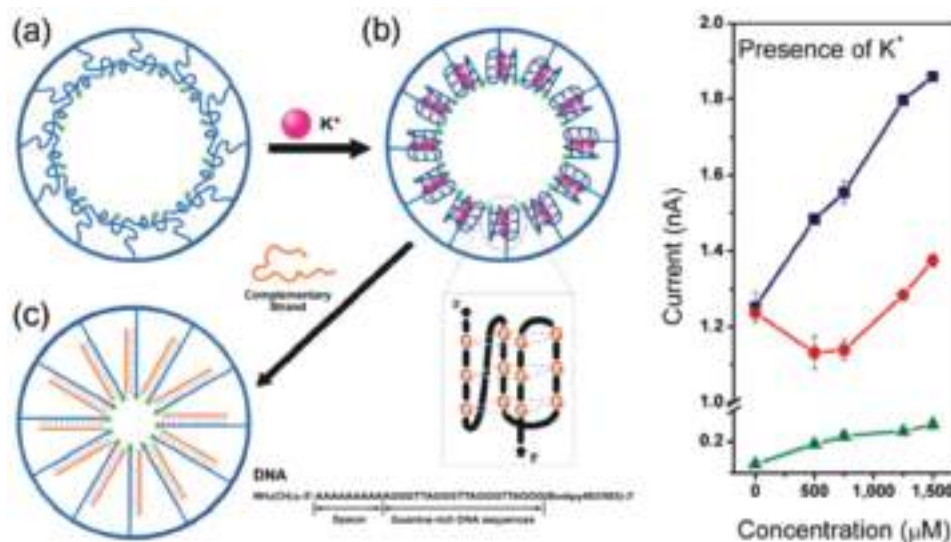


**Figure 6.** DNA complex structures. a) Schematic representation of the G4 DNA-functionalized nanochannels (left): in the absence of  $K^+$  (single stranded); b) in the presence of  $K^+$  (densely packed quadruplex); c) after adding complementary DNA strands (closely packed double-stranded DNA). Iontronic responsiveness (right): transmembrane current for increasing  $K^+$  concentration before DNA modification (squares); after G4 DNA functionalization (circles); and after adding the complementary DNA (triangles). a–c) Reproduced with permission.<sup>[168]</sup> Copyright 2009, American Chemical Society.

transformations switching from a random single-stranded conformation in the absence of  $K^+$  to a four-stranded quadruplex (G4) conformation in the presence of  $K^+$ . Consequently, the addition and/or removal of both chemical effectors ( $K^+$  and  $H^+$ ) results in the reversible ON/OFF switching of the iontronic signal.

Even oscillating pH changes have been employed for the modulation of complex DNA structures. Periodic oscillations between high and low conductivity states were first achieved in a DNA-free bullet-shaped PET single pore nanochannel by coupling to a chemical oscillator.<sup>[170]</sup> After chemical etching, the walls of the nanochannels present carboxylate groups, with a pKa value of 3.8. Thus, pH changes around this value produce significant variation in the surface charge density. The pH of the solution in the tip side of the membrane has stronger effect on the iontronic behavior of the nanochannels, so the chemical oscillator system  $NaBrO_3-Na_2SO_3-K_4Fe(CN)_6-H_2SO_4$  was placed in that compartment. As the chemical oscillator induces pH changes between about 4 and 6.5, appreciable periodic transmembrane conductivity changes were obtained as a consequence of the variation in the surface charge. It has been also shown how the oscillations frequencies can be modulated by varying the solution temperature in a continuous flowing conductivity cell.

Following this principle, an oscillating gating of the nanochannels was further performed by coupling a DNA motor to the nanochannels walls.<sup>[171]</sup> The cigar-like PET nanochannels were modified by covalent crosslinking of a single strand DNA oligomer able to produce a C-quadruplex depending on the pH values. At high pH, the DNA remains single strand and the nanochannels are in the open (ON) state. But the C-quadruplex is form when pH is lower than 5, producing the partial closure of the tip, lowering its conductivity (OFF state). This pH-gated nanochannel was then coupled to an oscillating reaction in bulk, which produces pH oscillations that, in turns, induce opening–closure cycles in the nanochannel. Then, the

transmembrane current oscillates as a result of the pH-driven conformational changes of the DNA oligomers.

### 5.1.2. Sensing through Hybridization Processes

The coupling of simple-structured DNA components to nanochannels has been also employed for oligonucleotide detection as modulator of the transmembrane ionic current using the hybridization as recognition and binding mechanism.

Early in 2005, Vlasiouk et al. used AAO membranes functionalized by covalently linked DNA to detect target DNA oligomers from the decrease of the transmembrane current upon DNA hybridization due to the partial blocking the pores.<sup>[172]</sup> As the sensing mechanism was based on the steric hindrance, it worked in pores of 20 nm diameter but hybridization could not be detected in 200 nm pores.

From that work, several investigations were devoted to the development of more complex responsive nanofluidic systems based on the DNA/RNA hybridization as a highly selective and stable recognition mechanism.

Following a different functionalization approach, Sun et al. developed nanofluidic channels for label-free, ultrasensitive, and highly sequence-specific detection of DNA.<sup>[173]</sup> In this case, the DNA probe oligonucleotides were electrostatically adsorbed on PEI-modified conical track-etched PET nanochannels. Then, immersion in BSA solution was pre-formed to avoid further non-specific adsorption. After that, DNA detection was realized by monitoring the rectification efficiency of the diode-like iontronic behavior upon hybridization. The as-prepared nanochannel presented a near ohmic behavior due to its closely null surface charge. After binding of the complementary negatively charged DNA target, the rectification increases owing to the increment in the net surface charge, yielding a binding-type dependency of the rectification factor on the target concentration.

The detection limit of this nanochannel sensor was  $10 \times 10^{-15}$  M for target DNA and the device was able to discriminate complementary DNA (c-DNA) from noncomplementary DNA and one-base mismatched DNA samples with high specificity, even in serum samples.

**DNA Superstructures:** Beyond double strands hybridization, DNA superstructures have been employed to create more efficient gating mechanisms in nanochannels. Jiang et al. developed an ATP-gated nanofluidic device that exhibits high ON/OFF ratios and a perfect electric seal at its closed state ( $\approx G\Omega$ ) based on DNA supersandwich-functionalized nanoporous AAO membranes.<sup>[174]</sup> Based on the reversibility and all-or-none gating properties, they showed the possibility of performing logic operations with these nanofluidic devices.

Initially, DNA capture probes (CP) were integrated into alumina nanochannels and after exposure to DNA probes P1 and P2 in solution, the hybridization process created long concatamers that efficiently block the passage of ions through the nanochannels (Figure 7a–d). The capture probes and P2 are DNA aptamers of ATP and, consequently, the addition of ATP to the solution leads to the disassembly of the oligonucleotide superstructure and the reopening of the nanochannel. In this particular configuration, the ATP-DNA interactions provide an efficient gating mechanism with ON/OFF ratios close to

$10^5$ – $10^6$ . The gating performance of this nanochannel device is remarkably high and can be attributed to the enhanced steric hindrance of the long, flexible DNA concatamers.

Based on the same mechanism, these authors achieved the sub-nanomolar and sub-micromolar sequence-specific DNA detection.<sup>[175]</sup> This sensing scheme was further improved by resorting to more complex DNA nanostructures displaying multiple binding sites. In this case, track-etched PET nanochannel membranes were modified with predesigned capture DNA probes. In the presence of target DNA, alternating units of signal probes (S1 and S2) are successively hybridized giving rise to long concatamers (Figure 7e–g).

The formation of these DNA superstructures inside the nanochannels efficiently blocks ionic transport across the membrane, thus leading to a decrease in the transmembrane ionic current or iontronic signal. If an aptamer sequence, specific to a small molecule, is introduced in the DNA probe; then, the presence of such target molecule triggers the disassembly of the preformed supersandwich structures. By using this strategy, the authors were able to detect oligonucleotides and ATP with detection limits of  $10 \times 10^{-15}$  M and  $1 \times 10^{-9}$  M, respectively.

Gou et al. also adopted a hierarchical assembly strategy to build up DNA structures into cylindrical nanochannel arrays in track-etched PET membranes.<sup>[176]</sup> The produced 3D crosslinked DNA superstructures switched the ionic transmembrane

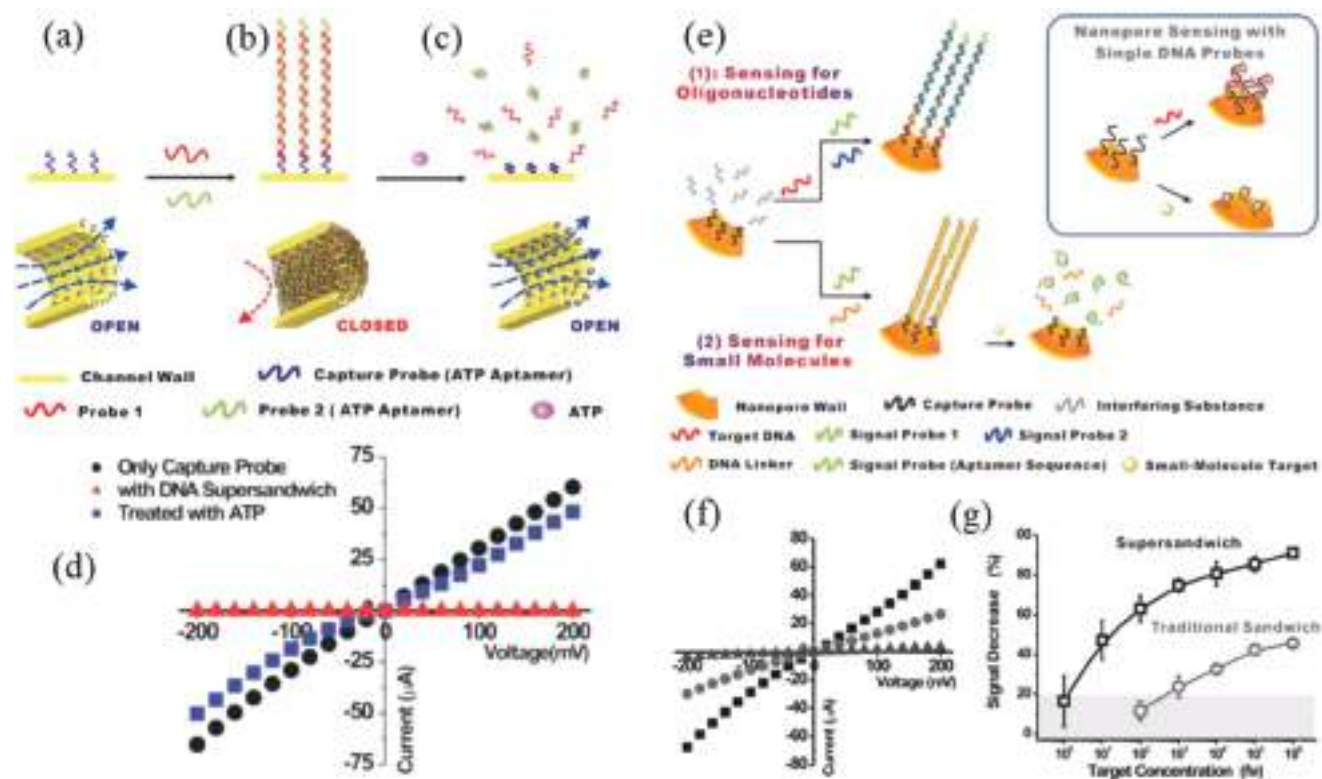


**Figure 7.** DNA superstructures. Schematic representation of the DNA supersandwich functionalization steps of the alumina nanochannels: a) DNA capture probes anchoring; b) concatamers formation; and c) ATP-driven disassembling. d) The OPEN/CLOSED states are verified by the  $I$ - $V$  response after each functionalization step. a–d) Reproduced with permission.<sup>[174]</sup> Copyright 2012, American Chemical Society. e) Comparison of the single-target strand conventional approach and supersandwich-amplified approach for DNA nanochannels functionalization. f)  $I$ - $V$  iontronic response for DNA detection: before (squares) and after adding  $10 \times 10^{-15}$  M (circles) and  $1 \times 10^{-9}$  M (triangles) DNA target. g) Dose–response of the traditional and supersandwich-functionalized nanochannels. e–g) Reproduced with permission.<sup>[175]</sup> Copyright 2013, Wiley-VCH.



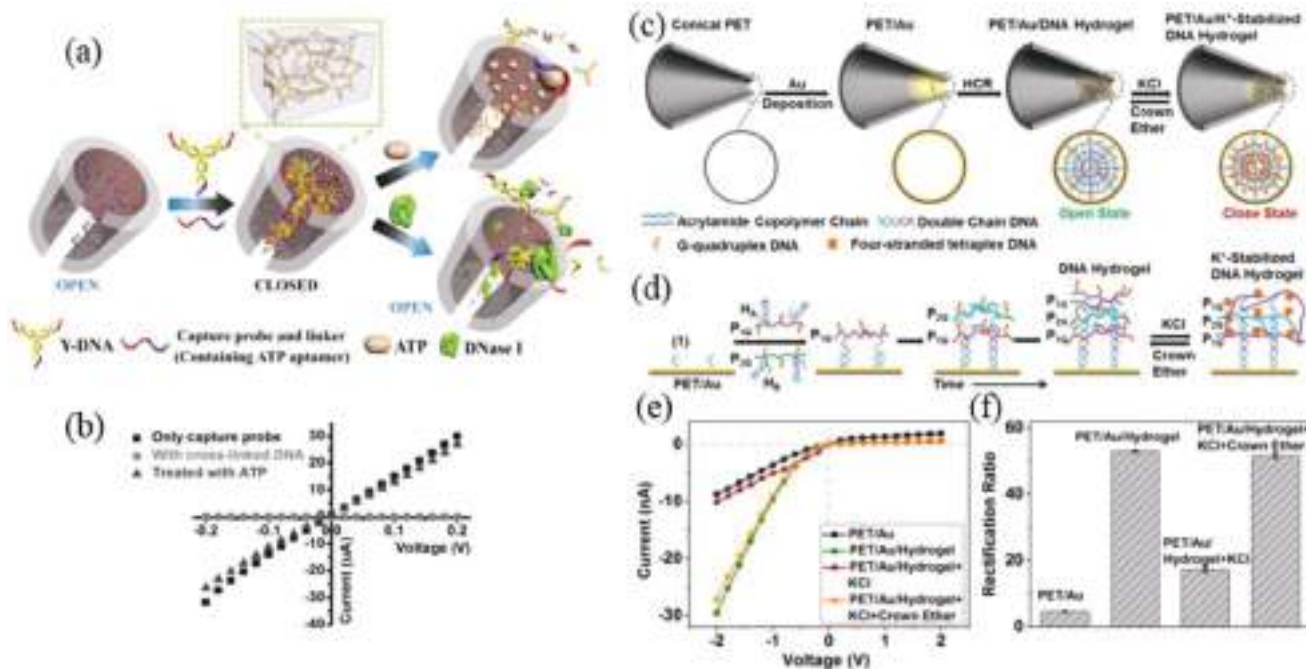


**Figure 8.** Hybridization-based detection. a) Sequence of modification of the solid-state nanopores with crosslinked DNA superstructures: firstly, ss-DNA are crosslinked to the nanopore walls; then, the Y-DNA are self-assembled in the presence of the linker; and finally, disassembly is produced by ATP or DNAase I. b) Iontronic response: efficient gating mechanism by assembly of DNA superstructures and ATP disassembly with ON/OFF ratio  $\approx 2000$ . a,b) Reproduced with permission.<sup>[176]</sup> Copyright 2015, Wiley-VCH. c) Schematic illustration of the functionalization steps: Au sputtering, DNA hydrogels assembly by HCR, and association of the G4 DNA units in the presence of  $K^+$ . d) Scheme of the integrated molecular system. e)  $I$ - $V$  iontronic response and f) rectification ratio after each modification step measured in  $0.1\text{ M LiCl } 10 \times 10^{-3}\text{ M Tris}$  buffer pH 7. c-f) Reproduced with permission.<sup>[177]</sup> Copyright 2018, Wiley-VCH.

current with high ON/OFF ratios of  $10^3$ – $10^5$ . Owing to the size of the DNA superstructures, this particular gating mechanism was applicable in a wide range of nanochannels with opening diameters up to 650 nm.

The assembly strategy is depicted in **Figure 8a**, and it involves the use of 3-point-star motif (Y-DNA) that is synthesized from three single-stranded DNAs (ssDNA) (Y1, Y2, and Y3). The exposure of nanochannels modified with single-stranded capture probes to a solution containing Y-DNAs and linker sequences (35 mer) results in the formation 3D Y-DNA superstructures clogging the nanochannel (OFF state).

Furthermore, the linker and CP contained an aptamer for ATP in their sequence, providing a disassembly mechanism. In the presence ATP, both the linker and CP bind ATP with higher affinities, dissolving the DNA superstructure and reopening the nanochannels as revealed by the increment in the transmembrane ionic current (ON state).

**Hybridization Chain Reaction (HCR):** The HCR constitutes a clever self-assembly process triggered by an initiator as it happens in chemical chain reactions. HCR can be concisely described as follows: when a single-stranded DNA initiator is added to a stable mixture of two hairpin DNA oligonucleotides (H1 and H2), it opens a hairpin of one species (H1), exposing a new single-stranded region that promotes the opening of the other hairpin (H2), having a complementary sequence and exposing a newly free segment, which is identical to the original initiator. The resulting chain reaction leads to the formation of

a double helix that grows until one of the components (H1 or H2) is exhausted.<sup>[178]</sup>

In 2017, Zhao et al. developed a signal amplification strategy based on the HCR in a label-free nanochannel biosensor for detection of DNA targets in a porous AAO membrane.<sup>[179]</sup> For this purpose, cylindrical AAO nanochannels were successively functionalized with APTES, sulfo-SMCC and 5'-thiol DNA CP. Then, the membranes were incubated in the target mRNA solution. The designed DNA CP was used to capture target DNA via complementary hybridization. Finally, the membrane was incubated in the solution containing the H1 and H2 DNA hairpin probes. The DNA target triggered the HCR to form large DNA superstructure causing the blockage on the nanochannel and the consequent decrease in the transmembrane ionic current. The developed nanochannel sensor achieved a sensitivity of  $30 \times 10^{-15}\text{ M}$  with a wide linear dynamic range from  $0.1 \times 10^{-12}$  to  $10 \times 10^{-12}\text{ M}$ , and good performance also in real samples.

More recently, DNA hydrogels were assembled onto the tip side of the conical nanochannel through HCR for high ionic current and rectification behaviors.<sup>[177]</sup> For that, the H1 and H2 DNA hairpin probes containing G-rich regions, able to produce G-quadruplex, were firstly incorporated to polyacrylamide copolymers, yielding hairpin-grafted polymers P1G and P2G. The Au-coated tip side is modified with thiolated nucleic acid (1), the initiator of the HCR and then immersed in a solution containing both polymers P1G and P2G. Thus, the surface-bound initiator triggers the HCR and a DNA hydrogel is obtained (Figure 8c–f). In the presence of  $K^+$  ions,

the G-quadruplex in the P1G and P2G residues is stabilized yielding a more rigid state of the hydrogels. On the other hand, by soaking in 18-crown-6-ether solutions, the  $K^+$  are released, leading to the dissociation of the G-quadruplex and softening the DNA hydrogel structure. So, the reversible switching between the stiff  $K^+$ -stabilized and soft  $K^+$ -free states, provides a gating mechanism of the nanochannel with excellent cyclability.

The hydrophilic network of DNA hydrogels bearing negative charges favors the enhancement of the ion current and the rectification factor. However, the presence of potassium ions partially neutralizes the negative charges of the DNA tethers, decreases the hydrophilicity, increases the stiffness of the superstructure and, consequently, leads to a decrease in the rectification ratio.

The same modification with DNA hydrogels was also performed in both tip sides of cigar-shaped nanochannels, yielding a nanofluidic system with to four possible states: i) open/open; ii) close/close; iii) close/open; iv) open/close. The closed state is achieved by previous incubation of the corresponding side in a  $K^+$  rich solution. Just in the case of asymmetric configurations (open/close or close/open), diode-like behaviors were obtained.

*Peptide Nucleic Acids (PNAs) and Phosphorodiamidate Morpholino Oligomers (PMOs):* Hybridization driven by pair base specific interaction is not restricted to the use of DNA or RNA single strands. Some other artificial synthetic templates without the natural phosphate-ribose structure but still keeping the recognition of complementary DNA sequences has been developed. A clear example is the PNA, whose backbone is composed of repeating *N*-(2-aminoethyl)-glycine units connected by peptide bonds. Having no charged phosphate groups in the backbone, the binding between PNA and DNA complementary strands is even stronger than between DNA/DNA strands due to the lack of phosphate-phosphate electrostatic repulsion. PNA oligomers have been also employed as DNA recognition elements in nanofluidic systems. By modifying the walls of gold-decorated nanochannels in track-etched PC membranes with PNA oligomers, Gyurcsanyi and co-workers achieved the label-free quantification of complementary DNA sequences.<sup>[180]</sup> The working principle relies on the decrease in the passage of anionic markers through PNA-modified nanochannels upon hybridization of complementary DNA strands. This method exhibits a marked dependence on the ionic strength, thus implying that the main mechanism operating into the nanochannel is the electrostatic exclusion of the anionic markers resulting from the presence of negatively charged DNA strands.

Other artificial hybridizing template is the PMO. In this case, the DNA bases are attached to a backbone of methylenemorpholine rings linked through phosphorodiamidate groups. Recently, PMO-functionalized conical PET nanochannels (EDC/NHSS chemistry) were employed for the label-free detection of microRNAs (miRNAs) with remarkable sensitivity and sequence specificity.<sup>[181]</sup> One of the attractive features of this sensing strategy relies on the fact that the hybridization efficiency between PMO and target miRNAs is enhanced by neutral character of the PMO backbone and its high sequence-specific affinity. By using these sensing platforms target miRNAs were detected in serum samples with a limit

of detection of  $10 \times 10^{-15}$  M as well as specifically discriminate complementary miRNAs (Let-7b) from noncomplementary miRNAs (miR-21) and one-base mismatched miRNAs (Let-7c). The diode-like behavior became more asymmetric after hybridization due to the increase of the high current branch. The relative change in this current intensity served as analytical parameter as it showed a binding dependence on the miRNA concentration. The miRNAs detection from the changes in the transmembrane ionic current was ascribed to the change of surface charge density when PMO/miRNAs hybridization occurred.

### 5.1.3. DNAzymes

Following a different approach, the use of DNAzymes has recently constituted a new strategy for coupling of DNA components to promote responsiveness in nanofluidic channels. Deoxyribozymes, also called DNAzymes, are DNA oligonucleotides that are capable of performing a specific chemical reaction, often with a catalytic effect.

Zhai and co-workers introduced a highly specific  $Cu^{2+}$ -induced self-cleaving DNAzyme into conical multipore track-etched PET membranes to create a copper-responsive nanofluidic system.<sup>[182]</sup> The selected DNAzyme (DNA(1)) displays a significant site-specific cleavage only when  $Cu^{2+}$  is present in the range from  $10 \times 10^{-9}$  to  $1 \times 10^{-3}$  M, which a non-linear response to copper concentration. This DNAzyme was integrated to the nanochannels by grafting of a short oligonucleotide (DNA(2)), which partially hybridizes with DNA(1) to form a double stranded structure (dsDNA) (Figure 9a). Before cleavage of the dsDNA, the noncomplementary parts of DNA(1) relax to a loosely packed single-stranded structure and the nanochannel presents a diode-like behavior with high cation-driven current owing to negative charges on both strands. After adding  $Cu^{2+}$ , the catalytic DNA(1) strand breaks into three fragments and a main fragment dissolves into the solution, leading to a decrease of the negative charge density. This results in a diminution of the cation-driven current with a sensitive response property in a range of  $10^{-8}$  to  $10^{-6}$  M in neutral 0.1 KCl solutions. No appreciable effects were observed in the presence of other divalent cations, proving the specificity to  $Cu^{2+}$ .

In a similar approach, a nanopore detection system based on both DNA supersandwich and  $Zn^{2+}$ -requiring DNAzymes was reported in cylindrical multipore track-etched PET membranes.<sup>[183]</sup> Initially, a CP is chemically grafted to the nanochannels walls. In the presence of the sessile probe (SP) of the substrate, a partial hybridization with the CP takes place. This event is then amplified by adding the auxiliary probe1 (AP1) and auxiliary probe2 (AP2), which hybridize to each other from the free end of the substrate probe, inducing the supersandwich structure. Later, the DNAzyme strand (DS), can partially hybridize with the SP to form a DNAzyme. In the presence of  $Zn^{2+}$  the DS becomes catalytic and it cleaves the SP, dissociating the DNA superstructure (Figure 9c).

A dramatic reduction of the transmembrane current takes place after the formation of the DNA supersandwich structures. However, when adding  $1 \times 10^{-3}$  M  $Zn^{2+}$ , the current curves recover nearly to those of purely CP-modified PET membrane. Thus, the increment in the ionic conductance was employed



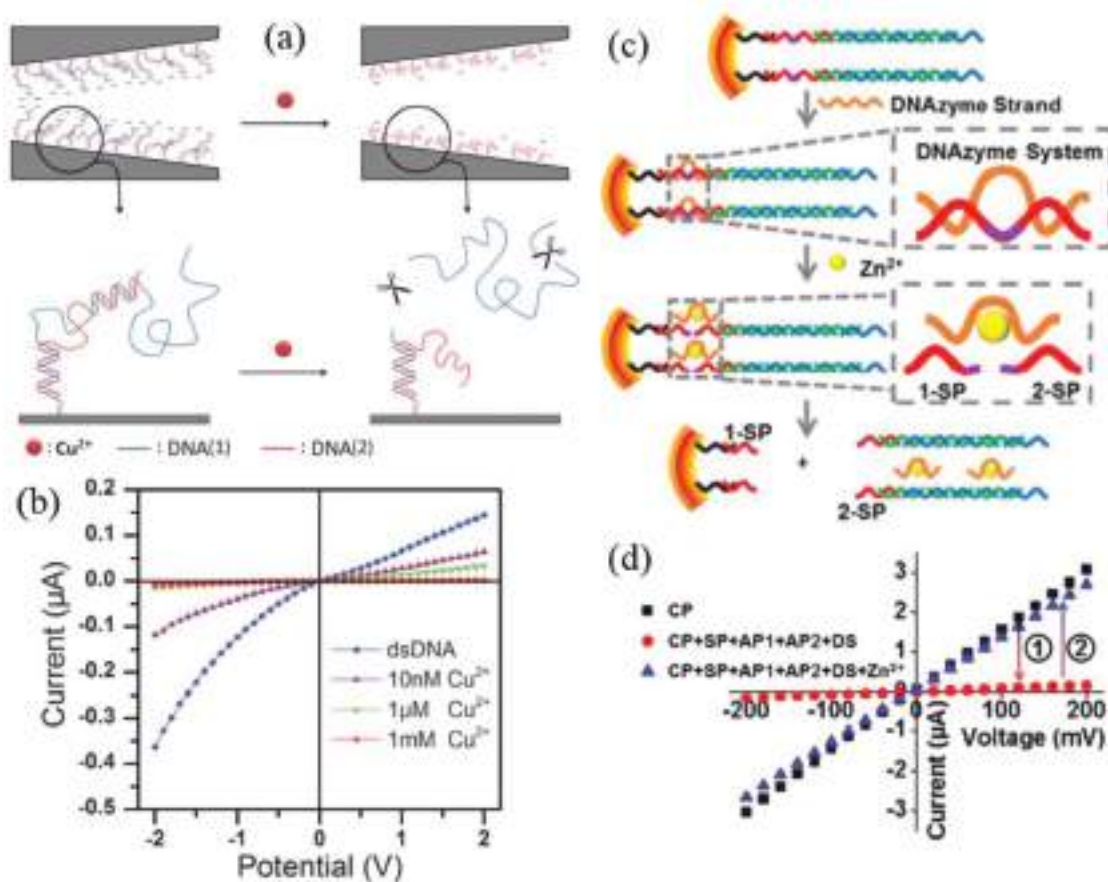


**Figure 9.** DNAzyme-based detection. a) Scheme of the functionalization steps and b) iontronic response of the nanochannels modified with dsDNA. Initially the system shows high conductance due to negative charges; in the presence of Cu<sup>2+</sup>, DNA(1) cleaves specific sites and the negative charge density decreases (lower cation-driven conductance). a,b) Reproduced with permission.<sup>[182]</sup> Copyright 2016, Royal Society of Chemistry. c) Schematic representation of the construction of DNA supersandwich structures for Zn<sup>2+</sup> detection. In the presence of Zn<sup>2+</sup>, the DNAzyme produces the cleavage of the DNA supersandwich. d) *I*–*V* iontronic response before (1) and after (2) adding Zn<sup>2+</sup> solution. c,d) Reproduced with permission.<sup>[183]</sup> Copyright 2016, Royal Society of Chemistry.

for the detection of Zn<sup>2+</sup>, reaching a reliable detection limit of  $1 \times 10^{-9}$  M without interference by other divalent cations.

#### 5.1.4. Specific Ion Binding by ssDNA

A different approach for specific ion-induced gating of the transmembrane transport in nanochannels is based on the use of short DNA fragments with sequences able to form stable complexes with a given cation. These DNA fragments have a random conformation that induces steric hindrance when bound to the nanochannel walls. However, a particular folded conformation is reached by specific ion binding, increasing the effective pore size. Such conformational transitions have been verified by circular dichroism.

Within this framework, Tian et al. presented an iontronic system sensitive to mercury (II) ions (Hg<sup>2+</sup>) based on ssDNA with an ion-specific thymine–thymine (T–T) base, which forms stable T–Hg<sup>2+</sup>–T complexes.<sup>[184]</sup> They employed single pore conical PI nanochannels modified with gold nanoparticles by sputtering and then by chemisorption of 5′-thiol-ended T-rich

ssDNA. In the presence of Hg<sup>2+</sup> ions, the stretched T-rich ssDNA switches into duplex structures through the formation of T–Hg<sup>2+</sup>–T complexes. This superstructural reorganization promotes a partial increase in the effective nanochannel size that is iontronically detected as an increase in transmembrane current (ON state) (Figure 10). Then, in the presence of Hg<sup>2+</sup> ions are removed from T–Hg<sup>2+</sup>–T complex and the original configuration is recovered. The reversible switching of the nanochannel properties can be observed by sequentially exposing the nanochannel to Hg<sup>2+</sup> (ON state) and cysteine (Cys) (OFF state) solutions. Blank experiments also showed that no significant changes were found in the presence of other metal ions, such as Cd<sup>2+</sup>, Pb<sup>2+</sup>, and Mg<sup>2+</sup>.

Following the same synthetic and mechanistic approach, Gao et al. presented a silver cation-selective nanofluidic system, using a ssDNA with specific cytosine–cytosine (C–C) mismatch base pairs which are able to bind Ag<sup>+</sup> by strong and stable C–Ag<sup>+</sup>–C complexes.<sup>[185]</sup> As in the previous case, the binding of Ag<sup>+</sup> induces a hairpin-like structure of the ssDNA which partially increases the effective pore size and high ionic current (ON state). Once again, when cysteine is introduced, the Ag<sup>+</sup> is

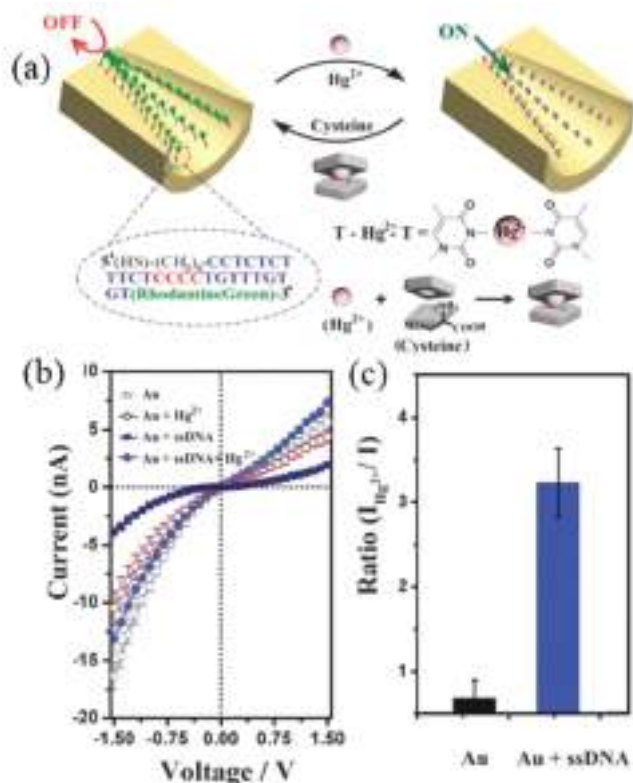


**Figure 10.** ssDNA binding. a) Scheme of the integrated molecular system for  $Hg^{2+}$  detection based on the grafting with T-rich ss-DNA. In the presence of this cation, the formation of duplex structures by T- $Hg^{2+}$ -T pairing opens the pore. b) Asymmetric  $I$ - $V$  iontronic response after different of the functionalization. c) Current (at 1.5 V) ratios for the naked and functionalized nanochannels in the presence of  $Hg^{2+}$ . a–c) Reproduced with permission.<sup>[184]</sup> Copyright 2013, Royal Society of Chemistry.

pulled out from the C- $Ag^+$ -C complexes and the C-rich ssDNA adopts a random structure causing higher steric hindrance (OFF state).

The same principle was later utilized for the simultaneous responsiveness to  $Ag^+$  and  $Hg^{2+}$  in funnel-shaped alumina nanochannels covalently modified with ssDNA, taking advantage of the specific interaction between  $Hg^{2+}$  ions and T bases as well as  $Ag^+$  ions and C bases.<sup>[186]</sup> By varying the pH of the solution,  $Hg^{2+}$  and  $Ag^+$  ions could be sensed individually.

## 5.2. Host–Guest Supramolecular Interactions

Supramolecular self-assembly has promoted the nanoarchitectonics of interfaces with precise control and directed functionalities. Particularly, cucurbit[n]uril<sup>[187]</sup> and pillar[n]arenes<sup>[188]</sup> constitute supramolecular hosts with outstanding ability for host–guest based supramolecular switches. In this subsection we revise some recent works on the use of supramolecular hosts for providing functional properties to solid-state nanochannels. These few examples and some others presented in the following sections illustrate the enormous potential of host–guest-based modulation of the ionic transport in nanofluidic channels.

Jiang and co-workers presented a  $Hg^{2+}$ -driven gating mechanism in solid-state conical nanopores based on competitive host–guest interactions of pillar[5]arenes.<sup>[189]</sup> A mercaptoacetic acid-pillar[5]arene (MAP5) was designed and synthesized specifically for  $Hg^{2+}$  association by host–guest interactions. In this system, 1,6-hexanediamine (HDA) was crosslinked to the surface of the PET membranes by EDC/NHSS chemistry. This amine was then employed to bind the MAP5 based on molecular recognition interactions. However, in the presence of  $Hg^{2+}$  in solution, the MAP5 prefers the interaction with this divalent cation and is removed from the HDA-modified surface. In that way, the competitive interaction of  $Hg^{2+}$  and the alkylamine group is the key of the gating mechanism of the nanochannel iontronic behavior in KCl solution. After HDA modification, the nanochannel walls are positive due to the amine protonation and the diode-like behavior presents high rectification factors. By addition of the MAP5 (negatively charged) to the solution, the negative surface charge is restored as a consequence of the binding to the amine moieties and the diode-like behavior becomes inverted, being selective to  $K^+$  (ON state). A subsequent addition of  $Hg^{2+}$  caused the release of MAP5 and a partial decrease of the negative surface charge, causing the decrease of the conductivity of the nanochannels (OFF state). This effect resembles the poisoning of  $K^+$  protein channels by  $Hg^{2+}$ . By alternating MAP5 and  $Hg^{2+}$  solutions, good reversibility was shown for this system, with low interference by other divalent cations.

In a more recent work, a reversible gating effect was achieved on single conical nanochannels by host–guest interaction-driven LbL supramolecular assemblies.<sup>[190]</sup> The walls of the etched PET channels were modified by chemical anchoring of a self-assembly precursor (NapDA), having a naphthalene pendant group which can be employed for further interaction with the host molecule—cucurbit[8]uril (CB[8]). The NapDA-modified channels present a gating effect depending on the concentration of CB[8] in solution in NaCl solution. Moreover, as the CB[8] units also interact with the  $K^+$ , in the presence of this cation the initial dissociated state of NapDA-modified channel is restored, providing a reversible gating mechanism. The CB[8] units bound to the NapDA-modified channels could be further modified by adding a three-armed naphthalene derivative (BTNI). As the BTNI has extra naphthalene groups, it can bind a new layer of CB[8] and so on, yielding an LbL modification procedure.

Following a completely different approach, the nonenzymatic borate-free glucose gating was obtained by the introduction of the chiral pillar[6]arene-based host–guest systems into nanochannels.<sup>[191]</sup> The working principle is based on differences in the binding strength of chiral pillar[6]arene and glucose enantiomers that, in turn, results in the modulation of the surface charges on nanochannel walls. Thus, the chiral nanochannels can be switched OFF by D-glucose and be switched ON by L-glucose, with good reversibility (Figure 11a,b). In this work, chiral alanine-decorated pillar[6]arene (L-AP6) was synthesized by a condensation reaction. Then, the L-AP6 (host) was associated to guest AZO moieties covalently bound to the etched PET nanochannel. The transmembrane current in 0.1 M KCl continuously decreased after each modification step as a consequence of the decrease of the negative surface charge and increase of hydrophobicity. Moreover, after adding  $1 \times 10^{-3}$  M glucose, the current further decreased in the case of D-Glu (OFF state),

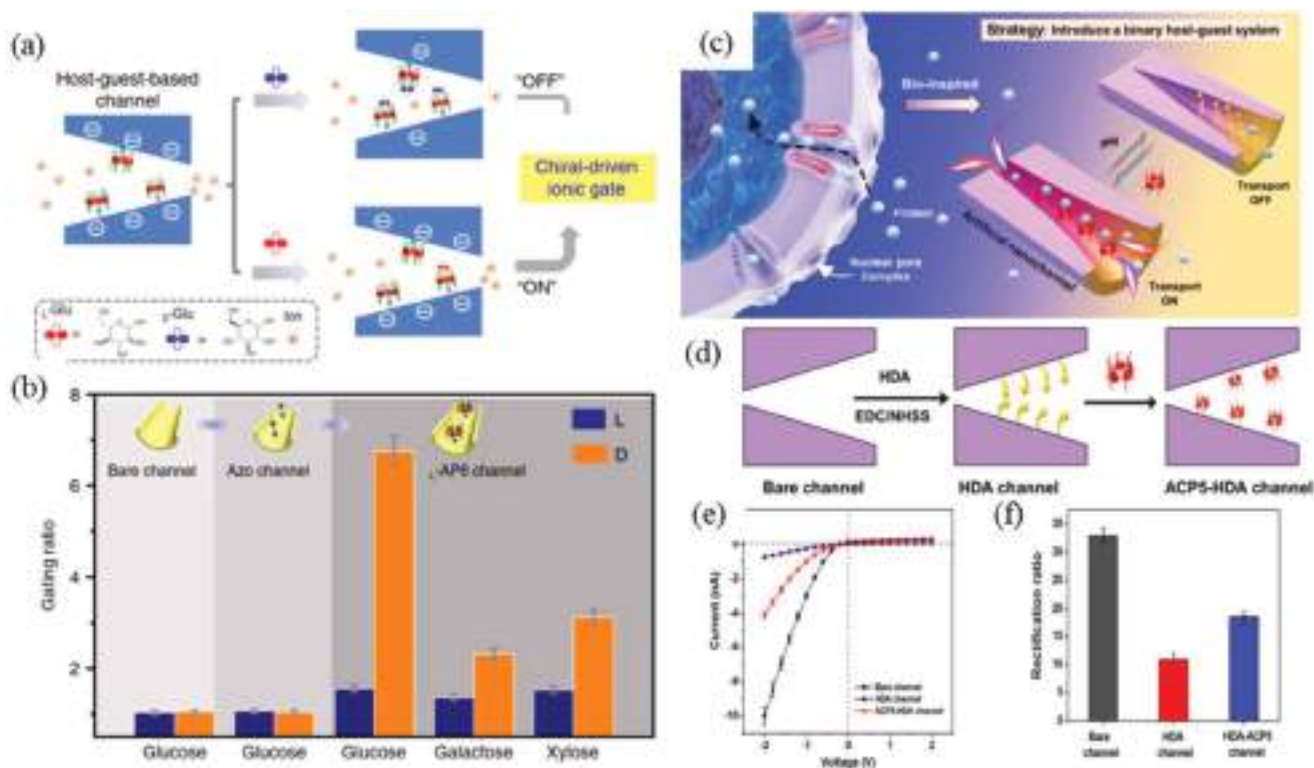


**Figure 11.** Host-guest supramolecular interactions. a) Scheme of the integrated molecular system for the glucose-enantiomer-driven gating mechanism based on host-guest interactions. b) Gating ratios at  $-2$  V after adding different sugars at each stage of the modification. a,b) Reproduced under the terms of the CC-BY Creative Commons Attribution 4.0 International License (<http://creativecommons.org/licenses/by/4.0/>).<sup>[191]</sup> Copyright 2018, The Authors. Published by Springer Nature. c) Bioinspired design of the host-guest-based pH-responsive nanochannel. d) Stages of the functionalization with HDA (guest) and ACP5 (host). e)  $I$ - $V$  ionic response and f) rectification ratio after each functionalization step in 0.1 M KCl PBS pH 7.2. c-f) Reproduced with permission.<sup>[192]</sup> Copyright 2018, American Chemical Society.

whereas it remained nearly unchanged in the case of L-Glu (ON state). After soaking in pure water, the bound D-glucose is released and the ON state is recovered, with good repeatability performance. The binding of glucose to the L-AP6-AZO complex occurs by multiple chiral hydrogen-bonding interactions and it is ten times more stable in the case of the enantiomer D. The effective surface  $pK_a$  changes upon D-glucose binding from 6.08 to 6.71, whereas it remains practically the same after L-glucose binding (6.14). Based on this  $pK_a$  shifts, the authors propose that differences in the surface charge would be responsible for the enantiomer-driven gating effect.

In addition, Li and co-workers presented another switchable nanochannel by introducing a pH responsible binary host-guest system.<sup>[192]</sup> Under pH regulation, this host-guest assembled system is capable of turning ON and OFF the histone translocation across the nanochannels. They designed a negatively charged host *N*-acetyl-cysteine pillar[5]arene (ACP5) that serves as receptor of the cationic histone. The conical etched PET nanochannels were modified by HDA crosslinking (EDC/NHSS) and then the membrane was soaked in  $1 \times 10^{-3}$  M ACP5 for self-assembling. At neutral pH, the ACP5/HDA-modified channel present cation-driven current rectification (negative surface charge). By lowering the pH to 4.5, the transmembrane current decreases, with a reversible switching performance. Moreover, the histone translocation was observed just when the ACP5 were bound to the HDA-modified nanopore, indicating

that ACP5 can act as a good receptor for facilitating histone transport. By alternating treatment with pH 4.5 solution and ACP5 solution, a highly robust OFF/ON gating of the histone translocation was achieved (Figure 11c-f).

### 5.3. Redox Sensitive and Electrochemically Actuated Nanofluidic Systems

#### 5.3.1. Redox Sensitive Nanochannels

Most redox sensitive nanofluidic devices are based on the effect of  $H_2O_2$  as molecular oxidizing species. In 2015, Ali et al. presented a  $H_2O_2$  sensitive nanochannels device by functionalization of single conical etched PET channels with an amine-terminated boronic ester carbamate (BEC-NH<sub>2</sub>) compound (EDC/PFP) (Figure 20).<sup>[193]</sup> In mild basic solution, the addition of  $H_2O_2$  hydrolyzes the arylboronic-ester into a corresponding phenol, which then undergoes oxidation and decarboxylation and 1,6-elimination reactions, leading to the generation of amine groups (positively charged). Thus, an inversion in the current rectification behavior is produced owing to the surface charge inversion and the increment of the hydrophilicity. These  $H_2O_2$ -generated amino groups can be further modified by reaction with succinic acid, leading to carboxylic moieties, inverting again the rectification behavior (Figure 12).



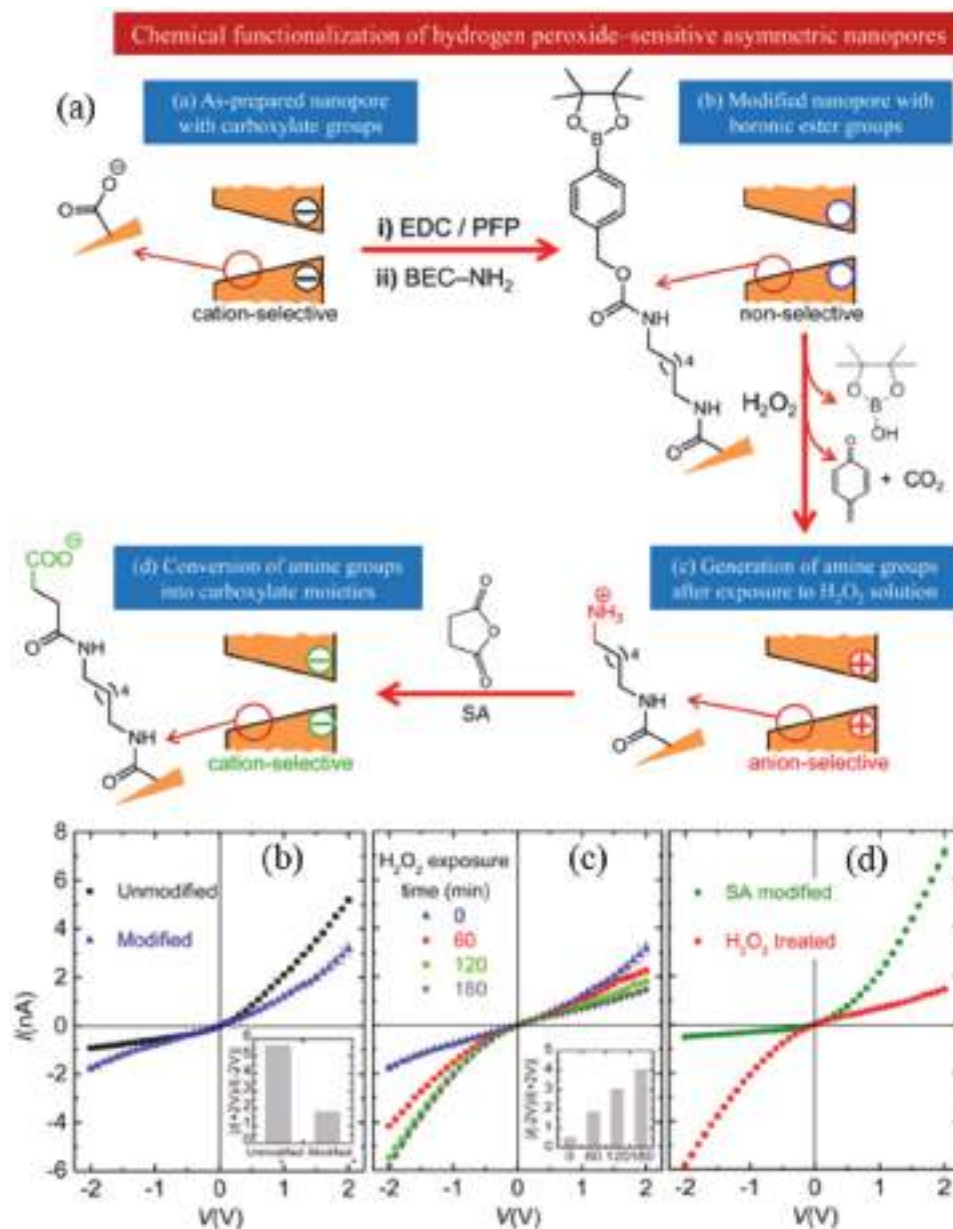


**Figure 12.** Redox-sensitive nanochannels. a) Functionalization procedure for the production of H<sub>2</sub>O<sub>2</sub>-sensitive nanochannels. b) *I-V* iontronic response before and after the chemical modification. c) *I-V* iontronic response of the modified nanochannel after exposing to H<sub>2</sub>O<sub>2</sub>. d) *I-V* iontronic response of the H<sub>2</sub>O<sub>2</sub>-treated nanochannel after exposing to succinic acid (SA). a–d) Reproduced with permission.<sup>[193]</sup> Copyright 2015, American Chemical Society.

With a different approach, Zhai and co-workers presented a redox sensitive nanochannels based on the biorelevant reaction of hydrogen peroxide with cytochrome *c* (cyt *c*).<sup>[194]</sup> For this, conically etched PET nanochannels were modified with cyt *c* by covalent crosslinking, employing ethylenediamine as spacer (EDC/PFP). In the presence of H<sub>2</sub>O<sub>2</sub>, ferrous cyt can be oxidized to the ferric species. The original situation can be then reestablished by treatment with ascorbic acid (AA). Cyt *c*-Fe<sup>2+</sup>-modified surface is nearly neutral and turns positive after H<sub>2</sub>O<sub>2</sub> treatment, which also increases the hydrophilicity leading to higher transmembrane ion current. Then, the ionic transport can be gated between ON/OFF states by H<sub>2</sub>O<sub>2</sub> and AA treatment.

More recently, a redox sensitive nanopore system has been developed by functionalization with nicotinamide units.<sup>[195]</sup> The nicotinamide derivative was synthesized and crosslinked to the walls of the conical etched PET nanochannels. This redox unit could be then reversibly reduced (by dithionite) and oxidized (by H<sub>2</sub>O<sub>2</sub>). As the oxidized form presents a quaternary pyridinium, an anion selective transport is achieved, whereas the reduced form is neutral and no rectification is observed. Thus, the redox reactions allowed reversibly switching the nanopore inner environment from a hydrophilic charged form (ON state) to a hydrophobic neutral one (OFF state).

Other redox sensitive system was reported on carbon nanopipets by employing redox probes in low concentration.<sup>[196]</sup> In

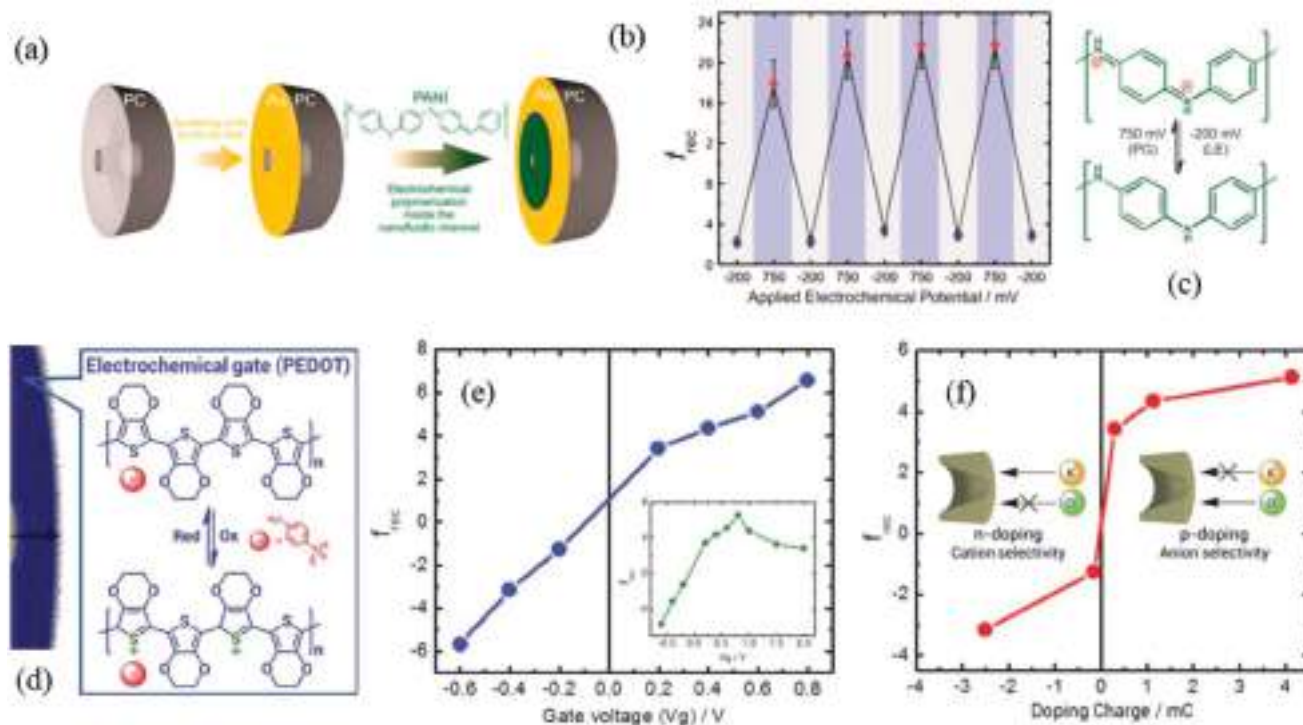


**Figure 13.** Conducting-polymer-modified nanochannels. a) Functionalization of the PC membranes with PANI by Au sputtering and electropolymerization. b) Electrochemically driven gating of the iontronic response in terms of the rectification factor at different applied potentials. c) Redox commutation of PANI. a–c) Reproduced with permission.<sup>[197]</sup> Copyright 2015, American Chemical Society. d) Electrochemically induced transitions of PEDOT responsible for conferring the FET-like iontronic behavior to the all-plastic nanofluidic device. e) Rectification factor of the PEDOT-modified nanochannel as a function of the applied (gate) potential. f) Rectification factor as a function of the doping degree of the PEDOT layer. d–f) Reproduced with permission.<sup>[198]</sup> Copyright 2017, Wiley-VCH.

the presence of  $\text{Fe}(\text{CN})_6^{3-/4-}$  and  $\text{Ru}(\text{NH}_3)_6^{3+/2+}$ , net surface charges are induced in the conducting carbon walls of the nanochannels, which modifies the ionic transport.

### 5.3.2. Electrochemically Actuated Systems

The electrochemical potential arises as a powerful variable for regulating the iontronic behavior in nanofluidic channels. The possibility of exploiting the redox characteristics of electroactive groups offers an interesting mechanism for tuning the transport properties of the nanofluidic devices by simply applying an electrochemically controlled “gating potential.” As already mentioned, the coupling between the applied potential and the modulation of the transmembrane ionic current requires electroactive materials, whose redox transformations yield surface charges in the nanochannels.

In 2015, Pérez-Mitta et al. presented an electrochemically actuated nanofluidic channel based on the electroactivity of a conducting polymer (polyaniline, PANI).<sup>[197]</sup> In this work, a PANI film was electrosynthesized on Au-sputtered PC single conical nanochannels. Owing to the decrease of the effective pore diameter and the presence of positive charges by PANI protonation, a highly rectifying behavior was achieved. Moreover, due to the potential dependence of the redox states of PANI, the state of charge of the PANI film can be readily modified by applying different electrochemical potentials to the metallized

membrane side. A continuous increment of the rectification ratio was achieved by oxidized the polymer film by turning the electrochemical potential. Furthermore, a reversible gating of the transmembrane current was achieved by alternating the applied potential between extreme values (Figure 13a–c).

The electrochemical modulation of the nanochannels iontronic response was also performed within an all-plastic device.<sup>[198]</sup> The fabrication of a field-effect tunable nanofluidic device was accomplished by modifying a conical etched PET nanochannel with a layer of the conducting polymer poly(3,4-ethylenedioxythiophene) (PEDOT). (Figure 13d–f). The PEDOT layer was chemically synthesized on the tip of the asymmetric channel by spin coating the monomer using ferric tosylate as oxidant and stabilizer. The PEDOT layer does not only enhance the rectification properties of the nanopore but it also allows changing the surface charge state by using a bipotentiostatic configuration to simultaneously apply an electrochemical potential to the nanopore membrane while recording the transmembrane current. Thus, for a given transmembrane voltage, the application of different gate voltages, i.e., electrochemical potentials, results in measurable changes in the nanochannel ionic conductance, in close resemblance to traditional field-effect transistor (FET) devices. This strategy permits rapid control of surface charge modulation and reversion with immediate effects on the rectification efficiency, thus providing a completely new concept for gating and actuation in nanofluidic channels.



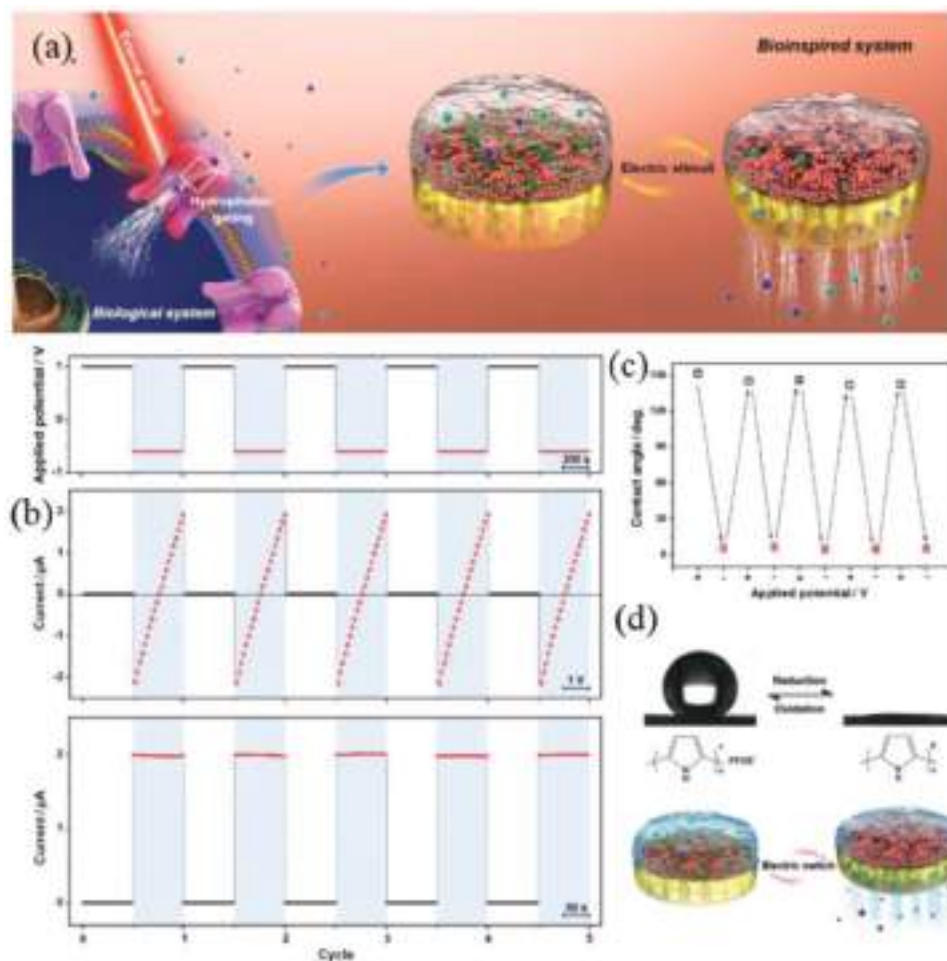


**Figure 14.** Electrochemically modulated hydrophobicity. a) Bioinspired electrochemically stimulated nanochannel based on the hydrophobic/hydrophilic transition of polypyrrole (PPy) film. b) Transient iontronic response after potential gating: ionic current–transmembrane voltage ( $I$ – $V$ ) and ionic current–time ( $I$ – $t$ ) properties under the alternate oxidation and reduction electrochemical potentials applied to the nanochannels. c) Changes of the contact angle for alternating electrochemical potential values. d) Chemical structure and contact angle images at the extreme applied potentials corresponding to the reduced and oxidized forms of PPy. a–d) Reproduced with permission.<sup>[200]</sup> Copyright 2018, Wiley-VCH.

Another nanochannel system responsive to electrochemical potential was prepared on AAO nanochannels.<sup>[199]</sup> AAO membranes were first sputtered with Pt and this metallic layer was employed for the electrosynthesis of a polypyrrole (PPy) coating. In the reduced state PPy is electrically neutral; however, upon oxidation it adopts a polycationic character due to the formation of polaron and bipolaron species. As a consequence, the electrochemical modulation of the oxidation state of PPy facilitates the reversible switching of the rectification factor and the ionic current passing through the nanochannel.

More recently, another electrically actuated hydrophobic-induced gating mechanism in AAO nanoporous membranes was obtained by functionalization with surfactant-doped PPy (Figure 14).<sup>[200]</sup> A PPy film was electrochemically synthesized on a gold-sputtered AAO membrane in the presence of perfluorooctanesulfonate anions (PFOS<sup>-</sup>). These anions act as dopants of the PPy in the oxidized state, conferring a hydrophobic behavior to the films. However, as the PPy is electrochemically reduced (in acetonitrile), the doping anions are released and the film turns hydrophilic. After further oxidation of the films

in acetonitrile in the presence of PFOS anions, the doping level is restored and so the hydrophobic character. Depending on the microscopic structure of these films, they could even present reversible superhydrophobicity/superhydrophilicity induced by electrochemical oxidation/reduction. Since the ionic transport is sensitive to the wetting of the walls of the nanochannels, the transmembrane current measured in aqueous solution depends on the hydrophobic/hydrophilic state of the PPy films. Thus, the ex situ oxidation of the PPy films in acetonitrile induces the doping with PFOS increasing the hydrophobicity. Consequently, the transmembrane ionic current in aqueous electrolytes markedly diminishes (OFF state). Conversely, as the PPy films are ex situ reduced, the films become hydrophilic and the ionic current increases (ON state). By a proper film microstructure (by an optimized electrosynthesis condition), gating factors of about  $10^5$  were obtained.

The use of conducting polymers in nanopore environments has been also explored by Ren et al.<sup>[201]</sup> as a strategy to attain selective single-molecule biosensing. By using nanopipette-based PPy ionic-FETs (or nanopore extended field-effect

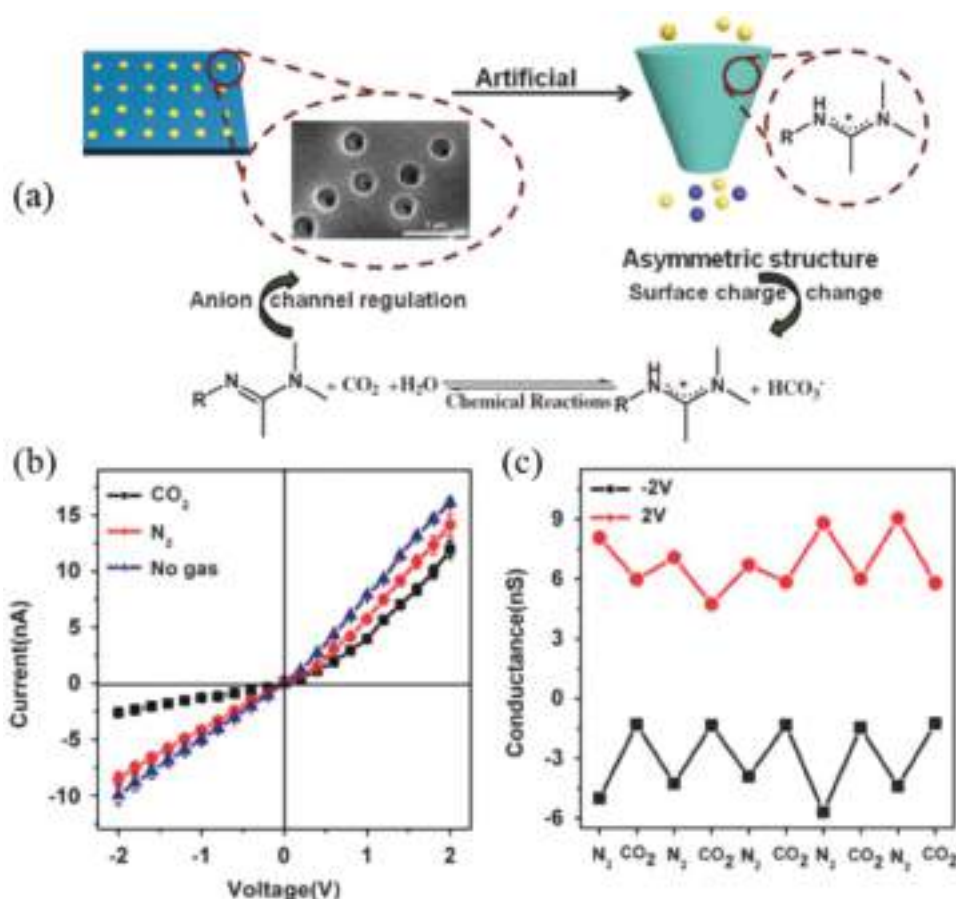


**Figure 15.**  $CO_2$ -activated bioinspired nanochannels. a) Reaction with amidine groups produces a net positive charge inside the pores. b)  $I-V$  iontronic response of the modified nanochannels after bubbling different gases. c) Reversibility of the  $CO_2$ -induced response. a–c) Reproduced with permission.<sup>[202]</sup> Copyright 2015, Nature Publishing Group.

transistor, nexFETs) these authors showed that it is feasible to control the transport of single-molecule DNA through a nanopore upon switching the gate voltage.

#### 5.4. Dissolved Gases as Chemical Effectors

Some recent works have studied the possibility of sensing dissolved gases via the changes in the iontronic response of solid-state nanochannels by coupling different molecular systems to the walls of the channels.

$CO_2$ . Zhai and co-workers presented a  $CO_2$ -induced ion gating mechanism in nanochannels by a  $CO_2$ -activated chemical reaction, which resembles the stomatal closure in response to  $CO_2$ .<sup>[202]</sup> They developed artificial nanochannels functionalized by two amidine-containing molecules with flexible and rigid molecular structures to provide  $CO_2$ -responsiveness. For that, amidine-containing molecules of (4-[4-(1-dimethylamino-ethylideneamino)-phenyl]-butyric acid) (DEPBA) and (12-(1-dimethylamino-ethylideneamino)-dodecanoic acid) (DEDA) were synthesized and attached to the surface of conical track-etched PET nanochannels by covalent crosslinking. The reaction of  $CO_2$  with amidine groups leads to the conversion of  $CO_2$ , water and amidine groups to bicarbonate and amidine

cations (Figure 15). The protonation of amidine groups turn the surface charge to positive, yielding an asymmetric anion-driven transmembrane current response. For example, while the rectification ratio of the DEPBA-modified channels is very low ( $\approx 1.64$ ) due to the small surface charge on the channel surface, it increases to 4.60 after bubbling  $CO_2$ . Since the chemical reaction of amidine groups with  $CO_2$  is reversible, the rectification vanishes again upon ventilation with  $N_2$ . The gas-gating mechanism is therefore reversible. Control experiments showed that the change in the rectification factor is owing to neither the pH change caused by bubbling  $CO_2$  nor the presence of bicarbonate anions.

Another  $CO_2$ -induced gating mechanism inspired by olfactory sensory neurons (OSN) of mosquitoes was presented more recently.<sup>[203]</sup> In that work, conical polyimide single nanochannels were chemically modified by anchoring (NHSS/EDC chemistry) (1-(4-amino-phenyl)-2,2,2-tri-fluoro-ethanone) (APTE) (Figure 16a–c). After etching, the polyimide channels are negatively charged, yielding a diode-like iontronic behavior when the transmembrane current is recorded. The chemical modification practically neutralizes the surface charge and increases the hydrophobicity of the walls of the nanochannels, yielding a hindrance of the ionic transport in a KCl solution (OFF state). However, when  $CO_2$  is dissolved in the solution, it partially produces

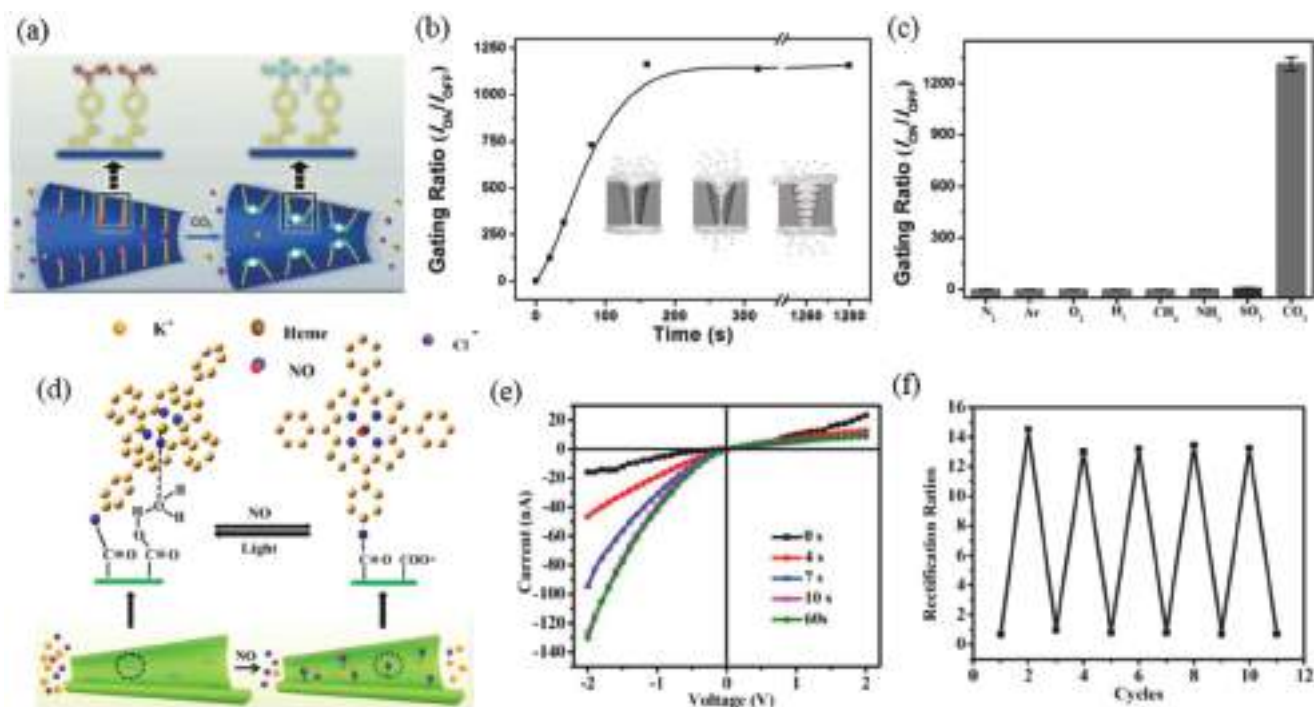


**Figure 16.** Gas-sensing nanochannels. a) Biomimetic CO<sub>2</sub>-responsive nanochannel based on the integration of APTG to the inner surface of the pores. b) Time response of the CO<sub>2</sub>-induced gating of the APTG-modified nanochannels. c) Selectivity of the gating effect on the iontronic response to CO<sub>2</sub>. a–c) Reproduced with permission.<sup>[203]</sup> Copyright 2016, Wiley-VCH. d) Scheme of the mechanism operating on the ferroporphyrin NO-responsive nanochannel. e) *I*–*V* iontronic response of the ferroporphyrin-modified channels after different NO ventilation times. f) Reversibility of the responsiveness by alternating cycles of NO bubbling and laser illumination. d–f) Reproduced with permission.<sup>[204]</sup> Copyright 2018, American Chemical Society.

carbonate. Carbonate can selectively coordinate to two adjacent molecules of APTG, conferring a negative charge to the surface of the nanochannels and restoring the diode-like behavior (ON state). So, the opening of the channel is indirectly caused by CO<sub>2</sub> as it happens in the protein channels of OSN. In that way, gating factors higher than 1000 were measured. Moreover, the system shows a high reproducibility as proved by cycling in solutions with and without dissolved CO<sub>2</sub>, whereas no interferences were observed by bubbling other gases to the solutions.

NO. A bioinspired gating mechanism based on the coupled effects of NO binding and light-induced dissociation on a ferroporphyrin was presented (Figure 16d–f).<sup>[204]</sup> In this work, conical multichannel PET membranes were chemically modified by crosslinking of an amino-ferroporphyrin to carboxylic groups of etched PET membranes. Since the crosslinking was incomplete, some of the remaining carboxylate groups can coordinate the Fe in the porphyrin, reducing the negative net surface charge as compared with the unmodified nanochannel. After bubbling NO in the solution, this molecule binds the free site in the Fe coordination displacing the carboxylate and inducing a more pronounced negative charge in the walls of the nanochannels. This effect can be monitored by an enhancement of the diode behavior of the nanochannel when the ionic transmembrane current was measured and the corresponding increase of the rectification factor. The response induced by NO was relatively rapid, reaching a saturation condition after 60 s of bubbling, and chemically specific as was not observed when other different gases were employed. The binding of the

NO to the porphyrin reversed by light and a marked decrease of the rectification was observed after irradiating the membrane with a 532 nm laser, due to the restoring of the carboxylate–porphyrin association. By successive bubbling and irradiation cycles, the excellent reversibility of the gating effect and the good stability of the iontronic behavior were demonstrated.

O<sub>2</sub>. A protein-gated nanoporous membrane based on the conformational changes of a peptide (CGGC) upon oxidation/reduction was recently presented.<sup>[205]</sup> The CGGC presents the possibility of producing an intramolecular disulfide S–S bond due to oxidation by dissolved oxygen, which induces a folding of the peptide structure that “opens” the channels. This disulfide bond can be then reduced by dithiothreitol, turning the peptide to a more extended conformation that “closes” the nanochannels (i.e., reduces the tip diameter). In that way, the peptides act as gatekeepers for the transport of small molecules through the cone-shaped multipore nanochannels in PET membranes, as probed by the gated transport of a fluorescent probe across the membrane. Also the ionic current can be gated by alternating DTT and O<sub>2</sub>, showing that the opening rate depends on the concentration of O<sub>2</sub> dissolved in the electrolyte solution.

### 5.5. Boronate-Containing Building Blocks: Sugar-Specific Interactions

The recognized ability of phenyl boronic acid to specifically coordinate to simple sugars<sup>[206]</sup> has been also exploited

in several nanopore systems. The mean charge of the phenyl boronic groups turns more negative after association to 1,2 and 1,3 diols, inducing changes in the iontronic behavior of the nanofluidic systems. As an example, single conical PET nanochannels were chemically modified by crosslinking with amino-phenyl boronic acid using EDC/NHSS chemistry.<sup>[207]</sup> After exposing the functionalized nanochannel to glucose solution at pH 7.4 the transmembrane ionic current decreased (OFF state). By immersing the membrane in pH 4.5, glucose is released from the channel surface, and the ionic current measured at pH 7.4 increased again (ON state). Following a similar approach, the crosslinking of amino-phenyl boronic acid to the carboxylic groups of etched conical PET nanochannels membranes was performed by only EDC.<sup>[208]</sup> This procedure yielded a glucose and fructose sensing nanofluidic system as revealed by the changes in both the conductance and the rectification efficiency.

Later, the boronic functionalization of a quartz nanopipette was performed by adsorption of a boronic moiety-containing polymer.<sup>[209]</sup> In this case, the addition of boronic units to poly(4-vinylpyridine) (PVP) was previously carried out by quaternization reaction with bromomethylphenylboronic acid. The modified nanopipette showed pH dependent transport and was sensitive to the presence of fructose in the millimolar range.

A similar behavior was reported for single glass conical nanopores modified with 4-carboxyphenylboronic acid (4CPB).<sup>[210]</sup> In this case, the APTES functionalization of the pore walls was previously performed and the iontronic behavior of the 4CPB-modified pore was sensitive to the presence of glucose in the millimolar range.

Also based on a boronic-appended polymer, a saccharide-driven gating effect was achieved by Zhang and co-workers in multiple nanochannels of AAO membranes.<sup>[211]</sup> In this case, the nanochannels (60 nm diameter) were chemically modified with chirality-responsive copolymers poly(3-(acryloylthioureido) phenylboronic acid-co-N-isopropylacrylamide) [P(ATPBA-co-NIPAAm)]. Although with different sensibility, these nanochannels were responsive to a series of saccharides in the sub-micromolar concentration range. In this case, the increase in the transmembrane current was attributed to the recognition of saccharide by the cooperative hydrogen bonding, which induces conformational changes that cause a variation of the wettability of the copolymer film.

More recently, the functionalization of nanopipettes with a copolymer of poly[4-vinyl phenylboronic acid] (PVPBA) and poly[2-(dimethylamino)ethylmethacrylate] (PDMAEM) via ATRP yielded a nanofluidic system with responsiveness toward pH, temperature and sugar concentration.<sup>[212]</sup> Owing to the presence of both boronic acid and tertiary amine groups, the nanofluidic devices presented strong pH dependence of the diode-like behavior, showing anion-selective and cation-selective transport in acidic and basic conditions, respectively. Additionally, as the PDMAEM presents a LCST transition at about 40–50 °C, the high temperature collapse induces an increment of the transmembrane current. Finally, rectification efficiency at neutral pH was dependent on the sub-millimolar concentration of glucose and fructose by reversible boronic esters formation.

In a completely different modification approach, the introduction of boronic moieties to a nanofluidic system was performed by electropolymerization of 3-aminophenylboronic

acid on Au-sputtered conical track-etched polycarbonate nanochannels.<sup>[213]</sup> The binding of sugar was used as a chemical effector inducing significant pKa shifts in the boronic moieties of the poly(aminophenylboronic acid) (PAPBA). In this way, the concentration of sugar was responsible for setting different proton-gated nanofluidic operations and switching the appearance of anion-driven and cation-driven rectification regimes over a wide pH range ( $1 < \text{pH} < 11$ ) (Figure 17).

## 5.6. Sensing and Detection of Biomarkers, Drugs, and Small Biomolecules

### 5.6.1. Enzymes as Active Building Blocks for Nanofluidic Sensors

Enzymes constitute smart building blocks for substrate-driven modulation of the transmembrane current in nanofluidic

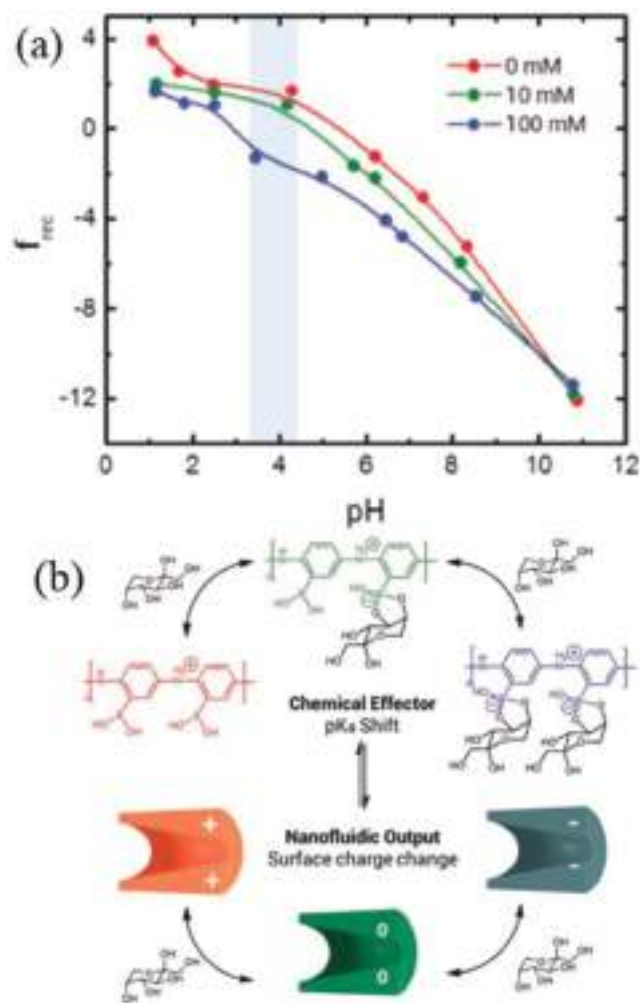


**Figure 17.** Sugar-responsive nanochannels. a) Variation of the rectification factor as a function of pH in the presence of different fructose concentrations (0,  $10 \times 10^{-3}$ ,  $100 \times 10^{-3}$  M) for a PAPBA-modified nanochannel. b) Mechanism of the effect of the sugar on the acid–base equilibrium and the iontronic responsiveness. a,b) Reproduced with permission.<sup>[213]</sup> Copyright 2018, American Chemical Society.



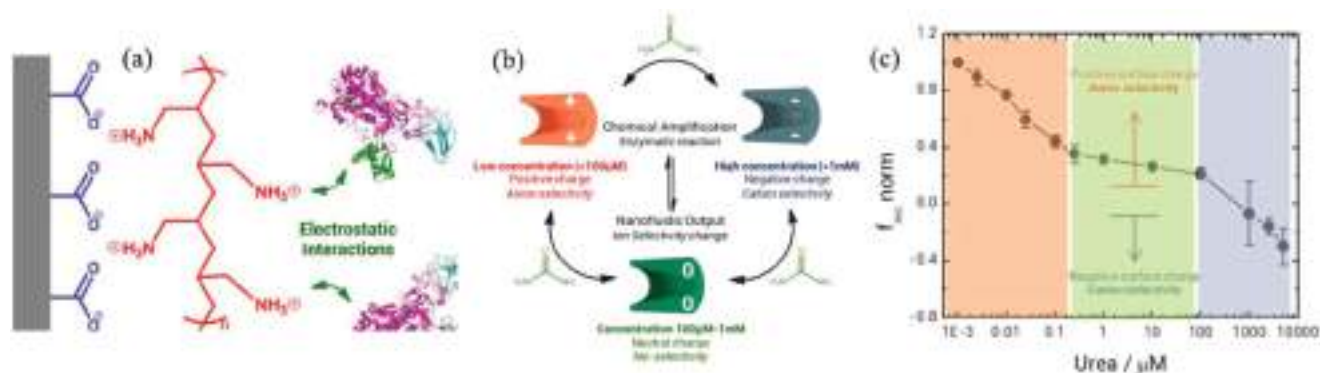


**Figure 18.** Enzyme-based urea detection. a) Electrostatic assembly for building up the urea-responsive nanofluidic device based on the integration of urease and PAH. b) Scheme showing the relationship between the urea degradation and the iontronic output by chemical amplification. c) Normalized rectification factors as a function of the urea concentration showing three regimes depending on the surface charge of the nanopore. a–c) Reproduced with permission.<sup>[216]</sup> Copyright 2018, American Chemical Society.

devices as they are naturally designed for the efficient and selective recognition of specific molecules.

In 2011, Ensinger and co-workers described a nanochannel platform for  $\text{H}_2\text{O}_2$  detection based in the covalent crosslinking of horseradish peroxidase (HRP) to single conical etched PET nanochannels using EDC/NHSS chemistry.<sup>[214]</sup> The HRP-nanochannel system detected nanomolar concentrations of  $\text{H}_2\text{O}_2$  with 2,2'-azino-bis(3-ethylbenzothiazoline-6-sulfonate) (ABTS) as the substrate. Addition of  $\text{H}_2\text{O}_2$  led to changes of the transmembrane current induced by the formation cationic products of the redox reactions accumulated in the nanochannel.

Also following an enzymatic approach, a glucose nanochannel biosensor based on the integration of glucose oxidase on conical PET nanochannels by covalent crosslinking (EDC/NHSS) was presented.<sup>[215]</sup> The modified channel presented an ohmic behavior due to its nearly null surface charge. In the presence of D-glucose, the transmembrane ionic current increases. This effect was ascribed to a change of local pH by the enzymatic activity. In the presence of oxygen molecules as the electron acceptor, the glucose oxidation reaction is a two-step catalytic redox reaction that produces protons, lowering the local pH. This pH shift below the isoelectric point of the enzyme causes the protonation of the protein surface amino groups, as revealed by zeta-potential measurements. Thus, a more asymmetric diode-like behavior arises. The increase of anion-driven ionic current could be detected even though the D-glucose concentration was as low as  $1 \times 10^{-9}$  M. A tip diameter of 30 nm was found to present the best sensing capability. On the other hand, no significant variation was observed when L-glucose was added, proving the enantiomeric selectivity.

More recently, a different coupling mechanism was employed for a urea nanochannel sensor using urease.<sup>[216]</sup> A weak polyelectrolyte was employed as reactive signal amplifier. Firstly, the electrostatic assembly of poly(allylamine) (PAH) on the etched bullet-like PET nanochannels was produced and then the urease was adsorbed on the PAH-modified channel. Urease catalyzes the hydrolysis of urea into ammonia and carbon dioxide causing a local pH increase and, consequently, a decrease in the protonation degree of the polyamine confined in the nanochannel, i.e., a diminution of positive charges. Thus, the local pH change is amplified by the presence of the

weak polyelectrolyte. Then, the urea concentration-dependent changes in the surface charge can be read out as a decrease in the rectification factor, which characterizes the asymmetric  $I$ - $V$  curves of the diode-like iontronic behavior of the functionalized nanochannel (Figure 18). This mechanism was demonstrated to be reversible and reproducible and the developed biosensing device was able to reach a limit of detection of  $1 \times 10^{-9}$  M.

#### 5.6.2. Integrated Molecular Systems for Enzyme-Free Detection

A wide variety of approaches has been developed within the last years to convert the interaction with specific target molecules into iontronic readouts in nanofluidic channels. The following selected systems reflect the variety of building blocks and nano-architectonic strategies.

**Biochemical Sensing: Histidine.** Jiang and co-workers reported a simple enantioselective sensing device based on a  $\beta$ -cyclodextrin (CD)-modified nanochannel system, which presented selective recognition of histidine enantiomers.<sup>[217]</sup> For this purpose, mono-6-amino- $\beta$ -CD was attached to etched conical PET nanochannels by EDC/NHS chemistry (Figure 19a–c). When exposed to L-His in the micrometer range, the modified nanochannel presented selective binding of L-His, decreasing the cation-driven transmembrane ionic current. In contrast, no significant changes were detected when solutions of D-His or other aromatic amino acids were employed. Using the current changes of the high conductance part of the diode-like  $I$ - $V$  curve, a binding behavior on the amino acid concentration was obtained.

**Acetylcholine.** Wen et al. introduced *p*-sulfonatocalix[4]-arene (SCX4) to the surface of a single conical track-etched PET nanochannel, using layer-by-layer assembly to achieve the highly sensitive recognition of Ach.<sup>[134]</sup> Owing to its anionic groups, SCX4 is an ideal host molecule to bind cationic organic guests in aqueous solution. SCX4 was adsorbed on the PEI-modified etched surface of the nanochannels by electrostatic interactions. After the adsorption of SCX4, the  $I$ - $V$  curve showed an Ohmic behavior, indicating a nearly null surface charge. The presence of Ach in the electrolyte solution led to an obvious change in the



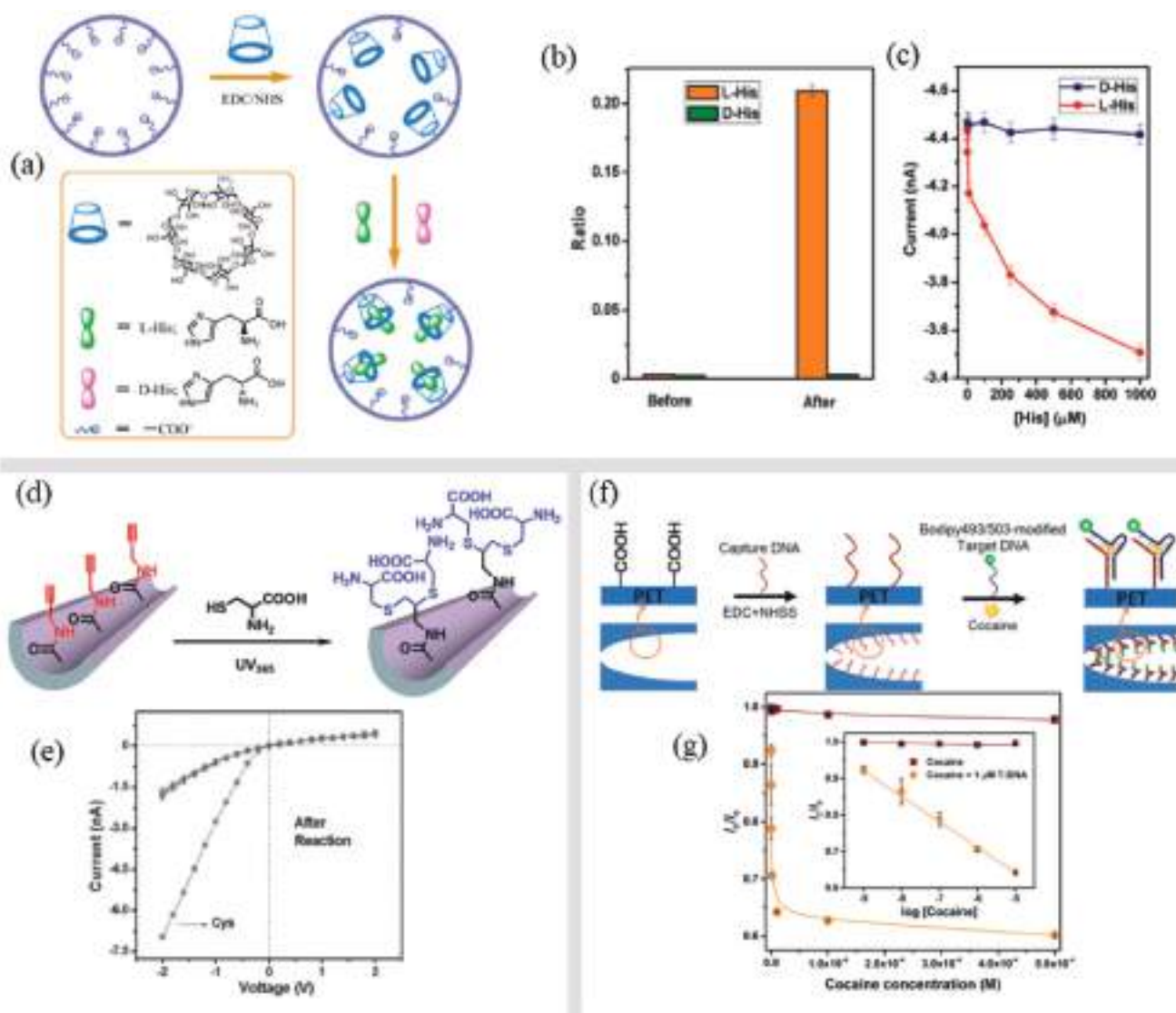


**Figure 19.** Biomolecules and drug sensing. a) Scheme of the functionalization with  $\beta$ -CD (host) and operation mechanism of the enantioselective histidine(guest)-responsive nanochannel. b) Current change ratios in the presence of  $1 \times 10^{-3}$  M D-His and L-His before and after the functionalization with  $\beta$ -CD. c) Current–concentration profiles of the  $\beta$ -CD-modified nanochannel showing the enantioselectivity of the nanofluidic device. a–c) Reproduced with permission.<sup>[217]</sup> Copyright 2011, American Chemical Society. d) Thiol-yne click reaction strategy for the development of cysteine-responsive nanochannels. e) *I*–*V* iontronic response after UV-induced functionalization. d,e) Reproduced with permission.<sup>[218]</sup> Copyright 2013, Wiley-VCH. f) Bullet-like nanochannel functionalization with ssDNA (capture) for cocaine detection. In the presence of the target DNA, a double strand is formed partially blocking the nanochannel. g) Current ratio with different concentrations of cocaine with and without the target aptamer. Linear relation in the inset proves the suitability of the proposed device for cocaine detection. f,g) Reproduced with permission.<sup>[219]</sup> Copyright 2018, American Chemical Society.

rectified ionic current, even at  $1 \times 10^{-9}$  M concentration. Due to the fact that each Ach molecule bears a positive charge, the formation of SCX4–Ach complexes prompts an increase in surface charge on the nanochannel walls with a concomitant effect on the rectification properties of the nanofluidic device. The current intensity corresponding to the high current branch steadily increased as Ach was added to the solution, following a Langmuir-type of binding dependence on the Ach concentration.

Cysteine. Sun et al. reported the fabrication of a nanochannel sensing platform displaying high Cys specificity and sensitivity.<sup>[218]</sup> The sensing mechanism relies on the formation

of selective covalent bonds by a photoinitiated thiol-yne click reaction and ultimately facilitates the detection of cysteine in complex matrices with no interferences.

The nanochannel walls are decorated with acetylene moieties and then under UV irradiation, the triple bond specifically reacts with cysteine (Figure 19d,e). The reaction of cysteine with the surface-yne groups confer negative charges to the nanochannel walls, as cysteine molecules are negatively charged under the working conditions (pH 7.38), and the appearance of negative surface charges triggers an enhancement of the iontronic response. Noteworthy, the high selectivity of this method

is not affected by the presence of higher concentrations of other amino acids and metabolites, even in urine samples.

**Uric Acid.** He et al. proposed a nonenzymatic route for sensing uric acid (UA) based on the application of glass capillary-based nanopores.<sup>[220]</sup> Glass nanopores were preconditioned with an ultrathin Au film, deposited by electroless plating, followed by the molecular assembly 2-thiouracil (2-TU). The experimental evidence indicates that hydrogen bonding interactions are responsible for the formation of UA-2-TU pairs or adducts on the nanopore walls, thus leading to changes in the ionic current. These changes in the magnitude of ionic current were employed for the detection of UA.

**L-Tryptophan.** The stereo-selective recognition of the L-enantiomer of tryptophan (L-Trp) amino acid was studied on conical PET nanopores by using several chemical modification steps.<sup>[221]</sup> In a first step the etched membranes were modified by dopamine (DOPA) polymerization. Then, the anchoring of bovine serum albumin (BSA) was achieved by Michael addition. BSA was proved to selectively bind the L-enantiomer of Trp. The selectivity was quantified in terms of the rectification factor. The nanopore was responsive to L-Trp in the 100  $\mu\text{m}$  nanopore was responsive to but only exhibiting a linear response in the millimolar range. Blank experiments confirmed that BSA-modified nanopores show no significant affinity toward phenylalanine (D-/L-Phe), D-tyrosine and D-tryptophan amino acids.

**Adenosine.** An adenosine-gated nanopore was built on PET membranes mimicking the adenosine receptors in living cells, which change their conformation after binding to adenosine allowing the cellular signaling.<sup>[222]</sup> In this case, an aptamer was assembled on a gold-modified PET single conical nanopore. The aptamer partially blocks the pore yielding low transmembrane current values (OFF state). The binding of adenosine to the aptamer moiety induces a conformational change that opens the pore (ON state). After adding adenosine deaminase to the solution, the adenosine is transformed into inosine, which is not recognized by the aptamer and the pore closes again. This results in a reversible gating mechanism. The gating effect is enhanced in nanochannels with tip diameter about 20 nm, reaching ON/OFF factors higher than 600.

**Histamine:** A histamine sensor was developed based on a metal ion displacement mechanism using PET conical nanochannels modified with metal-nitrilotriacetic (NTA-Ni<sup>2+</sup>) chelates.<sup>[223]</sup> The chemical modification was accomplished by covalently grafting *N,N*-bis(carboxymethyl)-L-lysine (BCML) followed by exposure to Ni<sup>2+</sup> ions. BCML immobilization and ulterior Ni<sup>2+</sup> ion complexation confer the nanochannel a given surface charge density. Then, when the (NTA-Ni<sup>2+</sup>)-modified pore is exposed to a histamine solution, the displacement of the surface complex formation equilibrium renders an increase in the negative surface charge by regeneration of free NTA moieties. High reversibility and low interference by other neurotransmitters was observed. Moreover, the increment of the negative surface charge on the concentration of histamine followed a binding isotherm, indicating that, in the timescale of the measurements, pseudo-equilibrium can be supposed and the histamine quantification can be effectively performed.

**Drug Sensing: Naproxen.** An innovative strategy for detecting chiral drugs using unmodified nanochannels was recently

presented.<sup>[224]</sup> The method is based on the use of *N*-acetyl-L-cysteine capped gold nanoparticles (NALC-AuNP) as chiral selectors for the enantioselective recognition of S-Naproxen (S-Npx) in the presence of R-Naproxen (R-Npx). When the conical etched nanochannel was exposed into  $1 \times 10^{-3}$  M R-Npx or S-Npx, the transmembrane ionic current remains the same. After injecting the NALC-AuNP in the working solution, the ionic current decreases, but this change is more marked in the presence of S-Npx. For instance, the transmembrane ionic current gradually decreases upon increasing S-Npx concentration (0 to  $1 \times 10^{-3}$  M), whereas it remains almost constant when the same experiment is carried out in the presence of R-Npx. The sensing mechanism has been ascribed to the preferred interaction between S-Npx and the NALC-AuNP through hydrogen bonds, which reduces the surface charge of AuNP causing aggregation more efficiently than in the case of the R-Npx (as proved by dynamic light scattering (DLS) measurements). As a consequence, the aggregates block the nanochannel more efficiently and the ionic current decreases more rapidly. The detection limit achieved by this method was  $1 \times 10^{-9}$  M.

**Inositol.** Inspired by Ca<sup>2+</sup> ionic channels, a biomimetic inositol phosphate-responsive nanopore device was built on AAO membranes.<sup>[225]</sup> Inositol phosphate (InsP) is a signaling molecule and can be specifically recognized in the nanomolar range by a *N*-isopropylacrylamide-co-4-(3-acryloylthioureido) benzoic acid copolymer (PNI-co-ATBA) by hydrogen bond formation with the ATBA moieties. The AAO nanochannels were chemically modified with the copolymer via SI-ATRP. The copolymer immobilized on the inner surface of the nanochannels becomes expanded by complexation with InsP, leading to a sharp decrease in the size of nanochannels, which further decreased the transmembrane ionic current (ohmic behavior). The effect was more pronounced for InsP than for other phosphate species.

**Cocaine.** A cocaine sensor based on an aptamer-modified nanochannel was recently reported.<sup>[219]</sup> Bullet-shaped PET single nanochannel walls were modified by anchoring a C-aptamer which is then recognized by cocaine and other target DNA aptamer (T-aptamer) (Figure 19f,g). The iontronic behavior appreciably changes in the presence of both cocaine and T-aptamer, but it remains the same when just one of them is present in the solution. The binding of both cocaine and T-aptamer molecules onto the C-aptamer anchors on the nanochannel wall led to a significant decrease in the effective pore size, thereby decreasing the transmembrane current and the rectification factor. The relative decrease in the transmembrane current at +2 V was linear on the logarithm of the cocaine concentration in the micromolar range up to  $1 \times 10^{-9}$  M (at fixed T-aptamer concentration). This effect was also selective toward cocaine over other similar drugs such as atropine and tropinone.

## 5.7. Iontronic Sensing of Specific Ions

Despite their small size, ions can effectively produce marked changes in the transmembrane conductance, as they are able to significantly alter the surface charge density of the nanochannels walls due to their intrinsic charge. By coupling the

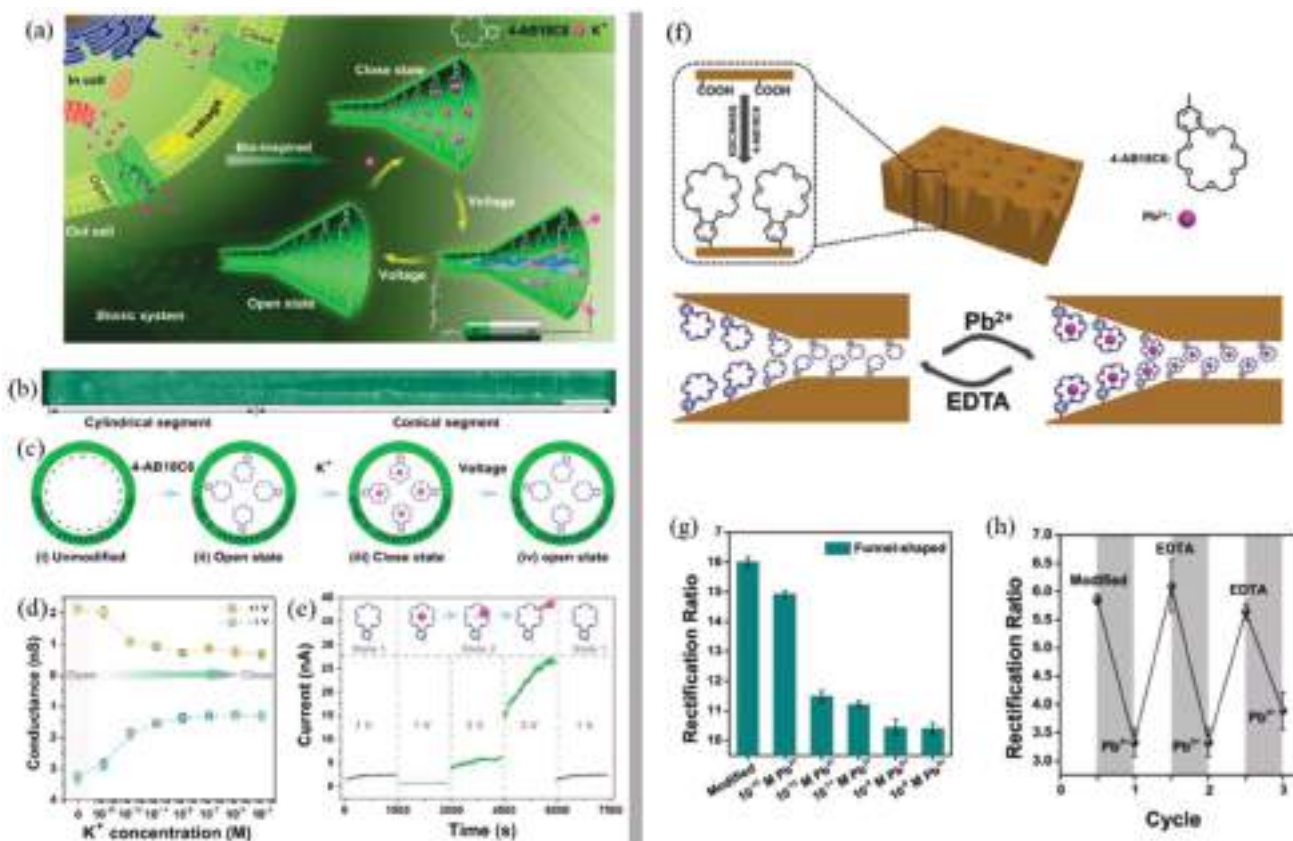


**Figure 20.** Crown moieties for ion detection. a) Scheme of the biomimetic voltage-responsive potassium-activated ionic gating in the 4-AB18C6-functionalized funnel-shaped nanochannels. b) Cross-sectional SEM image of a single nanochannel. c) Schematic representation of the sequential functionalization and voltage-induced gating. d) Dependence of the ionic conductance on the K<sup>+</sup> concentration and external voltage. e) Ionic current at different stages depicted in (c). a–e) Reproduced with permission.<sup>[228]</sup> Copyright 2017, American Chemical Society. f) Scheme of the Pb<sup>2+</sup>-gated 4-AB18C6-modified funnel-shaped nanochannels. g) Dependence of the rectification ratio on the Pb<sup>2+</sup> concentration in the sub-nanomolar range. h) Responsive switching ability of the 4-AB18C6-modified funnel-shaped nanochannels upon alternative addition of Pb<sup>2+</sup> and EDTA. f–h) Reproduced with permission.<sup>[229]</sup> Copyright 2018, Royal Society of Chemistry.

adequate chemical building blocks to the channel surface, the selective and efficient association of such a particular anion or cation can be performed. The following discussed systems illustrate the wide range of mechanisms employed in the last years for ion-induced gating and ion sensing in nanofluidic channels.

### 5.7.1. Crown Ethers for Specific Cation Recognition

Crown ethers are useful ligands (hosts) for specific cations.<sup>[226]</sup> Their selective cation binding properties are attributed to the molecular matching the cavity size and the corresponding cation diameter. Moreover, cations fitting into the crown ether cavity are further stabilized by interactions with the surrounding oxygen atoms. Therefore, several works have been focused on the use of ether crown moieties for detecting and sensing specific cations with nanofluidic channels. The following systems correspond to recent explanatory examples.

Na<sup>+</sup> and K<sup>+</sup>. In 2015, the selective detection of Na<sup>+</sup> and K<sup>+</sup> cations has been reported to be achieved by functionalizing etched polyimide single conical nanochannels with 4'-aminobenzo-15-crown-5 and 4'-aminobenzo-18-crown-6, respectively.<sup>[227]</sup>

The molecular recognition of these alkaline ions leads to the formation cationic complexes on the nanochannel walls, thus resulting in changes in surface charge, wettability and effective pore size. However, the iontronic behavior was different for each cation due to the different affinities. Na<sup>+</sup>-activated nanochannels exhibited an “ON/OFF” gating of the nanochannel, whereas K<sup>+</sup>-activated nanochannels were able to switch the rectified ionic transport between cation- and anion-driven conditions.

K<sup>+</sup>. In another work, an ultrasensitive K<sup>+</sup>-driven gated nanochannel system was recently prepared on PET funnel-shaped nanochannels by covalent crosslinking of 4'-aminobenzo-18-crown-6 molecules (EDC/NHSS) (Figure 20a–e).<sup>[228]</sup> By previous incubation in a K<sup>+</sup>-containing solution, the surface charge and wettability of the nanopore surface is changed a consequence of the irreversible potassium binding, altering the ionic transport, even when measured in a K<sup>+</sup>-free buffer. However, the original response can be then restored by applying high transmembrane potentials, yielding a potential-driven K<sup>+</sup> release. The system was proved to be sensitive down to 10<sup>-15</sup> M with a reversible response to cycling between K<sup>+</sup>-bound closed (OFF) and K<sup>+</sup>-free open states (ON).



Cs<sup>+</sup>. A cesium-sensitive nanochannel system was presented based on the decoration of an asymmetric PET nanochannel with a calix[4]arene-crown derivative, which selectively recognizes Cs<sup>+</sup> by host–guest interactions.<sup>[230]</sup> For that purpose, a NH<sub>2</sub>-terminated derivative of a calix[4]arene-crown was synthesized and then coupled to the remaining carboxylate groups of etched PET single pore nanochannels. The experimental data revealed that in the presence of Cs<sup>+</sup> ions the transmembrane current increases due the formation of positively charged calix-crown–Cs<sup>+</sup> complexes on the pore surface. In this working principle, the complexation process produces an asymmetrical distribution of cationic groups into the asymmetric nanochannel and triggers an inversion of the rectification behavior. These ideas were also supported by theoretical calculations. On the contrary, other alkali cations did not appreciably change the diode-like behavior, proving the selectivity.

Li<sup>+</sup>. A lithium-sensitive nanofluidic device was recently reported.<sup>[231]</sup> In this case, the aminoethyl-benzo-12-crown-4 (BC<sub>12</sub>C<sub>4</sub>–NH<sub>2</sub>) was synthesized and crosslinked to the carboxylate groups of the etched PET conical nanochannels (EDC/PFP chemistry). The BC<sub>12</sub>C<sub>4</sub> specifically binds Li<sup>+</sup> by supra-molecular host–guest interactions. The generation of positively charged B<sub>12</sub>C<sub>4</sub>–Li<sup>+</sup> complexes on the pore surface induces a diode-like behavior. The nanofluidic device is able to recognize the lithium ion in the micromolar to millimolar range even in the presence of high concentrations of potassium ions.

Pb<sup>2+</sup>. A system sensitive toward Pb<sup>2+</sup> was prepared on funnel-shaped multipore PET nanochannels (Figure 20f–h).<sup>[229]</sup> The nanochannels were chemically modified by crosslinking (EDC/NHSS) of 4'-aminobenzo-18-crown-6 (4-AB18C6) a Pb<sup>2+</sup> chelating agent. The surface charge of the modified nanochannel is negative, so current rectification is developed. Upon addition of Pb<sup>2+</sup> to the electrolyte solution, the ions are specifically bound to the crown moieties, decreasing the net negative charge and the corresponding rectification factor. The effect could be appreciated even in the presence of 10<sup>–15</sup> M Pb<sup>2+</sup> concentration and it was more marked than in the presence of other divalent cations, proving the selectivity. Also, the addition of EDTA restored the unbound situation, showing an excellent reversibility. Additionally, this novel solid-state nanopore geometry was shown to be more stable than the conical ones.

### 5.7.2. Other Molecular Mechanisms for Ion Sensing

In this subsection, we present other strategies developed within the last years for performing the selective detection and/or quantification of specific simple ions. The sensors range from simple nude etched polymer nanochannels<sup>[232]</sup> to channels functionalized with more sophisticated integrated molecular systems.<sup>[233]</sup>

Zn<sup>2+</sup>. In 2010, Jiang and co-workers reported a novel zinc-activated ion nanochannel obtained by immobilizing zinc finger peptides (EDC/NHSS chemistry) into a single conical PET nanochannel.<sup>[234]</sup> One of the main characteristics of zinc finger peptides/proteins is their ability to switch their conformation according on the presence of zinc ions. In the absence of zinc the transmembrane ionic current recorded is

small (“OFF state”); however, in the presence of zinc, the peptidic architecture switches to a finger-like conformation, promoting an increase in the effective channel diameter (“ON state”). As expected, due to the molecular size of the switchable “gatekeepers” this interesting gating effect becomes more pronounced in the case of nanochannels with tip diameters ≈30 nm.

Ca<sup>2+</sup>. Some years later, Zhai and co-workers presented a calcium-gated nanofluidic system based on the incorporation of calcein to conical PET nanochannels.<sup>[235]</sup> Calcein (2',7'-bis[*N,N*-bis-(carboxymethyl) aminomethyl]fluorescein) is a tetradentate ligand with four carboxyl groups, which chelate Ca<sup>2+</sup> with high efficiency. One of the carboxylic groups in calcein was employed for covalent attachment to the nanopore surface employing ethylenediamine as linker in a two steps functionalization (EDC/PFP chemistry). In basic solutions, the carboxylate groups confer a high negative surface charge to the pores, yielding markedly asymmetric current curves (cation-driven current, diode-like behavior). In the presence of calcium, the formation of chelates with the bound calcein moieties reduces the negative surface charge and, concomitantly, the transmembrane cation-driven current and the rectification efficiency, with a sensing range down to 0.01 × 10<sup>–3</sup> M.

Fluoride. The phenyl boronic moiety does not only react with sugars, it also efficiently reacts with fluoride. This phenomenon has been also employed in the construction of fluoride-gated nanochannels. Jiang and co-workers prepared a fluoride-responsive system by crosslinking of 4-aminophenylboronic acid (4APBA) on single conical polyimide nanochannels (EDC/NHSS).<sup>[236]</sup> The 4APBA immobilized on the nanochannels can form negatively charged tetrahedral fluoride adducts, including mono-, di-, and trifluoride adducts upon addition or removal of fluoride in solution (Figure 21a–c). The specific responsiveness of 4APBA to fluoride was proved by <sup>19</sup>F-NMR and UV–vis and fluorescence spectroscopy. The etched single polyimide nanochannel presented rectification behavior in 0.1 M NaNO<sub>3</sub> at pH 6.77 owing to its negative charge. After 4APBA functionalization, transmembrane current decreased markedly owing to the change in surface charge, effective pore size, and wettability. When 100 × 10<sup>–9</sup> M fluoride was added, the current increased again due to the F<sup>–</sup> binding to boron, which increases the negative surface charge and changes the surface wettability. This gating mechanism was not observed with chloride, bromide or iodide, proving the selectivity of the borate–fluoride interaction. Moreover, when soaking in NaOH solution, fluoride is replaced by –OH again, allowing the evaluation of the gating cycling performance, displaying high stability and reproducibility.

By designing a specific host molecule, Nie et al. created other fluoride sensor based on a nanofluidic channel.<sup>[238]</sup> They designed and synthesized 1,3-dipropargylaza-*p*-tert-butylcalix[4] crown (C4CE), in which the alkynyl group served for anchoring to the nanochannels and the three –NH– groups were used as the recognition unit for F<sup>–</sup> as hydrogen-bonding donors. Thus, the ionic recognition is not produced by the crown-ether (as in the case of cations) but by an external functional group. In a first modification step, azidopropan-1-amine (APAM) was attached to the surface of a single conical etched PET nanochannel (EDC/NHS coupling). Then the C4CE was coupled by



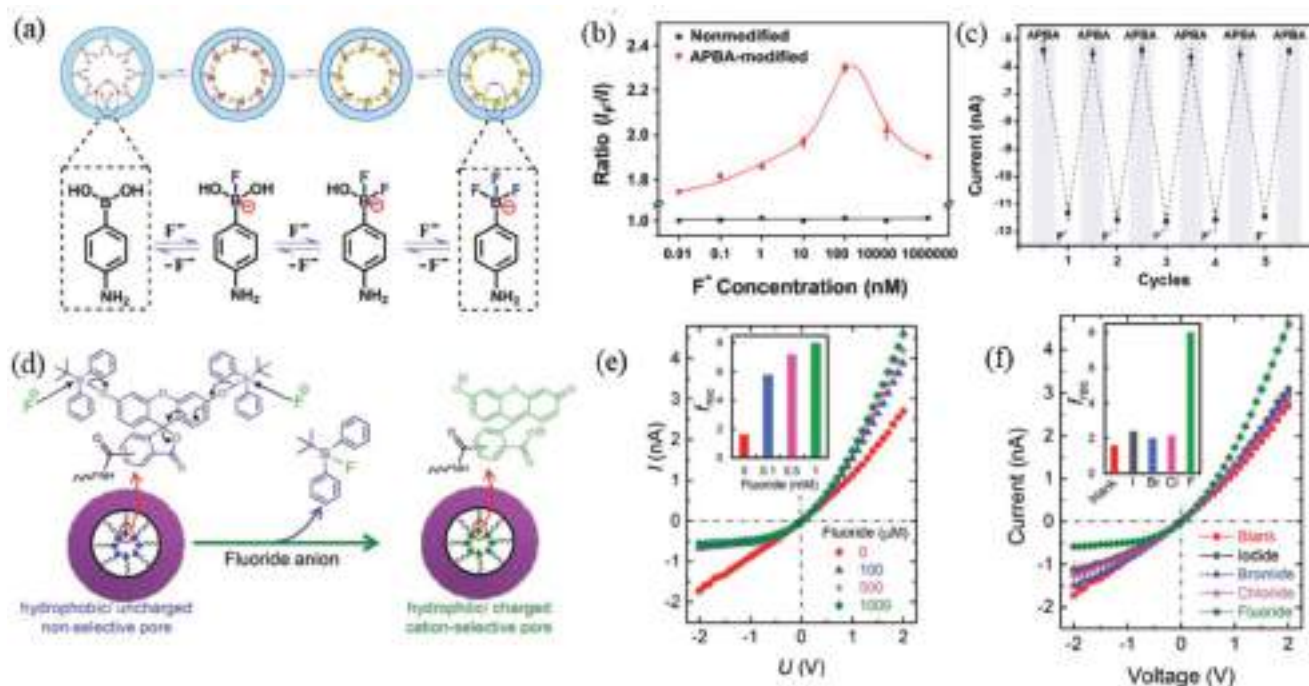


**Figure 21.** Fluoride responsiveness. a) Schematic representation of the reversible switching among the fluoride binding states in the APBA-functionalized nanochannels. b) Dependence of the change in the ionic current as a function of the fluoride concentration. c) Responsive switchability of the fluoride-driven ionic gate in terms of the ionic current at  $-2$  V upon addition and removal of fluoride. a–c) Reproduced with permission.<sup>[236]</sup> Copyright 2014, American Chemical Society. d) Scheme of the mechanism operating in the fluoride-responsive nanochannels. Fluoride removes the tert-butyl-diphenylsilyl (TBDPS) groups by cleavage of the Si–O bonds. e)  $I$ – $V$  iontronic response for increasing fluoride concentrations. f)  $I$ – $V$  iontronic response in the presence of different anions showing the nanofluidic device selectivity toward fluoride. d–f) Reproduced with permission under the terms of the CC-BY Creative Commons Attribution 3.0 Unported License (<https://creativecommons.org/licenses/by/3.0/>).<sup>[237]</sup> Copyright 2016, The Royal Society of Chemistry.

the click chemistry of the azide group ( $-N_3$ ) and the alkynyl group ( $-C\equiv CH$ ).

The reported experimental observations indicated a remarkable change in the ionic current upon adding  $F^-$  ions to the supporting electrolyte (0.1 M KCl). An increase in the concentration of  $F^-$  ions was manifested as an increase in the transmembrane current due to generation of negative surface charges on the nanochannel walls. The specificity of this approach was corroborated by additional blank experiments confirming that the exposure to other ions did not generate the same iontronic response. The detection limit was about  $1 \times 10^{-6}$  M and the dependence of the rectification factor on the fluoride concentration was satisfactorily fitted to a Langmuir isotherm, suggesting a direct relationship with the nanochannel surface charge density. Desorption of fluoride was efficiently performed by using  $Ca^{2+}$  solutions, providing a recycling mechanism.

The use of nanochannels modified with silylated fluorescein moieties was proposed by Ensinger and co-workers as a strategy to fabricate a fluoride-sensing nanofluidic device. (Figure 21d–f).<sup>[237]</sup> This route relies on harnessing the characteristics of fluorescein molecules derivatized with tert-butyl-diphenylsilyl (TBDPS) groups. By using simple coupling chemistries the derivatized fluorescein ( $Fcn$ -TBDPS- $NH_2$ ) molecules were grafted to the walls of etched PET nanochannel. In the presence of fluoride, the uncharged TBDPS moieties are removed by the fluoride-induced cleavage of the silicon–oxygen bond, thus leading to the generation of anionic groups on the nanochannel surface. This induces a cation-driven diode-like behavior in the

originally ohmic neutral  $Fcn$ -TBDPS-functionalized nanochannels. On the other hand, no significant changes were observed in the presence of other anions, proving the selectivity of the gating mechanism toward fluoride ions.

**Chloride.** A chloride-gated nanofluidic system was built on polyimide nanochannels by a two-step functionalization with 5-aminoisophthalic acid (AIPA) and 4-butylbenzenamine (BBA).<sup>[239]</sup> The di-isophthalamide moiety acts as a chloride binding site with high selectivity toward other halogen anions. The  $I$ – $V$  curves measured in  $NaNO_3$  show that in the presence of chloride there is an important increase in the cation-driven current and a diode-like behavior arises as a consequence of both the increase in the surface charge and the hydrophilicity of the nanopore walls. By using solutions with and without chloride, it is possible to reversibly achieve ON and OFF states respectively.

**Pyrophosphate.** The selective detection of pyrophosphate (PPi) was achieved on a Zn-complex modified single conical nanopore.<sup>[240]</sup> To achieve this goal, the PET-etched pore surface was chemically functionalized by a binder with two di(2-picolyl)amine [bis(DPA)] groups via carbodiimide coupling chemistry. After complexing two  $Zn^{2+}$  ions, this moiety can selectively bind pyrophosphate anions. The successive modification steps were followed by the change in the  $I$ – $V$  characteristics and the results were supported by numerical calculations (PNP model), revealing that the initial positive surface charged of the bis( $Zn^{2+}$ -DPA) complexes is inverted by the PPi binding in the sub-nanomolar range, with a saturation behavior above

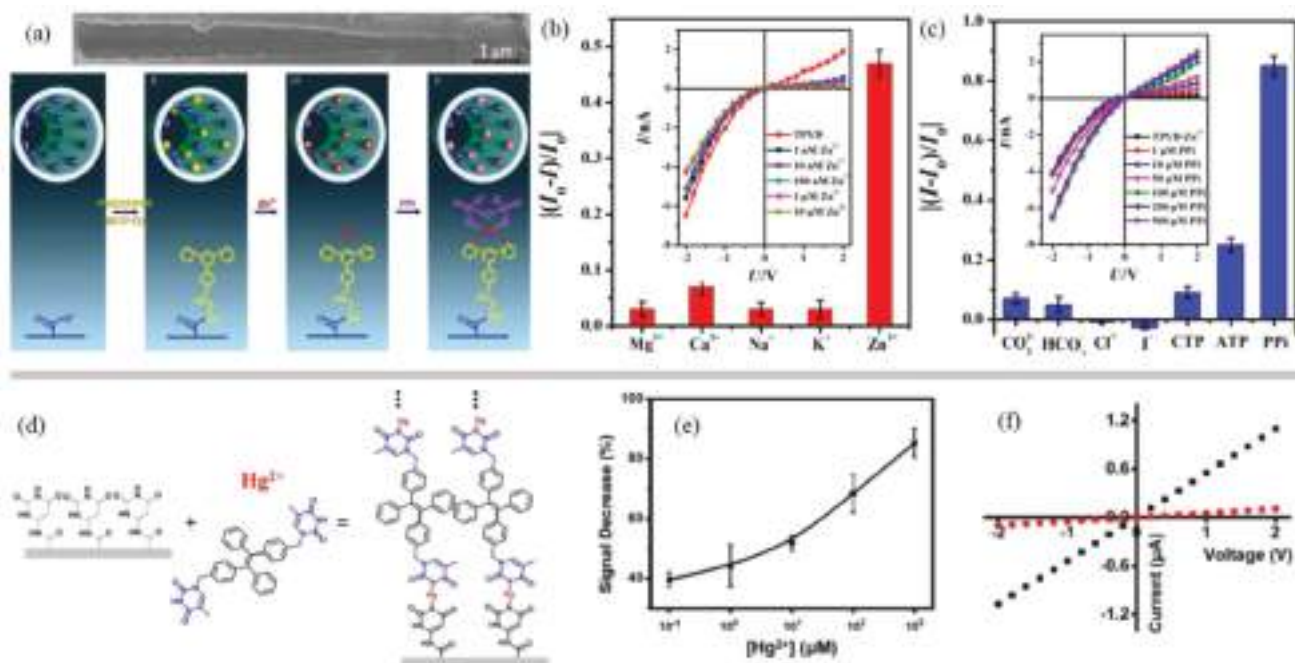


**Figure 22.** Ion sensing. a) SEM image of a single nanochannel cross-section and scheme of TPYD functionalization and mechanism of Zn<sup>2+</sup> and PPI selective recognition. b) Selectivity toward Zn<sup>2+</sup> in terms of the relative change of the iontronic response and *I*–*V* response for increasing Zn<sup>2+</sup> concentrations (inset). c) Selectivity toward PPI in terms of the relative change of the iontronic response and *I*–*V* response for increasing PPI concentrations (inset). a–c) Reproduced with permission.<sup>[241]</sup> Copyright 2017, Wiley-VCH. d) Scheme of the formation process of the chemical complexes between the TPE-2T and Hg<sup>2+</sup> on 6-aminouracil-modified nanochannels. e) Dose–response toward Hg<sup>2+</sup> in terms of the iontronic current at 2 V. f) *I*–*V* iontronic response of 6-aminouracil-modified cylindrical multipore membrane before (squares) and after (circles) adding Hg<sup>2+</sup> and TPE-2T to the electrolyte solution. d–f) Reproduced with permission.<sup>[233]</sup> Copyright 2016, American Chemical Society.

$1 \times 10^{-6}$  M. No changes are observed when other similar phosphate anions are added nor in the absence of Zn<sup>2+</sup> in the complex, proving the high selectivity of this system.

The sequential determination of Zn<sup>2+</sup> and pyrophosphate was then proposed based on the EDC/NHSS chemical modification of conical PET single nanochannels with a chelating agent (*N'*-[4-[(2,2':6',2''-terpyridine)-4-yl]benzyl]ethane-1,2-diamine, TPYD) in other work by Jiang and co-workers (Figure 22a–c).<sup>[241]</sup> The TPYD molecule selectively recognizes zinc among other cations and then the zinc coordinated to TPYD is employed for the binding of pyrophosphate. The TPYD-functionalized nanochannel inner surfaces are initially negative and then the surface charge is reduced by Zn<sup>2+</sup> coordination, which decreases the current rectification factor. This allows detecting the presence of Zn<sup>2+</sup> ions in the nanomolar range. Then, when a Zn-containing TPYD-functionalized nanochannel is exposed to pyrophosphate anions in solution, the rectification factor increases again as a consequence of the increment in the negative surface charge, allowing the detection of PPI selectively in the presence of a variety of anions in the micromolar range. Although the selective detection of both Zn<sup>2+</sup> and PPI was proved by changes in the rectification factor, no analytical quantifications were reported.

Cr<sup>3+</sup>. Zhai et al. proposed the use of unmodified asymmetric single pore PET nanochannels for the sensing of Cr<sup>3+</sup>.<sup>[232]</sup> After etching, the internal surface of the membrane is grafted with a high density of carboxyl and hydroxyl groups. At near neutral pH, bare nanochannels present highly asymmetric *I*–*V* curves

(cation-driven rectification behavior) due to their high negative surface charge. In the presence of Cr<sup>3+</sup>, both the current intensity and the rectification factor decrease as a consequence of the ion binding. Monitoring the changes in the rectification factor, a detection limit of  $16 \times 10^{-9}$  M was obtained. The authors also showed that the lack of selectivity inherent in the pristine etched nanochannel can be overcome by the addition of a chelator with a strong binding affinity toward interfering metal ions instead of Cr<sup>3+</sup>. Thus, the selective detection of Cr<sup>3+</sup> in the presence of EDTA at pH 8 was possible as the Cr<sup>3+</sup> chelation by EDTA was weaker than the chelation by the –COOH groups on the nanopore surface.

Fe<sup>3+</sup>. Recently, the detection of Fe<sup>3+</sup> was reported in funnel-shaped PET nanochannels functionalized with DOPA by crosslinking to the COOH groups of the etched channels (EDC/NHS chemistry).<sup>[15]</sup> By increasing Fe<sup>3+</sup> concentrations, different Fe<sup>3+</sup>–DOPA chelates are formed in the channel, affecting the wettability and charge distribution, thus inducing changes in the iontronic behavior. By employing a narrow cylindrical segment (diameter close to 10 nm) as the critical section, they were able to reach ultratrace level (down to  $10^{-12}$  M) of detection. The chelates can be then dissociated by adding EDTA to the solution, which forms a more stable complex with Fe<sup>3+</sup>. Then, responsive switching was achieved by addition and removal of Fe<sup>3+</sup>, with intermediate immersions in EDTA solutions.

Hg<sup>2+</sup>. Xu et al. proposed a novel method named dual-signal-output nanopore system for Hg<sup>2+</sup> detection.<sup>[233]</sup> For this purpose, they synthesized a complex molecule containing two

thymine moieties: 1,1'-(((1,2-diphenylethene-1,2-diyl)bis(4,1-phenylene))bis(5-methylpyrimidine-2,4(1H,3H)-dione, TPE-2T. This molecule forms a special chelate complex due to the linkage between thymine and  $\text{Hg}^{2+}$  and presents aggregation-induced emission, so its formation can be also monitored by fluorescence spectroscopy.

Firstly, multiple etched cylindrical PET nanochannels were modified with 6-aminouracil by EDC/NHSS chemistry as capture probe. Then, in the presence of low concentrations of  $\text{Hg}^{2+}$  and TPE-2T, the formation of  $(\text{TPE-2T-Hg}^{2+})_n$  complexes anchored to the nanochannel surface takes place (Figure 22d–f). This aggregation leads to the reduction of the nanochannel effective diameter, which can be monitored by a decrease in the transmembrane conductance (denoted as “plug”). Moreover, the nanochannels can be unplugged by adding  $\text{S}^{2-}$  anions, which breaks the aggregates by inducing  $\text{HgS}$  precipitation. In that way, they could not only perform reversible plug-unplug processes, but also achieve successive reliable  $\text{Hg}^{2+}$  calibration curves using the same membrane.

$\text{Cu}^{2+}$ . More recently, a  $\text{Cu}^{2+}$  sensitive nanofluidic device was prepared by functionalization of porous AAO membranes with polyglutamic acid (PGA) by simple adsorption.<sup>[242]</sup> Copper ions can form  $\text{Cu-PGA}$  complexes with PGA due to the interaction with the oxygen and nitrogen atoms of the carboxyl and amide groups, respectively. In addition, it was recently confirmed the existence of sub-nanometric ion channels in the barrier layer of the AAO membranes.<sup>[243]</sup> This provides a strong geometry-asymmetry, which results in unique ionic rectification phenomenon. Thus, the PGA-modified membrane presented a highly asymmetric transmembrane current behavior owing to its high negative surface charge. However, in the presence of  $\text{Cu}^{2+}$ , PGA chelates with the positive charge of  $\text{Cu}^{2+}$ , causing a decrease of the transmembrane current. Although the decrease is more pronounced for high copper concentrations, the detection limit is as low as femtomolar range. By lowering the pH, the interaction between  $\text{Cu}$  ions and PGA can be dissociated, providing a reutilization mechanism, with good reversibility. Even the  $\text{Cu}^{2+}$  determination in real blood samples was successfully performed.

### 5.8. Nanopores and Nanochannels Responsive to Physical Stimuli

The possibility of modifying iontronic signals upon exposition to physical stimuli presents great importance not only from the sensorics point of view but also for remote control devices based on nanofluidic channels. The transduction of environmental physical signals into changes in the transmembrane conductance or the symmetry of the iontronic behavior has been achieved by designing and constructing smart molecular systems coupled to nanochannels. In this last section, we review some recent clever strategies for conferring responsiveness toward physical stimuli to nanofluidic channels.

#### 5.8.1. Light-Driven Transformations and Photostimulated Processes

Several approaches have been addressed for incorporating light responsiveness to nanofluidic channels. A simple approach

reported involves the usage of a photoactive electrolyte.<sup>[244]</sup> Under UV irradiation, an additional proton dissociation is induced in the 8-hydroxypyrene-1,3,6-trisulfonate, shifting its charge from  $(-3)$  to  $(-4)$ . This increment in the net charge is possibly responsible for an exclusion effect in the tip of L-histidine-modified asymmetric PET nanochannels which, in turn, changes the transmembrane transport properties. In the absence of light, the equilibrium is returned to the formation of the  $(-3)$  species. Thus nanofluidic conditions can be switched between dark and light in a reversible way.

Another reported example of light responsiveness was based on the functionalization of asymmetric PET nanochannels with a photolabile pyrene derivative.<sup>[245]</sup> The functionalized surface presents no charged groups, showing an ohmic iontronic behavior. However, after UV irradiation, the cleavage of the pyrene derivative is produced yielding a carboxylate surface group and releasing the pyrene moiety. The appearance of a negative surface charge then induces a diode-like iontronic behavior. Of course, this light-induced gating mechanism is not reversible.

A different route for reversible light responsiveness is based on the coupling of light-dependent protonation equilibrium to the walls of the channels. Some years ago, for example, Zhang et al. employed nanochannels made of  $\text{TiO}_2$ , which is itself a photoactive material.<sup>[246]</sup> Under continuous UV light excitation, the photogenerated electrons are trapped by hydroxylated titanium surface inducing a negative surface charge. More recently, the effect of UV light on the nanochannels walls was also shown to produce charge alterations, but in a completely different system. In this case, a bioinspired photodriven ion pump system in which the cations flow against the electrochemical gradient (uphill) powered by the light was achieved in conical etched PET nanochannels.<sup>[247]</sup> Due to the UV photoabsorption of benzoic acid derivative dimers on the inner surface of the nanochannel, the irradiation induces the dissociation of the hydrogen bonds yielding more mobile charged groups.

A different approach is based on the functionalization of the walls of nonphotoactive nanochannels with molecules whose acid–base equilibrium is regulated by light. This is the case of track-etched polyimide nanopores modified with malachite-green derivatives<sup>[248]</sup> that upon exposure to UV light release hydroxide ions and the pore walls switch from neutral to cationic characteristics. This switch in the surface charge triggers the conductance, switching from “OFF” (ohmic behavior) to “ON” (anion-selective rectifying behavior) states. Interestingly, in the absence of UV irradiation, the nanochannel restores its nonselective, Ohmic behavior. Subsequent illumination/darkness cycles demonstrated that the molecular systems exhibit good photostability and reversibility.

In this line, light responsiveness has been also achieved by modification of the asymmetric PET nanochannels walls by a spiropyran derivative (EDC/NHS chemistry).<sup>[249]</sup> Under UV irradiation, the spiropyran molecule suffers a transition to an open structure, changing its state from a neutral hydrophobic molecule to a hydrophilic one with a phenolic function that can yield a negatively charged group at high pH. On the other hand, at low pH, the open form of the spiropyran presents a positive charge. The closed form can be restored by stopping the illumination, so the nanofluidic device presents a gating from low-conductance



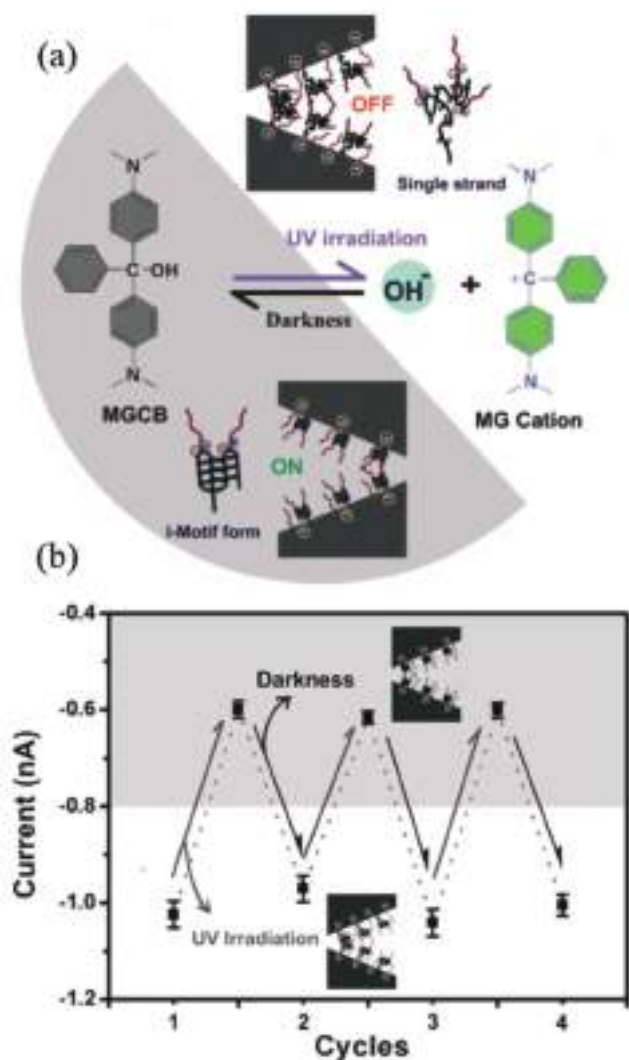


**Figure 23.** Photodriven gating. a) The photochemical reaction of MGCB produces  $\text{OH}^-$ , increasing the pH up on irradiation. The C4-DNA conformation switches between *i*-motif (ON) and single strand (OFF) depending on the pH of the solution. b) Reversibility of the ON/OFF response upon irradiation cycles in terms of the current at  $-1$  V. a, b) Reproduced with permission.<sup>[251]</sup> Copyright 2012, Wiley-VCH.

nonrectifying state (OFF state) to a high conductance diode-like behavior (ON state) under UV illumination. Additionally, due to the pH dependence of the charge of the open spiropyran, the gating mechanism results into cation-selective or anion-selective rectification regimes depending on the solution pH.

In a similar approach, multipored PET membranes were functionalized with spiropyrans coupled to long PEG chains. The purpose of using a photoactive/macromolecular architecture was to amplify the gating properties of the nanopore.<sup>[250]</sup> The characterization of the ionic transport properties showed that the nanopore switches from open to closed states upon UV and visible irradiation, respectively. The reported data indicate that not only the light-driven actuation of the spiropyrans but also the self-assembly of the PEG–spiropyran building blocks play an important role in the gating properties of the nanodevice.

Using a different actuation mechanism, Jiang and co-workers proposed the application of photoinduced pH changes coupled to C4-DNA motors as a methodology to create light-controlled nanochannels.<sup>[251]</sup> These DNA nanostructures form *i*-motif structures under slightly acidic conditions, but the structure switches to single strands under mild alkaline conditions. PET nanochannels modified with C4-DNA motors were coupled to malachite green carbinol (MGCB) as the photoinduced  $\text{OH}^-$  ion emitter. Under UV irradiation, the malachite green derivative releases  $\text{OH}^-$  ions, increasing the pH and triggering the conformational switch into single-stranded structures that, in turn, results in a decrease in the effective pore size and the transmembrane current. (Figure 23). In this way, illumination–darkness cycles can produce pH variations that yield a reversible modulation of the transmembrane current.

A similar mechanistic approach was then employed for a drug delivery proof of concept based on the photodriven gating in mesoporous silica nanoparticles.<sup>[252]</sup> In this case, the MGCB is also employed to produce pH local shift under UV irradiation. This pH increment induces a conformational change in the surface-bound ssDNA, triggering the pore opening.

In a more complex methodology, light-responsive biomimetic nanochannels were prepared using host–guest interactions between a negative pillararene (P6A) host and a positive azobenzene (AZO) guest on a conical PET single pore.<sup>[253]</sup> The inner wall of the nanochannel was decorated with the positively charged AZO molecules (EDC/NHS chemistry). The soluble negatively charged P6A can form the supramolecular inclusion compound with the *trans* conformation of AZO but not with the *cis* conformation. As the *cis*–*trans* transition can be reversibly promoted by light, the effective charge of the nanopores is also modulated by irradiation at the adequate wavelength. The positive surface charge of the AZO-modified nanochannel is reversed by formation of the supramolecular complex, so the alternation between cation-driven and anion-driven rectification states can be reversibly achieved by light (Figure 24a–c).

More recently, a completely different approach for light-responsive nanofluidic channels was presented based on the changes in the hydrophobicity of the nanochannels walls induced by light.<sup>[255]</sup> The walls of PET asymmetric channels were functionalized using azobenzene derivatives. Azobenzene derivatives can be reversibly isomerized between *cis* and *trans* conformations by UV (365 nm) and visible light (430 nm), respectively. This conformational change can be employed to control the inclusion (*cis* state) or exclusion (*trans* state) into  $\beta$ -CD via host–guest reactions. The binding of the CD, in turn, produces an increase in the hydrophilicity of the pores, inducing higher conductance. Thus, under visible irradiation and CD in the solution, an increment in the transmembrane current is obtained, yielding a light-dependent gating mechanism.

### 5.8.2. Reversible Physicochemical Transformations Triggered by Temperature Changes

Some years ago, the thermal effect on the molecular transport through ion-tracked PET membranes modified by grafting with PNIPAM hydrogel.<sup>[256]</sup> From that work, several groups have employed the thermoresponsiveness of PNIPAM to modulate



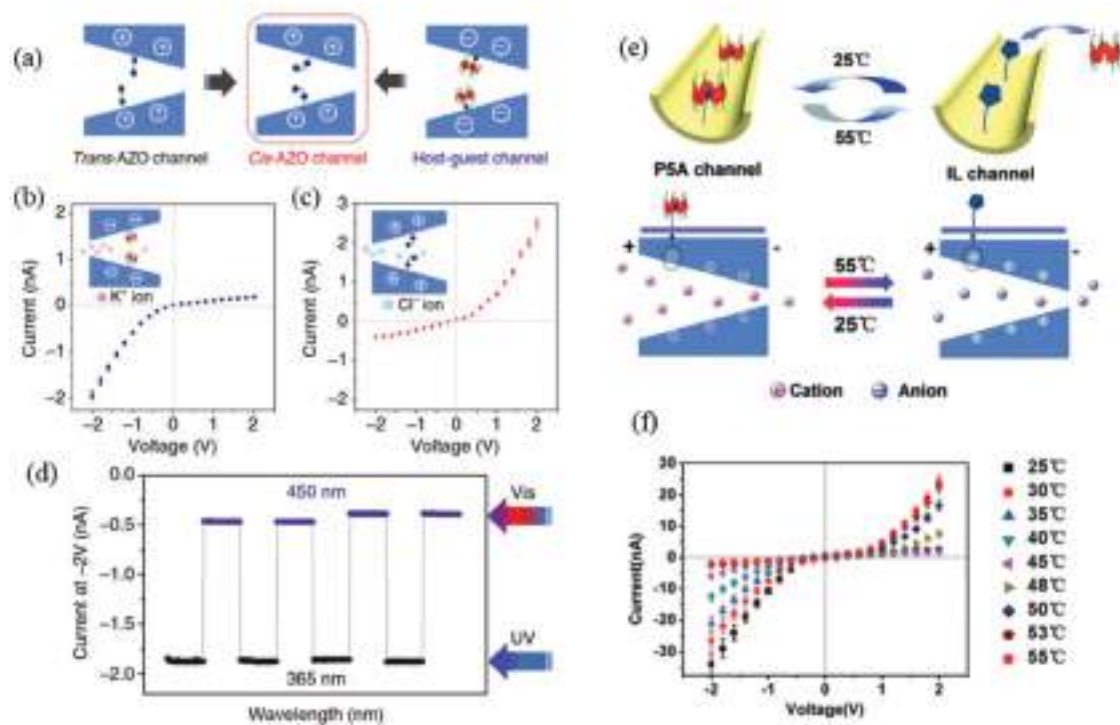


**Figure 24.** Light and temperature responsiveness by host-guest interactions. a) Scheme of the light-responsive nanofluidic device based on the functionalization with the photoactive AZO molecule (guest) and its host-guest interaction with P6A. b) *I*-*V* response (cation-driven current) after visible light irradiation. c) *I*-*V* iontronic (anion-driven current) response after UV light irradiation. d) Reversibility of the different states of the P6A-based nanochannels in terms of the ionic current as alternating irradiation cycles. a-d) Reproduced under the terms of the CC-BY Creative Commons Attribution 4.0 International License (<http://creativecommons.org/licenses/by/4.0/>).<sup>[253]</sup> Copyright 2017, The Authors. Published by Springer Nature. e) Scheme describing the thermosensitive nanofluidic device based on the interaction between P5A (host) and IL (guest). f) *I*-*V* iontronic response for increasing temperatures. e, f) Reproduced with permission.<sup>[254]</sup> Copyright 2017, Wiley-VCH Verlag GmbH & Co.

the ionic transport in nanochannels. Actually, the functionalization of nanochannels with PNIPAM has been extensively studied using different synthetic approaches,<sup>[153,257–260]</sup> even from a molecular dynamics point of view.<sup>[261]</sup>

Alem et al. studied the influence of temperature on the conductance of cylindrical etched nanopores on PET membranes modified with polymer brushes of PNIPAM.<sup>[257]</sup> As the temperature increases, the collapse of the brushes is produced and the effective diameter of the nanochannels increases, enhancing the ionic current. Yameen et al. described the modification of single polyimide track etched nanopores with PNIPAM brushes in order to create a thermoresponsive nanochannel, with reversible thermal gating in the 23–40 °C range.<sup>[153]</sup>

In a more recent work, PNIPAM chains were also crosslinked to the COOH surface groups of etched PET nanochannels (EDC/PFP chemistry), but using a grafting-to functionalization approach.<sup>[258]</sup> The reversible thermal collapse was reported to strongly modify the diffusion of small charged molecules, producing a gating effect.

A similar approach was reported by Guo et al., but employing the grafting-from functionalization of conical PET nanochannels by RAFT polymerization of PNIPAM brushes.<sup>[259]</sup> In this case, the transition between a rectifying state at temperature below 34 °C and a nonrectifying regime above 38 °C was observed as a consequence of the collapse of the polymer chains on the nanopores walls, which reduces the number of adsorbed anions.

More recently, the SI-RAFT polymerization of PNIPAM was also shown to produced temperature-gated cation-selective ionic transport in mesoporous SiO<sub>2</sub> thin films.<sup>[261]</sup>

Beyond the predominance of PNIPAM as an effector of thermal changes, some other physicochemical systems have been also utilized in temperature-responsive nanochannels. For example, asymmetric block copolymer modified nanochannel membranes with temperature and pH ion transport modulation have been prepared.<sup>[262]</sup> In this case, PET membranes were modified by coating with a PS-*b*-PDMAEMA copolymer, which presents a transition between extended and collapsed conformations modulated by both pH and temperature changes. After modification with the PS-*b*-PDMAEMA copolymer, the original diode-like behavior of the negatively charged nanopores becomes inverted and enhanced as a consequence of the introduction of the positive charges in the PDMAEMA moieties. At temperatures higher than 45 °C, the LCST transition yields a collapsed state that increased the effective nanochannel diameter, producing higher transmembrane currents.

In other example, the high temperature gating of conductance of AAO membranes was achieved by grafting of poly(benzyl methacrylate) (PBzMA) brushes by SI-ATRP.<sup>[263]</sup> In this work, (1-ethyl-3-methylimidazolium bis(trifluoromethanesulfone)imide ([EMIm][NTf<sub>2</sub>]), a room-temperature ionic liquid (RTIL), was employed as electrolyte. The PBzMA suffers a LCST transition in this RTIL at about 120–150 °C. At high temperature,

the collapsed polymer brushes efficiently block the transport of organic charge carriers through the nanochannels. However, once the nanochannels are closed they could not be immediately reopened to their original size by cooling down, showing a hysteresis in the swelling behavior. One advantage of this kind of thermally actuated nanofluidic system is that the operative range of responsiveness could be tuned by selecting the appropriate pair polymer–RTIL.

A completely new strategy to fabricate a temperature-sensitive nanochannel based on the introduction of molecular switches was presented recently.<sup>[254]</sup> For this purpose, a polyimide conical single nanochannel was decorated by anchoring a positively charged ionic liquid (IL) by EDC/NHS chemistry. On the other hand, a negatively charged pillar[5]arene (P5A) was specially synthesized. This P5A molecule can act as host for the IL and the resulting host–guest equilibrium is very sensitive to temperature changes. The supramolecular complex is formed at room temperature but it can be dissociated by increasing the temperature at 55 °C. The IL-modified nanochannel presents a positive surface charge, but it turns to negative by host–guest complex formation, changing the transmembrane transport from anion-driven to cation-driven. Thus, the P5A-based functional nanochannel acts as thermally driven molecular gates that can be controlled by simply tuning the working temperature in the range 25–55 °C (Figure 24e–f).

Using a hybrid strategy, Liu et al. created multifunctional nanochannels exhibiting four different states controlled by three independent stimuli: light, pH, and temperature.<sup>[264]</sup> The use of host–guest interactions between 3-amino-3-deoxy- $\alpha$ -cyclodextrin ( $\alpha$ -CD) and azobenzene was utilized to modify the responsiveness of poly-L-lysine (PLL) and PNIPAM. In this approach  $\alpha$ -CD is bound to the surface of cylindrical (34 nm diameter) etched PET channels (EDC/NHSS), whereas the polymers (PLL and PNIPAM) are grafted to azobenzene. The AZO-polymer binds to surface  $\alpha$ -CD reducing the transmembrane current, which can be restored to the original value by UV irradiation (the AZO group switches to the cis form, dissociating the host–guest complex). Concomitantly, as PLL adopts diverse conformations depending on the protonation state, the AZO–PLL modified nanochannel also presents pH responsiveness. On the other hand, in the case of the AZO–PNIPAM, the bound system presents thermal responsiveness provided by the LCST transition of PNIPAM. Due to the reversible coupling of the responsive AZO–polymers to the channels, the system was referred to as a plug and play template.

### 5.8.3. Transport Properties of Nanochannels Modulated by Magnetic Fields

A nanochannel modulated by moderate magnetic fields inspired by the homing-pigeon mechanosensitive ion channels was recently reported.<sup>[265]</sup> In pigeons, magnetite clusters associated to the membrane of certain neurons are responsible for the membrane deformation that causes the pore opening induced by changes in the magnetic field. Based on this idea, PET membranes containing conical single nanochannels were imprinted with a magnetic ink in order to generate magnetic bars. These bars allow transducing a magnetic field

into a mechanical deformation of the membrane increasing the opening of the nanochannel. In that way, the presence of a magnetic field induces an ON state that can be monitored by an increase in the transmembrane ionic current. In the absence of the magnetic stimulus, the pores partially close and the current diminishes (OFF state). The alternation ON/OFF was shown to be reversible and the magnet-induced gating was shown to be rapid and dependent on the magnetic field intensity. The magnetic field was shown to be responsible for a mechanical deformation of the PET membrane, without altering either the surface charge equilibrium or the hydrophobicity of the nanochannels. Based on this effect, the ionic current, the rectifying factor, and the conductance of the conical nanochannel could be reversibly changed by an external magnetic field.

### 5.8.4. Pressure-Sensitive Nanofluidic Devices

In close resemblance to mechanosensitive ion channels in which physical strain active signals, White and co-workers<sup>[266]</sup> developed nanofluidic devices whose ionic readout was modulated by exerting mechanical forces. By using cone-shaped glass nanopores, these authors showed that the ionic rectification can be controlled by varying the pressure. Experimental data revealed that under low ionic conditions the ionic rectification was determined by the rate of the pressure-driven electrolyte flow passing through the nanopore. Indeed, experiments performed with nanopores displaying different tip radii, 185 and 30 nm, indicated that the nanopore tip size was another important variable. This has been ascribed to the pressure-induced disruption of cation and anion distributions within the nanopore. When no mechanical stress is applied, the nanopore displays rectifying characteristics due to the presence of residual negative charges on the glass surface. Then, upon applying pressure across the larger pore (185 nm) the rectification disappears and an Ohmic  $I$ – $V$  response is observed (Figure 25). However, similar experiments performed on the smaller pores (30 nm) revealed no changes in the rectification properties. These results that the interplay between mechanical pressure and fluid dynamics in charged interfaces can be exploited to create pressure-responsive nanofluidic devices.

### 5.8.5. Nanofluidic Devices Controlled by Local Electric Fields

In some examples described in previous sections we have discussed the role of the applied potential in combination with other molecular entities, e.g., DNA of conducting polymers, as an interesting input to control the transport properties of nanochannels. These notions were further extended to create electrically addressable nanofluidic devices. Kalmán et al. reported the modification of a conical track-etched nanopore with a gold gate located in the tip.<sup>[76]</sup> The fabrication process involved the deposition of successive layers of titanium, gold, titanium, and then silicon dioxide. These authors reported that upon applying a negative voltage, a gating effect was observed for positive transmembrane voltages. Then, by changing the electric potential applied to the “gate” the ionic current passing through the pore was switched from a rectifying to an ohmic regime. The working principle of this device

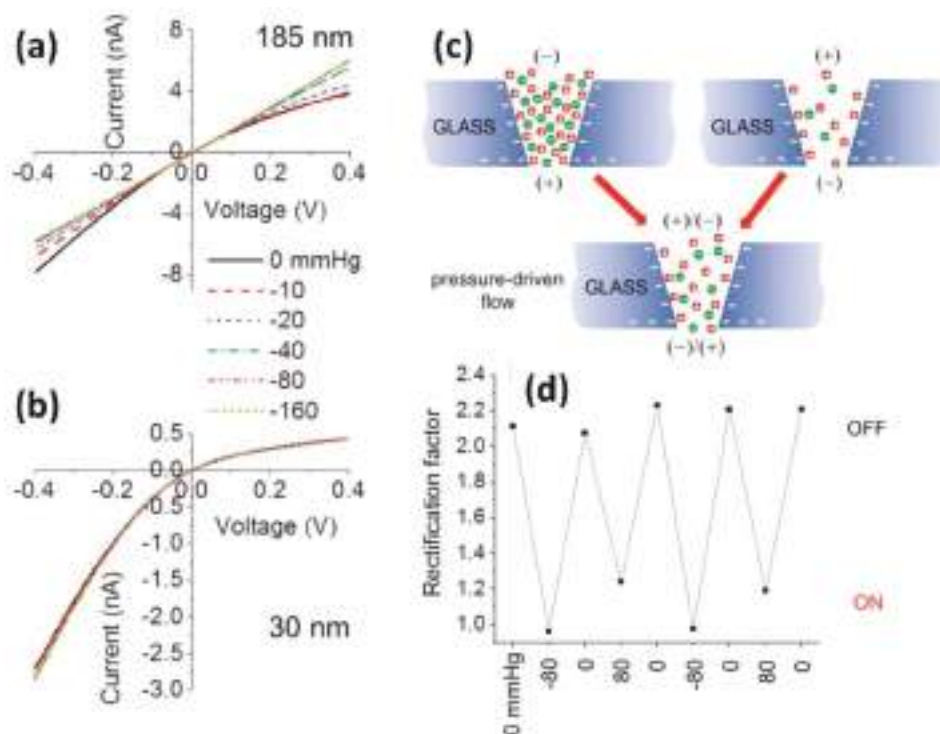


**Figure 25.** Pressure-driven actuation. a, b) Pressure-dependent  $I$ - $V$  responses of cone-shaped glass nanopores with radii of 185 (a) and 30 nm (b). Electrolyte: 0.01 M KCl solution containing  $0.1 \times 10^{-3}$  M PBS buffer (pH 7.3). c) Simplified illustration describing the ion distribution close to the tip of a negatively charged conical glass nanopore under different polarization conditions and in the absence and in the presence of pressure-driven flow. d) Variation in the rectification factor upon pressure switching. a-d) Reproduced with permission.<sup>[266]</sup> Copyright 2011, American Chemical Society.

relies on the fact that the local electric field generated by the gate alters the ionic distributions at the pore entrance with a concomitant effect on the transport properties.

## 6. Innovation, Technology Transfer and Commercial Aspects—From the Lab to the Marketplace

Each year, new technologies emerge and continue changing our lives. Sometimes, these technologies only provide incremental benefits, but on occasion, something new emerges that is truly disruptive and shifts the existing paradigm. For example, after several years of development, biological nanopores have entered the market resulting in substantial price reductions for direct DNA/RNA sequencing. Oxford Nanopore Technologies developed a portable, real time, long-read and low cost nanopore DNA sequencer device that has been designed to bring easy biological analyses. In March 2018, as a marginal note, it has been announced that Oxford Nanopore Technologies has raised \$140 million in new financing, with plans to use the proceeds toward commercial expansion efforts, including a new manufacturing facility, and the development of new products.<sup>[267]</sup>

Genia Technologies also developed a single-molecule and semiconductor based DNA sequencing platform using nanopore technology.<sup>[268–270]</sup> This nanopore-based platform offers

real-time, single molecule analysis requiring neither complicated optics or fluidics instrumentation nor labeling or amplification steps. Genia Technologies has been acquired by Roche in 2014,<sup>[271]</sup> and according to this pharmaceutical company the goal behind this acquisition is to introduce disruptive technologies to the market. In principle, the technology platform developed by Genia can significantly contribute to reduce the price of sequencing while increasing speed and sensitivity. In a similar way, Illumina has made substantial investments to obtain licenses and develop the nanopore sequencing technologies.<sup>[272–274]</sup> Even though these technologies and commercial products exclusively rely on the use of biological nanopores, a careful look at the invention claims listed in the corresponding patents reveals that these technologies are conceived to be compatible with solid-state nanopores. For instance, in some inventions QuantaPore<sup>[275]</sup> has resorted to hybrid nanopore platforms involving the combined use of biological and solid-state nanopores.<sup>[276]</sup>

Even though biological nanopores took the lead in commercial applications, solid-state nanopores are moving forward at a rapid pace and steadily reaching the marketplace. Two Pore Guys (now Ontera) has developed a fascinating technology that offers the promise of point-of-care liquid biopsy.<sup>[277]</sup> This technology is based on solid-state nanopores and can detect, differentiate and count molecules quickly and economically with a faster time to results than technologies currently being developed.<sup>[278–280]</sup> The developed platform detects and quantifies an array of molecules fully compatible with diagnostics,

food testing, agricultural and environmental applications. Along similar lines, Electronic Biosciences<sup>[281]</sup> is developing innovative nanopore platforms to create new technologies for molecular analysis.<sup>[282,283]</sup> These platforms are based on glass nanopore membranes originally developed in the laboratory of Prof. Henry White at the University of Utah and licensed for use by Electronic Biosciences.

It is no wonder that one of the most valuable assets of high technology companies is a comprehensive intellectual property portfolio—in which patents are key elements. It is widely accepted that a patent portfolio may be used for a variety of business objectives, such as bolstering market position, demonstrating a high level of expertise, protecting research and development efforts, generating revenue, as well as encouraging favorable crosslicensing or settlement agreements.

At the same time, we should note that patenting rates and patent propensity are currently used as proxies for measuring technological innovations in a particular field. Or, in other words, both the scientific community and the technological world recognize that patents provide a fairly good—although not perfect—representation of innovation activities.

The increasing number of patent applications filed by large companies reflects the involvement of the industry and shows their interest in converting interesting discoveries in solid-state nanopores into innovation and exploiting them commercially. Companies such as IBM,<sup>[284,285]</sup> Intel,<sup>[286]</sup> Agilent Technologies,<sup>[287,288]</sup> Roche,<sup>[289]</sup> and Samsung<sup>[290,291]</sup> have filed patent applications related to fabrication, functionalization, measurement, and applications of solid-state nanopores. In this regard, a special mention must be made to the achievements of Oxford Nanopore Technologies in terms of development and commercialization of DNA/RNA sequencing equipment.<sup>[292]</sup> As a pioneer in nanopore technologies, this company has been playing a leading role in this emerging market area since its foundation in 2005 and, at the moment, this is the only company that has been successful in commercializing nanopore-based platforms for single molecule sensing.

With the recent advances in DNA sequencing and the concomitant positive impact on biotechnology, solid-state nanopore devices received ample attention from industry as a potential source of commercial success. Just to put things into context, the disruptive effect of nanopores on DNA sequencing technologies could be compared to the revolutionizing impact of integrated circuits on electronics. With this commercial potential, it is no exaggeration to say that nanopores are poised to become one of the most dynamic segments of the global biosensors market.

## 7. Conclusions and Outlook—Unlocking Untapped Potential

“If we are to achieve things never before accomplished we must employ methods never before attempted”

Francis Bacon

During the past decade, solid-state nanopores have gained a particular relevance as a new class of devices offering a new dimension in the design of advanced platforms for nanofluidic applications. Solid-state nanopores have now come a long way

and borne many fruits. Today we have a mature discipline whose high standards are challenging to meet. Yet, it represents a unique and versatile toolbox to construct nanofluidic platforms for multiple applications.

There has been a continuous avalanche of growth and development in the science and technology of solid-state nanopores and device applications. The thrust of the advances has involved the improvement of our understanding of the physics of nanofluidic devices as well as an increased mastery in the design, construction and functionalization of inorganic and polymeric nanochannels of different dimensions.

Over the past decade, research on solid-state nanopores has evolved significantly from curiosity-driven research to practical applications. Indeed, the patent applications filed by large companies reflect the involvement of the industry and show the potential commercial value of solid-state nanopores and nanochannels.

Advances in the molecular functionalization and surface engineering of nanopore and nanochannels walls have made it possible to produce functional heterostructures in nanofluidic devices exhibiting engineered ion transport properties that are not available in nature. Concomitantly, advances in the fabrication of nanopores, nanochannels and nanopipettes of differing structural properties have provided new opportunities for technological innovation in nanofluidics (**Figure 26**). These fabrication technologies, taken jointly with versatile functionalization techniques have facilitated the development of a number of high performance nanofluidic devices displaying fast processing capabilities for reliable transduction of ionic signals, this being an area of fundamental interest to engineers.

Within just little more than a decade of pioneering work demonstrating the utility of nanopores our understanding of such systems at the nanoscale and our ability to control their functions and properties have granted access to a range of nanofluidic devices with potential applications that could lead, in a not too distant future, to commercial technologies. It may be that some of the potential applications that were identified are never produced on an industrial scale, whereas others that are currently unforeseen could achieve a major commercial success. What is evident is that several indicators, e.g., filed patents and startups, suggest that the ingenuity and creativity of scientists and engineers are gradually unlocking the door that allows solid-state nanopores to enter the marketplace. We should also bear in mind that many potential practical applications of nanopores and nanofluidic devices are still in the conceptual stage of development and will have to tackle some challenging technical issues, such as reproducibility and repeatability of the nanomanufacturing protocols.

It seems evident that, apart from DNA sequencing, one of the emerging niche areas for solid-state nanopores is the (bio) chemical sensing of bioactive molecules, where the ability to specifically recognize a target molecule and reproducibly generate an ionic signal may lead to reliable sensing platforms based on “iontronic” principles. Within this framework, we envisage that one of the promising areas is the ultrasensitive detection of drugs for pharmaceutical or even forensics applications.

Looking at nature for design inspiration is essential to create new nanopore devices. We know that biological pores exploit the harmony of supramolecular and covalent interactions and



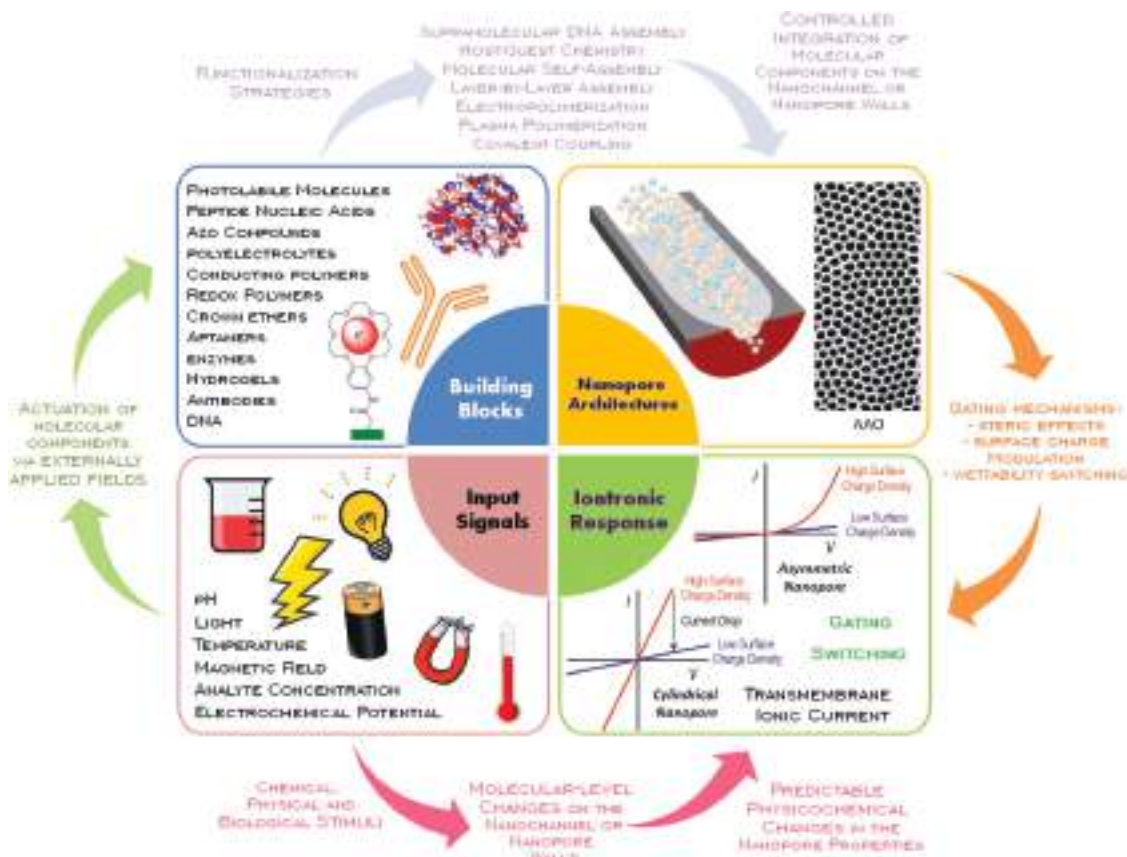


**Figure 26.** Conceptual illustration describing the combination of responsive molecular components and nanopore architectures in order to design nanofluidic architectures capable of transducing biological, chemical, and physical stimuli into predictable “iontronic” signals. The figure includes an SEM image of nanoporous anodic aluminum oxide (AAO).

the spatial organization of molecular entities to create architectures with adjustable, but specific, transport functions. Hence, we believe that the main challenge lying ahead is the rational integration of functions stemming from multicomponent (bio)molecular systems confined in the nanopore. In order to achieve this goal, it will be necessary to exert control over the molecular assembly, tailoring and, confinement conditions of (bio)molecular arrays capable of performing concerted functions with different levels of sophistication. Ideally, these concerted functions will be responsible for transducing multiple inputs in predefined ionic signals by exploiting spatial and physicochemical effects on the nanochannel walls. This is particularly important, especially in the light of the fact that these effects depend nontrivially on charge distributions, steric constraints, equilibrium displacements, or local changes in ionic concentration. In this regard, the interplay between molecular organization and supramolecular interactions in nanopore confinement is a subject that deserves further attention. As is well known, strong confinement within the nanopore can enhance interfacial interactions with the pore walls and strongly affect the physicochemical identity of the confined molecular systems. In consideration of these factors, we hypothesize that new functional capabilities can emerge from incorporation of integrated chemical systems in confined environments.

As already discussed in previous sections, the integration of switchable, stimuli-responsive units on the nanochannel walls is the bedrock of nanofluidic devices. The molecular design of solid-state nanopores revolves around the idea of deliberately introducing predesigned molecular components that might exhibit two or more easily distinguishable and predictable physicochemical states that can be conveniently exploited to transduce a particular biological, chemical or physical input into an “iontronic” signal. It is with this idea in mind that different approaches have been developed in order to construct of nanofluidic devices responsive to environmental variables, physical stimuli and even the presence of biological inputs, such as DNA or enzymes. In this sense, an interesting route which can be followed is the integration of molecular machines powered by chemical, photochemical, and electrochemical inputs for signal processing at the molecular and nanoscale level. In the past years a plethora of artificial molecular machines have been designed and constructed in solution and on surfaces, and very interesting concepts for molecular nanoactuation induced by external inputs have been duly demonstrated. It is plausible to consider that, the integration of molecular machines in nanopore devices could lead these nanosystems to a new level of functionality with additional capacity to control molecular transport and ionic signals through stimuli-induced specific and directional mechanical(molecular) movements.

On the other hand, biological molecules, such nucleic acids and enzymes, exhibit incredible functions with high specificity and efficiency, which cannot be replicated by any synthetic material. Therefore, when we talk about biosensing applications of solid-state nanopores, the controlled integration and use of biological molecules sounds like a rational way to construct nanodevices capable of detecting analytes with high specificity and accuracy. Recent advances in this matter clearly indicate that the development of novel bioactive nanopores introducing multifunctionalities of biological origin represents an amazing research line offering promising prospects for innovation in biosensing.

As mentioned above, there are also a range of interesting applications for solid-state nanopores outside biochemical and drug sensing. Examples may include energy conversion or nanofluidic logic devices. In this context, one additional challenge is to demonstrate radically new applications for solid-state nanopores and nanochannels in an effort to greatly expand the scope of areas that these devices will impact on.

The nanopore technologies discussed here not only herald a new era in integrative design of nanofluidic devices, but also give the reader a perspective of the bright future in the development of practical applications, that are even more promising if we consider that they can help find new and affordable solutions to the social (health), economic (energy), and environmental issues affecting our lives.

Looking back at what has been done over these past years, we cannot fail to be impressed by the wealth of experimental approaches for designing nanofluidic platforms. But what is more enthralling is how much there is still waiting to be done. We hope that this review does accomplish the twin objectives of portraying a dynamic, emerging field involving the utilization of nanopores, nanochannels and nanopipettes as a unified whole, and of elaborating the fascinating science (and technology!) in the several constituting parts. We believe that the juxtaposition of different approaches and perspectives in one place will stimulate new ideas and concepts in nanopore research. In very much the same way, we hope that every reader can envisage new possibilities and horizons for solid-state nanopores, just after reading these pages.

## Acknowledgements

G.P.-M. acknowledges a doctoral scholarship from CONICET. W.A.M. and O.A. are CONICET fellows and acknowledge financial support from Universidad Nacional de La Plata (PPID-X016), CONICET (PIP-0370) and ANPCyT (PICT-2017-1523 and PICT2016-1680). Financial support provided by the German Academic Exchange Service (DAAD) is also recognized and acknowledged (G.P.-M.). C.T. and M.E.T.-M. thank the LOEWE project iNAPO funded by the Ministry of Higher Education, Research and the Arts (HMWK) of the Hessen state.

## Conflict of Interest

The authors declare no conflict of interest.

## Keywords

nanochannels, nanofluidic devices, nanopores, sensing, surface functionalization

Received: March 6, 2019

Revised: May 16, 2019

Published online:

- [1] Z. Long, S. Zhan, P. Gao, Y. Wang, X. Lou, F. Xia, *Anal. Chem.* **2018**, *90*, 577.
- [2] M. Lepoitevin, T. Ma, M. Bechelany, J.-M. Janot, S. Balme, *Adv. Colloid Interface Sci.* **2017**, *250*, 195.
- [3] K. Xiao, L. Chen, G. Xie, P. Li, X.-Y. Kong, L. Wen, L. Jiang, *Nanoscale* **2018**, *10*, 6850.
- [4] X. Huang, X. Kong, L. Wen, L. Jiang, *Adv. Funct. Mater.* **2018**, *28*, 1801079.
- [5] G. Pérez-Mitta, A. G. Albesa, C. Trautmann, M. E. Toimil-Molares, O. Azzaroni, *Chem. Sci.* **2017**, *8*, 890.
- [6] Z. Zhang, L. Wen, L. Jiang, *Chem. Soc. Rev.* **2018**, *47*, 322.
- [7] K. Xiao, L. Wen, L. Jiang, *Small* **2016**, *12*, 2810.
- [8] G. Pérez-Mitta, C. Trautmann, M. E. Toimil-Molares, O. Azzaroni, in *Chem. Modif. Nanopores Nanochannels*, Elsevier, Norwich, NY, USA **2017**, pp. 61–83.
- [9] Y. Lin, Y.-L. Ying, R. Gao, Y.-T. Long, *Chem. - Eur. J.* **2018**, *24*, 37.
- [10] R. Li, X. Fan, Z. Liu, J. Zhai, *Adv. Mater.* **2017**, *29*, 1702983.
- [11] S. Chen, Y. Tang, K. Zhan, D. Sun, X. Hou, *Nano Today* **2018**, *20*, 84.
- [12] X. Hou, *Adv. Mater.* **2016**, *28*, 7049.
- [13] Y. Zhu, K. Zhan, X. Hou, *ACS Nano* **2018**, *12*, 908.
- [14] M. Wang, H. Meng, D. Wang, Y. Yin, P. Stroeve, Y. Zhang, Z. Sheng, B. Chen, K. Zhan, X. Hou, *Adv. Mater.* **2019**, *31*, 1805130.
- [15] B. Niu, K. Xiao, X. Huang, Z. Zhang, X.-Y. Kong, Z. Wang, L. Wen, L. Jiang, *ACS Appl. Mater. Interfaces* **2018**, *10*, 22632.
- [16] S. J. Lee, S. Y. Lee, *Appl. Microbiol. Biotechnol.* **2004**, *64*, 289.
- [17] J. C. T. Eijkel, A. van den Berg, *Microfluid. Nanofluid.* **2005**, *1*, 249.
- [18] Y. Lin, Y.-L. Ying, Y.-T. Long, *Curr. Opin. Electrochem.* **2018**, *7*, 172.
- [19] T. Albrecht, *Curr. Opin. Electrochem.* **2017**, *4*, 159.
- [20] B. N. Miles, A. P. Ivanov, K. A. Wilson, F. Doğan, D. Japrun, J. B. Edel, *Chem. Soc. Rev.* **2013**, *42*, 15.
- [21] R. B. Schoch, P. Renaud, *Appl. Phys. Lett.* **2005**, *86*, 253111.
- [22] G. Job, F. Herrmann, *Eur. J. Phys.* **2006**, *27*, 353.
- [23] T. M. Squires, S. R. Quake, *Rev. Mod. Phys.* **2005**, *77*, 977.
- [24] M. Shankla, A. Aksimentiev, *J. Phys. Chem. B* **2017**, *121*, 3724.
- [25] R. Qiao, N. R. Aluru, *Phys. Rev. Lett.* **2004**, *92*, 1.
- [26] D. B. Wells, M. Belkin, J. Comer, A. Aksimentiev, *Nano Lett.* **2012**, *12*, 4117.
- [27] M. Tagliazucchi, I. Szleifer, in *Chem. Modif. Nanopores Nanochannels*, Elsevier, Norwich, NY, USA **2017**, pp. 27–60.
- [28] T. Deng, M. Li, Y. Wang, Z. Liu, *Sci. Bull.* **2015**, *60*, 304.
- [29] C. M. Edmonds, Y. C. Hudiono, A. G. Ahmadi, P. J. Hesketh, S. Nair, *J. Chem. Phys.* **2012**, *136*, 065105.
- [30] C. Duan, W. Wang, Q. Xie, *Biomicrofluidics* **2013**, *7*, 26501.
- [31] J. Kudr, S. Skalickova, L. Nejd, A. Moullick, B. Ruttkay-Nedecky, V. Adam, R. Kizek, *Electrophoresis* **2015**, *36*, 2367.
- [32] K. Healy, B. Schiedt, A. P. Morrison, *Nanomedicine* **2007**, *2*, 875.
- [33] C. Trautmann, in *Ion Beams Nanoscience and Technology* (Eds.: H. R., W. H., Z. Y.), Springer, Berlin **2009**, pp. 369–387.
- [34] J. Li, D. Stein, C. McMullan, D. Branton, M. J. Aziz, J. A. Golovchenko, *Nature* **2001**, *412*, 166.
- [35] M. M. Marshall, J. Yang, A. R. Hall, *Scanning* **2012**, *34*, 101.
- [36] A. T. Kuan, J. A. Golovchenko, *Appl. Phys. Lett.* **2012**, *100*, 1.
- [37] C. J. Lo, T. Aref, A. Bezryadin, *Nanotechnology* **2006**, *17*, 3264.

- [38] P. Chen, M. Y. Wu, H. W. M. Salemink, P. F. A. Alkemade, *Nanotechnology* **2009**, 20, 1.
- [39] A. L. Bianco, J. Gierak, É. Bourhis, A. Madouri, X. Lafosse, G. Patriarche, G. Oukhaled, C. Ulysse, J. C. Galas, Y. Chen, L. Auvray, *Microelectron. Eng.* **2006**, 83, 1474.
- [40] J. Yang, D. C. Ferranti, L. A. Stern, C. A. Sanford, J. Huang, Z. Ren, L.-C. Qin, A. R. Hall, *Nanotechnology* **2011**, 22, 285310.
- [41] J. Li, M. Gershow, D. Stein, E. Brandin, J. A. Golovchenko, *Nat. Mater.* **2003**, 2, 611.
- [42] Z. Siwy, P. Apel, D. Dobrev, R. Neumann, R. Spohr, C. Trautmann, K. Voss, *Nucl. Instrum. Methods Phys. Res., Sect. B* **2003**, 208, 143.
- [43] P. Y. Apel, I. V. Blonskaya, N. V. Levkovich, O. L. Orelovich, *Pet. Chem.* **2011**, 51, 555.
- [44] P. Y. Apel, A. P. Akimenko, I. V. Blonskaya, T. Cornelius, R. Neumann, K. Schwartz, R. Spohr, C. Trautmann, *Nucl. Instrum. Methods Phys. Res., Sect. B* **2006**, 245, 284.
- [45] Y. Sun, Z. Zhu, Z. Wang, Y. Jin, J. Liu, M. Hou, Q. Zhang, *Nucl. Instrum. Methods Phys. Res., Sect. B* **2003**, 209, 188.
- [46] F. Dehaye, E. Balanzat, E. Ferain, R. Legras, *Nucl. Instrum. Methods Phys. Res., Sect. B* **2003**, 209, 103.
- [47] D. Albrecht, P. Armbruster, R. Spohr, M. Roth, K. Schaupt, H. Stuhmann, *Nucl. Instrum. Methods Phys. Res., Sect. B* **1984**, 2, 702.
- [48] V. Picq, J. M. Ramillon, E. Balanzat, *Nucl. Instrum. Methods Phys. Res., Sect. B* **1998**, 146, 496.
- [49] B. E. Fischer, S. M. Metzger, *MRS Bull* **2000**, 25, 39.
- [50] M. E. Toimil-Molares, *Beilstein J. Nanotechnol.* **2012**, 3, 860.
- [51] Y. Zhang, X.-Y. Kong, L. Gao, Y. Tian, L. Wen, L. Jiang, *Materials* **2015**, 8, 6277.
- [52] P. Y. Apel, I. V. Blonskaya, S. N. Dmitriev, O. L. Orelovich, A. Presz, B. A. Sartowska, *Nanotechnology* **2007**, 18, 305302.
- [53] Z. Siwy, Y. Gu, H. A. Spohr, D. Baur, A. Wolf-Reber, R. Spohr, P. Apel, Y. E. Korchev, *Europhys. Lett.* **2002**, 60, 349.
- [54] A. J. Storm, J. H. Chen, X. S. Ling, H. W. Zandbergen, C. Dekker, *Nat. Mater.* **2003**, 2, 537.
- [55] U. F. Keyser, B. N. Koeleman, S. V. A. N. Dorp, D. Krapf, R. M. M. Smeets, S. G. Lemay, N. H. Dekker, C. Dekker, **2006**, 2, 473.
- [56] M.-Y. Wu, D. Krapf, M. Zandbergen, H. Zandbergen, P. E. Batson, *Appl. Phys. Lett.* **2005**, 87, 113106.
- [57] M. J. Kim, M. Wanunu, D. C. Bell, A. Meller, *Adv. Mater.* **2006**, 18, 3149.
- [58] M. J. Kim, B. McNally, K. Murata, A. Meller, **2007**, 205302, 16.
- [59] B. Radisavljevic, A. Radenovic, J. Brivio, V. Giacometti, A. Kis, *Nat. Nanotechnol.* **2011**, 6, 147.
- [60] R. M. M. Smeets, U. F. Keyser, D. Krapf, M.-Y. Wu, N. H. Dekker, C. Dekker, *Nano Lett.* **2006**, 6, 89.
- [61] C. Wei, A. J. Bard, S. W. Feldberg, *Anal. Chem.* **1997**, 69, 4627.
- [62] P. Hansma, B. Drake, O. Marti, S. Gould, C. Prater, *Science* **1989**, 243, 641.
- [63] P. Novak, C. Li, A. I. Shevchuk, R. Stepanyan, M. Caldwell, S. Hughes, T. G. Smart, J. Gorelik, V. P. Ostanin, M. J. Lab, G. W. J. Moss, G. I. Frolenkov, D. Klenerman, Y. E. Korchev, *Nat. Methods* **2009**, 6, 279.
- [64] Y. Shao, M. V. Mirkin, *J. Am. Chem. Soc.* **1997**, 119, 8103.
- [65] Q. Li, S. Xie, Z. Liang, X. Meng, S. Liu, H. H. Girault, Y. Shao, *Angew. Chem., Int. Ed.* **2009**, 48, 8010.
- [66] Sutter Instrument Company, *The Pipette Cookbook*, [https://www.sutter.com/PDFs/pipette\\_cookbook.pdf](https://www.sutter.com/PDFs/pipette_cookbook.pdf) (accessed: June 2019).
- [67] C. Gao, S. Ding, Q. Tan, L. Gu, *Anal. Chem.* **2009**, 81, 80.
- [68] B. Zhang, Y. Zhang, H. S. White, *Anal. Chem.* **2004**, 76, 6229.
- [69] J. H. Shim, J. Kim, G. S. Cha, H. Nam, R. J. White, H. S. White, R. B. Brown, *Anal. Chem.* **2007**, 79, 3568.
- [70] G. Wang, A. K. Bohaty, I. Zharov, H. S. White, *J. Am. Chem. Soc.* **2006**, 128, 13553.
- [71] B. Zhang, J. Galusha, P. G. Shiozawa, G. Wang, A. J. Bergren, R. M. Jones, R. J. White, E. N. Ervin, C. C. Cauley, H. S. White, *Anal. Chem.* **2007**, 79, 4778.
- [72] D. Emmrich, A. Beyer, A. Nadzeyka, S. Bauerdick, J. C. Meyer, J. Kotakoski, A. Götzhäuser, *Appl. Phys. Lett.* **2016**, 108, 163103.
- [73] D. Polcari, P. Dauphin-Ducharme, J. Mauzeroll, *Chem. Rev.* **2016**, 116, 13234.
- [74] Y. Tian, X. Hou, L. Jiang, *J. Electroanal. Chem.* **2011**, 656, 231.
- [75] X. Hou, H. Dong, D. Zhu, L. Jiang, *Small* **2010**, 6, 361.
- [76] E. B. Kalmán, O. Sudre, I. Vlasiouk, Z. S. Siwy, *Anal. Bioanal. Chem.* **2009**, 394, 413.
- [77] A. Asatekin, K. K. Gleason, *Nano Lett.* **2011**, 11, 677.
- [78] V. P. Menon, C. R. Martin, *Anal. Chem.* **1995**, 67, 1920.
- [79] K. B. Jirage, J. C. Hulteen, C. R. Martin, *Science* **1997**, 278, 655.
- [80] M. Nishizawa, V. P. Menon, C. R. Martin, *Science* **1995**, 268, 700.
- [81] S. B. Lee, C. R. Martin, *Anal. Chem.* **2001**, 73, 768.
- [82] C. C. Harrell, S. B. Lee, C. R. Martin, *Anal. Chem.* **2003**, 75, 6861.
- [83] P. Scopece, L. A. Baker, P. Ugo, C. R. Martin, *Nanotechnology* **2006**, 17, 3951.
- [84] F. Muench, L. Hussein, T. Stohr, U. Kunz, S. Ayata, I. Gärtner, H.-J. Kleebe, W. Ensinger, *Colloids Surf., A* **2016**, 508, 197.
- [85] F. Muench, S. Schaefer, L. Hagelüken, L. Molina-Luna, M. Duerrschnebel, H.-J. Kleebe, J. Brötz, A. Vaskevich, I. Rubinstein, W. Ensinger, *ACS Appl. Mater. Interfaces* **2017**, 9, 31142.
- [86] J. W. Elam, D. Routkevitch, P. P. Mardilovich, S. M. George, *Chem. Mater.* **2003**, 15, 3507.
- [87] M. S. Sander, M. J. Côté, W. Gu, B. M. Kile, C. P. Tripp, *Adv. Mater.* **2004**, 16, 2052.
- [88] V. Romero, V. Vega, J. García, R. Zierold, K. Nielsch, V. M. Prida, B. Hernando, J. Benavente, *ACS Appl. Mater. Interfaces* **2013**, 5, 3556.
- [89] H. Shin, D.-K. Jeong, J. Lee, M. M. Sung, J. Kim, *Adv. Mater.* **2004**, 16, 1197.
- [90] D. Jeong, J. Lee, H. Shin, J. Lee, J. Kim, M. Sung, *J. Korean Phys. Soc.* **2004**, 45, 12491252.
- [91] G. Triani, P. J. Evans, D. J. Attard, K. E. Prince, J. Bartlett, S. Tan, R. P. Burford, *J. Mater. Chem.* **2006**, 16, 1355.
- [92] C. Bae, S. Kim, B. Ahn, J. Kim, M. M. Sung, H. Shin, *J. Mater. Chem.* **2008**, 18, 1362.
- [93] A. Spende, N. Sobel, M. Lukas, R. Zierold, J. C. Riedl, L. Gura, I. Schubert, J. M. M. Moreno, K. Nielsch, B. Stühn, C. Hess, C. Trautmann, M. E. Toimil-Molares, *Nanotechnology* **2015**, 26, 335301.
- [94] N. Sobel, C. Hess, M. Lukas, A. Spende, B. Stühn, M. E. Toimil-Molares, C. Trautmann, *Beilstein J. Nanotechnol.* **2015**, 6, 472.
- [95] S. Cabello-Aguilar, S. Balme, A. A. Chaaya, M. Bechelany, E. Balanzat, J.-M. Janot, C. Pochat-Bohatier, P. Miele, P. Dejardin, *Nanoscale* **2013**, 5, 9582.
- [96] R. dela Torre, J. Larkin, A. Singer, A. Meller, *Nanotechnology* **2012**, 23, 385308.
- [97] P. Chen, T. Mitsui, D. B. Farmer, J. Golovchenko, R. G. Gordon, D. Branton, *Nano Lett.* **2004**, 4, 1333.
- [98] M. Lepoitevin, P. E. Coulon, M. Bechelany, J. Cambedouzou, J.-M. Janot, S. Balme, *Nanotechnology* **2015**, 26, 144001.
- [99] X. Hou, Y. Liu, H. Dong, F. Yang, L. Li, L. Jiang, *Adv. Mater.* **2010**, 22, 2440.
- [100] X. Hou, F. Yang, L. Li, Y. Song, L. Jiang, D. Zhu, *J. Am. Chem. Soc.* **2010**, 132, 11736.
- [101] P. Y. Apel, *Radiat. Meas.* **1995**, 25, 667.
- [102] I. Vlasiouk, Z. S. Siwy, *Nano Lett.* **2007**, 7, 552.
- [103] E. B. Kalmán, I. Vlasiouk, Z. S. Siwy, *Adv. Mater.* **2008**, 20, 293.



- [104] M. Ali, B. Schiedt, R. Neumann, W. Ensinger, *Macromol. Biosci.* **2010**, *10*, 28.
- [105] F. Xia, W. Guo, Y. Mao, X. Hou, J. Xue, H. Xia, L. Wang, Y. Song, H. Ji, Q. Ouyang, Y. Wang, L. Jiang, *J. Am. Chem. Soc.* **2008**, *130*, 8345.
- [106] N. Li, S. Yu, C. C. Harrell, C. R. Martin, *Anal. Chem.* **2004**, *76*, 2025.
- [107] M. Pevarnik, K. Healy, M. Davenport, J. Yen, Z. S. Siwy, *Analyst* **2012**, *137*, 2944.
- [108] R. Wei, V. Gatterdam, R. Wieneke, R. Tampé, U. Rant, *Nanotechnol.* **2012**, *7*, 257.
- [109] J. E. Wharton, P. Jin, L. T. Sexton, L. P. Horne, S. A. Sherrill, W. K. Mino, C. R. Martin, *Small* **2007**, *3*, 1424.
- [110] L. T. Sexton, L. P. Horne, S. A. Sherrill, G. W. Bishop, L. A. Baker, C. R. Martin, *J. Am. Chem. Soc.* **2007**, *129*, 13144.
- [111] S. Onclin, B. J. Ravoo, D. N. Reinhoudt, *Angew. Chem., Int. Ed.* **2005**, *44*, 6282.
- [112] M. Wanunu, A. Meller, *Nano Lett.* **2007**, *7*, 1580.
- [113] Y. Zhao, J.-M. Janot, E. Balanzat, S. Balme, *Langmuir* **2017**, *33*, 3484.
- [114] S. Liu, Y. Dong, W. Zhao, X. Xie, T. Ji, X. Yin, Y. Liu, Z. Liang, D. Momotenko, D. Liang, H. H. Girault, Y. Shao, *Anal. Chem.* **2012**, *84*, 5565.
- [115] L.-H. Yeh, M. Zhang, S. Qian, J.-P. Hsu, S. Tseng, *J. Phys. Chem. C* **2012**, *116*, 8672.
- [116] O. Azzaroni, K. H. A. Lau, *Soft Matter* **2011**, *7*, 8709.
- [117] P. Actis, B. Vilozny, R. A. Seger, X. Li, O. Jejelowo, M. Rinaudo, N. Pourmand, *Langmuir* **2011**, *27*, 6528.
- [118] F. M. Gilles, F. M. Boubeta, O. Azzaroni, I. Szleifer, M. Tagliuzucchi, *J. Phys. Chem. C* **2018**, *122*, 6669.
- [119] G. Pérez-Mitta, W. A. Marmisollé, A. G. Albesa, M. E. Toimil-Molares, C. Trautmann, O. Azzaroni, *Small* **2018**, *14*, 1702131.
- [120] A. P. Mártire, G. M. Segovia, O. Azzaroni, M. Rafti, W. Marmisollé, *Mol. Syst. Des. Eng.* **2019**, <https://doi.org/10.1039/C9ME00007K>.
- [121] E. Maza, C. von Bilderling, M. L. Cortez, G. Díaz, M. Bianchi, L. I. Pietrasanta, J. M. Giussi, O. Azzaroni, *Langmuir* **2018**, *34*, 3711.
- [122] J. J. Richardson, M. Bjornmalm, F. Caruso, *Science* **2015**, *348*, aaa2491.
- [123] G. E. Fenoy, B. Van der Schueren, J. Scotto, F. Boulmedais, M. R. Ceolín, S. Bégin-Colin, D. Bégin, W. A. Marmisollé, O. Azzaroni, *Electrochim. Acta* **2018**, *283*, 1178.
- [124] E. Piccinini, S. Alberti, G. S. Longo, T. Berninger, J. Breu, J. Dostalek, O. Azzaroni, W. Knoll, *J. Phys. Chem. C* **2018**, *122*, 10181.
- [125] M. L. Cortez, A. Lorenzo, W. A. Marmisollé, C. von Bilderling, E. Maza, L. Pietrasanta, F. Battaglini, M. Ceolín, O. Azzaroni, *Soft Matter* **2018**, *14*, 1939.
- [126] G. E. Fenoy, E. Maza, E. Zelaya, W. A. Marmisollé, O. Azzaroni, *Appl. Surf. Sci.* **2017**, *416*, 24.
- [127] E. Piccinini, C. Bliem, C. Reiner-Rozman, F. Battaglini, O. Azzaroni, W. Knoll, *Biosens. Bioelectron.* **2017**, *92*, 661.
- [128] N. E. Muzzio, D. Gregurec, E. Diamanti, J. Irigoyen, M. A. Pasquale, O. Azzaroni, S. E. Moya, *Adv. Mater. Interfaces* **2016**, *4*, 1600126.
- [129] M. Coustet, J. Irigoyen, T. A. Garcia, R. A. Murray, G. Romero, M. Susana Cortizo, W. Knoll, O. Azzaroni, S. E. Moya, *J. Colloid Interface Sci.* **2014**, *421*, 132.
- [130] M. Lorena Cortez, N. De Matteis, M. Ceolín, W. Knoll, F. Battaglini, O. Azzaroni, *Phys. Chem. Chem. Phys.* **2014**, *16*, 20844.
- [131] J. Irigoyen, S. E. Moya, J. J. Iturri, I. Llarena, O. Azzaroni, E. Donath, *Langmuir* **2009**, *25*, 3374.
- [132] M. Ali, B. Yameen, J. Cervera, P. Ramírez, R. Neumann, W. Ensinger, W. Knoll, O. Azzaroni, P. Ramı, R. Neumann, W. Ensinger, W. Knoll, O. Azzaroni, *J. Am. Chem. Soc.* **2010**, *132*, 8338.
- [133] T. Ma, P. Gaigalas, M. Lepoitevin, I. Plikusiene, M. Bechelany, J.-M. Janot, E. Balanzat, S. Balme, *Langmuir* **2018**, *34*, 3405.
- [134] L. Wen, Z. Sun, C. Han, B. Imene, D. Tian, H. Li, L. Jiang, *Chem. - Eur. J.* **2013**, *19*, 7686.
- [135] J. Cui, O. Azzaroni, A. del Campo, *Macromol. Rapid Commun.* **2011**, *32*, 1699.
- [136] T. A. García, C. A. Gervasi, M. J. Rodríguez Presa, J. I. Otamendi, S. E. Moya, O. Azzaroni, *J. Phys. Chem. C* **2012**, *116*, 13944.
- [137] O. Azzaroni, B. Trappmann, P. van Rijn, F. Zhou, B. Kong, W. T. S. Huck, *Angew. Chem., Int. Ed.* **2006**, *45*, 7440.
- [138] O. Azzaroni, S. E. Moya, A. A. Brown, Z. Zheng, E. Donath, W. T. S. Huck, *Adv. Funct. Mater.* **2006**, *16*, 1037.
- [139] B. Yameen, M. Álvarez, O. Azzaroni, U. Jonas, W. Knoll, *Langmuir* **2009**, *25*, 6214.
- [140] A. A. Brown, O. Azzaroni, L. M. Fidalgo, W. T. S. Huck, *Soft Matter* **2009**, *5*, 2738.
- [141] J. Cui, T.-H. Nguyen, M. Ceolín, R. Berger, O. Azzaroni, A. del Campo, *Macromolecules* **2012**, *45*, 3213.
- [142] J. M. Giussi, M. L. Cortez, W. A. Marmisollé, O. Azzaroni, *Chem. Soc. Rev.* **2019**, *48*, 814.
- [143] G. E. Fenoy, J. M. Giussi, C. von Bilderling, E. M. Maza, L. I. Pietrasanta, W. Knoll, W. A. Marmisollé, O. Azzaroni, *J. Colloid Interface Sci.* **2018**, *518*, 92.
- [144] B. Yameen, M. Ali, M. Álvarez, R. Neumann, W. Ensinger, W. Knoll, O. Azzaroni, *Polym. Chem.* **2010**, *1*, 183.
- [145] A. Calvo, B. Yameen, F. J. Williams, O. Azzaroni, G. J. A. A. Soler-Illia, *Chem. Commun.* **2009**, 2553.
- [146] A. Calvo, M. C. Fuertes, B. Yameen, F. J. Williams, O. Azzaroni, G. J. A. A. Soler-Illia, *Langmuir* **2010**, *26*, 5559.
- [147] B. Yameen, A. Kaltbeitzel, A. Langner, H. Duran, F. Müller, U. Gösele, O. Azzaroni, W. Knoll, *J. Am. Chem. Soc.* **2008**, *130*, 13140.
- [148] B. Yameen, A. Kaltbeitzel, A. Langer, F. Müller, U. Gösele, W. Knoll, O. Azzaroni, *Angew. Chem., Int. Ed.* **2009**, *48*, 3124.
- [149] A. Brunson, J. Cui, M. Ceolín, A. del Campo, G. J. A. A. Soler-Illia, O. Azzaroni, *Chem. Commun.* **2012**, *48*, 1422.
- [150] A. Brunson, C. Díaz, L. I. Pietrasanta, B. Yameen, M. Ceolín, G. J. A. A. Soler-Illia, O. Azzaroni, *Langmuir* **2012**, *28*, 3583.
- [151] O. Azzaroni, *J. Polym. Sci., Part A: Polym. Chem.* **2012**, *50*, 3225.
- [152] B. Yameen, M. Ali, R. Neumann, W. Ensinger, W. Knoll, O. Azzaroni, W. Knoll, *Chem. Commun.* **2010**, *46*, 1908.
- [153] B. Yameen, M. Ali, R. Neumann, W. Ensinger, W. Knoll, O. Azzaroni, *Small* **2009**, *5*, 1287.
- [154] B. Yameen, M. Ali, R. Neumann, W. Ensinger, W. Knoll, O. Azzaroni, *J. Am. Chem. Soc.* **2009**, *131*, 2070.
- [155] H. Ouyang, Z. Xia, J. Zhe, *Microfluid. Nanofluid.* **2010**, *9*, 915.
- [156] W. Guo, H. Xia, L. Cao, F. Xia, S. Wang, G. Zhang, Y. Song, Y. Zhang, L. Jiang, D. Zhu, *Adv. Funct. Mater.* **2010**, *20*, 3561.
- [157] Z. Zeng, Y. Ai, S. Qian, *Phys. Chem. Chem. Phys.* **2014**, *16*, 2465.
- [158] G. Chen, S. Das, *J. Phys. Chem. B* **2015**, *119*, 12714.
- [159] F. M. Gilles, M. Tagliuzucchi, O. Azzaroni, I. Szleifer, *J. Phys. Chem. C* **2016**, *120*, 4789.
- [160] G. Chen, J. Patwary, H. S. Sachar, S. Das, *Microfluid. Nanofluid.* **2018**, *22*, 112.
- [161] R. S. Maheedhara, H. S. Sachar, H. Jing, S. Das, *J. Phys. Chem. B* **2018**, *122*, 7450.
- [162] H. Zhang, X. Hou, J. Hou, L. Zeng, Y. Tian, L. Li, L. Jiang, *Adv. Funct. Mater.* **2015**, *25*, 1102.
- [163] C. C. Harrell, P. Kohli, Z. Siwy, C. R. Martin, *J. Am. Chem. Soc.* **2004**, *126*, 15646.
- [164] Y. Mao, S. Chang, S. Yang, Q. Ouyang, L. Jiang, *Nat. Nanotechnol.* **2007**, *2*, 366.
- [165] F. Wang, X. Liu, I. Willner, *Angew. Chem., Int. Ed.* **2015**, *54*, 1098.
- [166] S. F. Buchsbaum, G. Nguyen, S. Howorka, Z. S. Siwy, *J. Am. Chem. Soc.* **2014**, *136*, 9902.



- [167] D. Liu, S. Balasubramanian, *Angew. Chem., Int. Ed.* **2003**, *42*, 5734.
- [168] X. Hou, W. Guo, F. Xia, F. Q. Nie, H. Dong, Y. Tian, L. Wen, L. Wang, L. Cao, Y. Yang, J. Xue, Y. Song, Y. Wang, D. Liu, L. Jiang, *J. Am. Chem. Soc.* **2009**, *131*, 7800.
- [169] M. Liu, H. Zhang, K. Li, L. Heng, S. Wang, Y. Tian, L. Jiang, *Adv. Funct. Mater.* **2015**, *25*, 421.
- [170] H. Zhang, J. Hou, R. Ou, Y. Hu, H. Wang, L. Jiang, *Nanoscale* **2017**, *9*, 7297.
- [171] J. Wang, R. Fang, J. Hou, H. Zhang, Y. Tian, H. Wang, L. Jiang, *ACS Nano* **2017**, *11*, 3022.
- [172] I. Vlassiouk, P. Takmakov, S. Smirnov, *Langmuir* **2005**, *21*, 4776.
- [173] Z. Sun, T. Liao, Y. Zhang, J. Shu, H. Zhang, G. J. Zhang, *Biosens. Bioelectron.* **2016**, *86*, 194.
- [174] Y. Jiang, N. Liu, W. Guo, F. Xia, L. Jiang, *J. Am. Chem. Soc.* **2012**, *134*, 15395.
- [175] N. Liu, Y. Jiang, Y. Zhou, F. Xia, W. Guo, L. Jiang, *Angew. Chem., Int. Ed.* **2013**, *52*, 2007.
- [176] W. Guo, F. Hong, N. Liu, J. Huang, B. Wang, R. Duan, X. Lou, F. Xia, *Adv. Mater.* **2015**, *27*, 2090.
- [177] Y. Wu, D. Wang, I. Willner, Y. Tian, L. Jiang, *Angew. Chem., Int. Ed.* **2018**, *57*, 7790.
- [178] D. Evanko, *Nat. Methods* **2004**, *1*, 186.
- [179] T. Zhao, H. S. Zhang, H. Tang, J. H. Jiang, *Talanta* **2017**, *175*, 121.
- [180] G. Jagerszki, R. E. Gyurcsanyi, L. Hofler, E. Pretsch, *Nano Lett.* **2007**, *7*, 1609.
- [181] T. Liao, X. Li, Q. Tong, K. Zou, H. Zhang, L. Tang, Z. Sun, G.-J. Zhang, *Anal. Chem.* **2017**, *89*, 5511.
- [182] Y. Chen, D. Zhou, Z. Meng, J. Zhai, *Chem. Commun.* **2016**, *52*, 10020.
- [183] N. Liu, R. Hou, P. Gao, X. Lou, F. Xia, *Analyst* **2016**, *141*, 3626.
- [184] Y. Tian, Z. Zhang, L. Wen, J. Ma, Y. Zhang, W. Liu, J. Zhai, L. Jiang, *Chem. Commun.* **2013**, *49*, 10679.
- [185] L. Gao, P. Li, Y. Zhang, K. Xiao, J. Ma, G. Xie, G. Hou, Z. Zhang, L. Wen, L. Jiang, *Small* **2015**, *11*, 543.
- [186] H. Wang, S. Hou, Q. Wang, Z. Wang, X. Fan, J. Zhai, *J. Mater. Chem. B* **2015**, *3*, 1699.
- [187] X. L. Ni, X. Xiao, H. Cong, Q. J. Zhu, S. F. Xue, Z. Tao, *Acc. Chem. Res.* **2014**, *47*, 1386.
- [188] T. Ogoshi, T. A. Yamagishi, Y. Nakamoto, *Chem. Rev.* **2016**, *116*, 7937.
- [189] F. Zhang, J. Ma, Y. Sun, I. Boussouar, D. Tian, H. Li, L. Jiang, *Chem. Sci.* **2016**, *7*, 3227.
- [190] R. Fang, H. Zhang, L. Yang, H. Wang, Y. Tian, X. Zhang, L. Jiang, *J. Am. Chem. Soc.* **2016**, *138*, 16372.
- [191] Y. Sun, F. Zhang, J. Quan, F. Zhu, W. Hong, J. Ma, H. Pang, Y. Sun, D. Tian, H. Li, *Nat. Commun.* **2018**, *9*, 2617.
- [192] F. Zhang, J. Ma, Y. Sun, Y. Mei, X. Chen, W. Wang, H. Li, *Anal. Chem.* **2018**, *90*, 8270.
- [193] M. Ali, I. Ahmed, S. Nasir, P. Ramirez, C. M. Niemeyer, S. Mafe, W. Ensinger, *ACS Appl. Mater. Interfaces* **2015**, *7*, 19541.
- [194] Y. Xu, J. Jiang, Z. Meng, Q. Zhang, X. Li, J. Zhai, *J. Phys. Chem. C* **2016**, *120*, 17342.
- [195] M. Ali, I. Ahmed, P. Ramirez, S. Nasir, S. Mafe, C. M. Niemeyer, W. Ensinger, *Sens. Actuators, B* **2017**, *240*, 895.
- [196] D. Wang, M. V. Mirkin, *J. Am. Chem. Soc.* **2017**, *139*, 11654.
- [197] G. Pérez-Mitta, W. A. Marmisollé, C. Trautmann, M. E. Toimil-Molares, O. Azzaroni, *J. Am. Chem. Soc.* **2015**, *137*, 15382.
- [198] G. Pérez-Mitta, W. A. Marmisollé, C. Trautmann, M. E. Toimil-Molares, O. Azzaroni, *Adv. Mater.* **2017**, *1700972*, 1.
- [199] Q. Zhang, Z. Zhang, H. Zhou, Z. Xie, L. Wen, Z. Liu, J. Zhai, X. Diao, *Nano Res.* **2017**, *10*, 3715.
- [200] Q. Zhang, J. Kang, Z. Xie, X. Diao, Z. Liu, J. Zhai, *Adv. Mater.* **2017**, *1703323*, 1.
- [201] R. Ren, Y. Zhang, B. P. Nadappuram, B. Akpinar, D. Klenerman, A. P. Ivanov, J. B. Edel, Y. Korchev, *Nat. Commun.* **2017**, *8*, 586.
- [202] Y. Xu, M. Zhang, T. Tian, Y. Shang, Z. Meng, J. Jiang, J. Zhai, Y. Wang, *NPG Asia Mater.* **2015**, *7*, 1.
- [203] X. Shang, G. Xie, X.-Y. Kong, Z. Zhang, Y. Zhang, W. Tian, L. Wen, L. Jiang, *Adv. Mater.* **2017**, *29*, 1603884.
- [204] R. Li, X. Sui, C. Li, J. Jiang, J. Zhai, L. Gao, *ACS Appl. Mater. Interfaces* **2018**, *10*, 3241.
- [205] K. Xiao, K. Wu, L. Chen, X. Y. Kong, Y. Zhang, L. Wen, L. Jiang, *Angew. Chem., Int. Ed.* **2018**, *57*, 151.
- [206] T. D. James, K. R. A. S. Sandanayake, S. Shinkai, *Angew. Chem., Int. Ed. Eng.* **1996**, *35*, 1910.
- [207] Z. Sun, C. Han, L. Wen, D. Tian, H. Li, L. Jiang, *Chem. Commun.* **2012**, *48*, 3282.
- [208] Q. H. Nguyen, M. Ali, R. Neumann, W. Ensinger, *Sens. Actuators, B* **2012**, *162*, 216.
- [209] B. Viložny, A. L. Wollenberg, P. Actis, D. Hwang, B. Singaram, N. Pourmand, *Nanoscale* **2013**, *5*, 9214.
- [210] S. Zhao, Y.-B. Zheng, S.-L. Cai, Y.-H. Weng, S.-H. Cao, J.-L. Yang, Y.-Q. Li, *Electrochem. Commun.* **2013**, *36*, 71.
- [211] H. Wang, M. Yan, M. Zhang, *Chem. Commun.* **2015**, *51*, 2444.
- [212] Y.-B. Zheng, S. Zhao, S.-H. Cao, S.-L. Cai, X.-H. Cai, Y.-Q. Li, *Nanoscale* **2017**, *9*, 433.
- [213] G. Pérez-Mitta, W. A. Marmisolle, L. Burr, M. E. Toimil-Molares, C. Trautmann, O. Azzaroni, *Small* **2018**, *14*, 1703144.
- [214] M. Ali, M. N. Tahir, Z. Siwy, R. Neumann, W. Tremel, W. Ensinger, *Anal. Chem.* **2011**, *83*, 1673.
- [215] G. Hou, H. Zhang, G. Xie, K. Xiao, L. Wen, S. Li, Y. Tian, L. Jiang, *J. Mater. Chem. A* **2014**, *2*, 19131.
- [216] G. Pérez-Mitta, A. S. Peinetti, M. L. Cortez, M. E. Toimil-Molares, C. Trautmann, O. Azzaroni, *Nano Lett.* **2018**, *18*, 3303.
- [217] C. Han, X. Hou, H. Zhang, W. Guo, H. Li, L. Jiang, *J. Am. Chem. Soc.* **2011**, *133*, 7644.
- [218] Z. Sun, C. Han, M. Song, L. Wen, D. Tian, H. Li, L. Jiang, *Adv. Mater.* **2014**, *26*, 455.
- [219] J. Wang, J. Hou, H. Zhang, Y. Tian, L. Jiang, *ACS Appl. Mater. Interfaces* **2018**, *10*, 2033.
- [220] H. He, X. Xu, P. Wang, L. Chen, Y. Jin, *Chem. Commun.* **2015**, *51*, 1914.
- [221] M. Ali, S. Nasir, W. Ensinger, *Electrochim. Acta* **2016**, *215*, 231.
- [222] P. Li, X. Y. Kong, G. Xie, K. Xiao, Z. Zhang, L. Wen, L. Jiang, *Small* **2016**, *12*, 1854.
- [223] M. Ali, P. Ramirez, I. Duznovic, S. Nasir, S. Mafe, W. Ensinger, *Colloids Surf., B* **2017**, *150*, 201.
- [224] I. Boussouar, Q. Chen, X. Chen, Y. Zhang, F. Zhang, D. Tian, H. S. White, H. Li, *Anal. Chem.* **2017**, *89*, 1110.
- [225] Q. Lu, Q. Tang, Z. Chen, S. Zhao, G. Qing, T. Sun, *ACS Appl. Mater. Interfaces* **2017**, *9*, 32554.
- [226] F. A. Christy, P. S. Shrivastav, *Crit. Rev. Anal. Chem.* **2011**, *41*, 236.
- [227] Q. Liu, K. Xiao, L. Wen, H. Lu, Y. Liu, X.-Y. Kong, G. Xie, Z. Zhang, Z. Bo, L. Jiang, *J. Am. Chem. Soc.* **2015**, *137*, 11976.
- [228] K. Wu, K. Xiao, L. Chen, R. Zhou, B. Niu, Y. Zhang, L. Wen, *Langmuir* **2017**, *33*, 8463.
- [229] Y. Qian, Z. Zhang, W. Tian, L. Wen, L. Jiang, *Faraday Discuss.* **2018**, *210*, 101.
- [230] M. Ali, I. Ahmed, P. Ramirez, S. Nasir, J. Cervera, S. Mafe, C. M. Niemeyer, W. Ensinger, *Langmuir* **2017**, *33*, 9170.
- [231] M. Ali, I. Ahmed, P. Ramirez, S. Nasir, S. Mafe, C. M. Niemeyer, W. Ensinger, *Anal. Chem.* **2018**, *90*, 6820.
- [232] Q. Zhai, J. Wang, H. Jiang, Q. Wei, E. Wang, *Talanta* **2015**, *140*, 219.
- [233] X. Xu, R. Hou, P. Gao, M. Miao, X. Lou, B. Liu, F. Xia, *Anal. Chem.* **2016**, *88*, 2386.
- [234] Y. Tian, X. Hou, L. Wen, W. Guo, Y. Song, H. Sun, Y. Wang, L. Jiang, D. Zhu, *Chem. Commun.* **2010**, *46*, 1682.
- [235] Z. Meng, C. Jiang, X. Li, J. Zhai, **2014**.

- [236] Q. Liu, K. Xiao, L. Wen, Y. Dong, G. Xie, Z. Zhang, Z. Bo, L. Jiang, *ACS Nano* **2014**, *8*, 12292.
- [237] M. Ali, I. Ahmed, P. Ramirez, S. Nasir, J. Cervera, C. M. Niemeyer, W. Ensinger, *Nanoscale* **2016**, *8*, 8583.
- [238] G. Nie, Y. Sun, F. Zhang, M. Song, D. Tian, L. Jiang, H. Li, *Chem. Sci.* **2015**, *6*, 5859.
- [239] Q. Liu, L. Wen, K. Xiao, H. Lu, Z. Zhang, G. Xie, X.-Y. Kong, Z. Bo, L. Jiang, *Adv. Mater.* **2016**, *28*, 3181.
- [240] M. Ali, I. Ahmed, P. Ramirez, S. Nasir, C. M. Niemeyer, S. Mafe, W. Ensinger, *Small* **2016**, *12*, 2014.
- [241] Y. Zhang, R. Zhou, Z. Zhao, X.-Y. Kong, G. Xie, Q. Liu, P. Li, Z. Zhang, K. Xiao, Z. Liu, L. Wen, L. Jiang, *ChemPhysChem* **2017**, *18*, 253.
- [242] X. P. Zhao, S. S. Wang, M. R. Younis, X. H. Xia, C. Wang, *Anal. Chem.* **2018**, *90*, 896.
- [243] W. Chen, B. Jin, Y. L. Hu, Y. Lu, X. H. Xia, *Small* **2012**, *8*, 1001.
- [244] M. Zhang, Z. Meng, J. Zhai, L. Jiang, *Chem. Commun.* **2013**, *49*, 2284.
- [245] M. Ali, S. Nasir, P. Ramirez, I. Ahmed, Q. H. Nguyen, L. Fruk, S. Mafe, W. Ensinger, *Adv. Funct. Mater.* **2012**, *22*, 390.
- [246] Q. Zhang, Z. Liu, X. Hou, X. Fan, J. Zhai, L. Jiang, *Chem. Commun.* **2012**, *48*, 5901.
- [247] Z. Zhang, X. Y. Kong, G. Xie, P. Li, K. Xiao, L. Wen, L. Jiang, *Sci. Adv.* **2016**, *2*, 1.
- [248] L. Wen, Q. Liu, J. Ma, Y. Tian, C. Li, Z. Bo, L. Jiang, *Adv. Mater.* **2012**, *24*, 6193.
- [249] M. Zhang, X. Hou, J. Wang, Y. Tian, X. Fan, J. Zhai, L. Jiang, *Adv. Mater.* **2012**, *24*, 2424.
- [250] T. Ma, M. Walko, M. Lepoitevin, J. M. Janot, E. Balanzat, A. Kocer, S. Balme, *Adv. Mater. Interfaces* **2018**, *5*, 1.
- [251] L. Wen, J. Ma, Y. Tian, J. Zhai, L. Jiang, *Small* **2012**, *8*, 838.
- [252] D. He, X. He, K. Wang, J. Cao, Y. Zhao, *Adv. Funct. Mater.* **2012**, *22*, 4704.
- [253] Y. Sun, J. Ma, F. Zhang, F. Zhu, Y. Mei, L. Liu, D. Tian, H. Li, *Nat. Commun.* **2017**, *8*, 260.
- [254] R. Wang, Y. Sun, F. Zhang, M. Song, D. Tian, H. Li, *Angew. Chem.* **2017**, *129*, 5378.
- [255] G. Xie, P. Li, Z. Zhao, Z. Zhu, X. Y. Kong, Z. Zhang, K. Xiao, L. Wen, L. Jiang, *J. Am. Chem. Soc.* **2018**, *140*, 4552.
- [256] N. Reber, A. Kuchel, R. Spohr, A. Wolf, M. Yoshida, *J. Membr. Sci.* **2001**, *193*, 49.
- [257] H. Alem, A. S. Duwez, P. Lussis, P. Lipnik, A. M. Jonas, S. Demoustier-Champagne, *J. Membr. Sci.* **2008**, *308*, 75.
- [258] S. Nasir, M. Ali, W. Ensinger, *Nanotechnology* **2012**, *23*, 225502.
- [259] W. Guo, H. Xia, F. Xia, X. Hou, L. Cao, L. Wang, J. Xue, G. Zhang, Y. Song, D. Zhu, Y. Wang, L. Jiang, *ChemPhysChem* **2010**, *11*, 859.
- [260] S. Schmidt, S. Alberti, P. Vana, G. J. A. A. Soler-Illia, O. Azzaroni, *Chem. - Eur. J.* **2017**, *23*, 14500.
- [261] L. G. Lopez, R. J. Nap, *Phys. Chem. Chem. Phys.* **2018**, *20*, 16657.
- [262] Z. Zhang, G. Xie, K. Xiao, X.-Y. Kong, P. Li, Y. Tian, L. Wen, L. Jiang, *Adv. Mater.* **2016**, *28*, 9613.
- [263] Y. Zhou, W. Guo, J. Cheng, Y. Liu, J. Li, L. Jiang, *Adv. Mater.* **2012**, *24*, 962.
- [264] N. Liu, C. Li, T. Zhang, R. Hou, Z. Xiong, Z. Li, B. Wei, Z. Yang, P. Gao, X. Lou, X. Zhang, W. Guo, F. Xia, *Small* **2017**, *13*, 1600287.
- [265] G. Hou, D. Wang, K. Xiao, H. Zhang, S. Zheng, P. Li, Y. Tian, L. Jiang, *Small* **2018**, *14*, 1703369.
- [266] W.-J. Lan, D. A. Holden, H. S. White, *J. Am. Chem. Soc.* **2011**, *133*, 13300.
- [267] *Oxford Nanopore Raises £100M From International Investors*, <https://www.genomeweb.com/sequencing/oxford-nanopore-raises-100m-international-investors#.XHmtqIhKjIW> (accessed: June 2019).
- [268] R. Davis, R. Chen, *US20130244340A1*, **2013**.
- [269] R. Davis, R. Chen, *WO2013123450A1*, **2013**.
- [270] R. Chen, R. Davis, *WO2011097028A1*, **2011**.
- [271] *Roche Acquires Genia Technologies to Strengthen Next Generation Sequencing Pipeline*, <https://www.roche.com/media/releases/medcor-2014-06-02.htm> (accessed: June 2019).
- [272] J. G. Mandell, K. L. Gunderson, J. H. Gundlach, *US20150344945A1*, **2015**.
- [273] B. Boyanov, J. G. Mandell, K. L. Gunderson, J. Bai, L. Qiang, B. Baas, *US20170260582A1*, **2017**.
- [274] W. Meuleman, *EP3004378B1*, **2017**.
- [275] QuantaPore Inc., <https://quantapore.com/> (accessed: June 2019).
- [276] M. Huber, *US20160122812A1*, **2016**.
- [277] *Two Pore Guys*, <https://www.twoporeguys.com/> (accessed: June 2019).
- [278] T. J. Morin, D. A. Heller, W. B. Dunbar, *US20170074855A1*, **2017**.
- [279] T. J. Morin, T. Shropshire, W. B. Dunbar, D. A. Heller, H. Wang, *US20180023115A1*, **2018**.
- [280] T. J. Morin, *US20140329225A1*, **2014**.
- [281] *Electronic Biosciences*, <http://electronicbio.com/> (accessed: June 2019).
- [282] E. N. Ervin, J. J. Watkins, G. A. Barrall, *US20140106472A1*, **2014**.
- [283] A. D. Hibbs, G. A. Barrall, E. N. Ervin, D. K. Lathrop, *US20110162963A1*, **2011**.
- [284] Z. Li, C. Pei, F. Yang, *US20120040512A1*, **2012**.
- [285] S. Polonsky, S. M. Rosnagel, G. A. Stolovitzky, *US8003319B2*, **2011**.
- [286] X. Su, A. A. Berlin, *US7744816B2*, **2010**.
- [287] P. W. Barth, *US7075161B2*, **2006**.
- [288] C. A. Flory, *US7410564B2*, **2008**.
- [289] J. Feng, K. Liu, A. Radenovic, Y. Astier, *US20180073161A1*, **2018**.
- [290] J. Shim, D.-H. Lee, K. Eom, T. Jeon, H. Jeong, *US20140021047A1*, **2014**.
- [291] J. Lee, J. Park, *US20130240378A1*, **2013**.
- [292] *Oxford Nanopore Technologies*, <https://nanoporetech.com/> (accessed: June 2019).
- [293] B. A. Sartowska, O. L. Orellovitch, P. Y. Apel, I. V. Blonskaya, A. Presz, *Nukleonika* **2012**, *57*, 575.